이학박사학위청구논문

# 백색지방조직의 에너지대사 조절에서 지방조직 줄기세포의 역할 규명

# Roles of Adipose Stem Cells in the Energy Metabolism of White Adipose Tissue

2024 년 2 월

서울대학교 대학원

생명과학부

남 궁 한

# Roles of Adipose Stem Cells in the Energy Metabolism of White Adipose Tissue

**A dissertation submitted in partial fulfillment**

**of the requirement for degree of**

**DOCTOR OF PHILOSOPHY**

**To the Faculty of the**

**School of Biological Sciences**

**At**

**SEOUL NATIONAL UNIVERSITY**

**By**

**Hahn Nahmgoong**

**February, 2024**

**Data Approved**

_____

_____

_____

_____

_____

_____

# 백색지방조직의 에너지대사 조절에서 지방조직 줄기세포의 역할 규명

# Roles of Adipose Stem Cells in the Energy Metabolism of White Adipose Tissue

지도교수 김 재 범

이 논문을 이학박사 학위논문으로 제출함
2024 년 2 월

서울대학교 대학원

생명과학부

남 궁 한

남궁한의 이학박사 학위논문을 인준함
2024 년 2 월

위 원 장 _____ (인)

부위원장 _____ (인)

위 원 _____ (인)

위 원 _____ (인)

위 원 _____ (인)

# ABSTRACT

## Roles of Adipose Stem Cells in the Energy Metabolism of White Adipose Tissue

**Hahn Nahmgoong**

Adipose tissue is a central metabolic organ that stores excess energy and secretes various hormones and lipid metabolites to regulate whole-body energy homeostasis. In mammals, adipose tissue is largely divided into white adipose tissue (WAT), which is specialized in energy storage, and brown adipose tissue (BAT), which is specialized in non-shivering thermogenesis. Anatomically, WAT is categorized into visceral adipose tissue (VAT) and subcutaneous adipose tissue (SAT). In rodents, epididymal adipose tissue (EAT) and inguinal adipose tissue (IAT) are representative models of VAT and SAT, respectively.

A growing body of evidence indicates that EAT and IAT differ in their developmental origin, anatomical location, and response to metabolic stimuli. In mice, EAT arises postnatally from the somitic mesoderm, whereas IAT arises embryonically from the posterior lateral plate mesoderm. EAT interacts with intra-abdominal organs, such as the gut, whereas IAT protects the body from physical stress and cold environments. Furthermore, EAT and IAT exhibit different features in response to metabolic stimuli. In obesity, EAT exhibits low-grade chronic inflammation and fibrosis, whereas these phenomena are not highly manifested in IAT. Moreover, upon cold stimuli, thermogenic beige adipocytes are produced in IAT, but not in EAT.

Accumulating evidence suggests that distinct properties of adipose stem cells (ASCs) would mediate different characteristics of EAT and IAT. For instance, adipocytes derived from EAT or IAT ASCs are functionally different. In obesity, the formation of adipocytes from ASCs is enhanced specifically in EAT. Upon cold exposure, ASCs in IAT differentiate into beige adipocytes. Furthermore, it has been reported that ASCs in IAT inhibit inflammatory responses. Recent studies applied single-cell RNA sequencing (scRNA-seq) analysis have shown that ASCs are heterogeneous and composed of subpopulations. Nonetheless, depot-specific ASC subpopulations that exhibit different features of the two fat depots have not been properly explored.

In Chapter I, I comparatively analyze the adipogenesis processes in EAT and IAT. I find that differentiation of ASCs into white adipocytes is more active in EAT than in IAT, whereas $BST2^{high}$ ASCs are unique beige adipocyte precursors in IAT. EAT and IAT ASCs are composed of distinct clusters, which are categorized into three adipogenic stages. Committed preadipocytes, which have high adipogenic potential, are more abundant in EAT than in IAT because of the intrinsic characteristics of each ASC type. Obesogenic stimuli induce EAT-specific *de novo* adipogenesis, which is potentiated by the proliferation of EAT ASCs. In addition, IAT-specific $BST2^{high}$ ASCs, whose biogenesis is regulated by the lymph nodes, exhibit a strong potential to differentiate into beige adipocytes.

In Chapter II, I identify fibrotic $SDC1^{+}$ ASCs in EAT and anti-inflammatory $CXCL14^{+}$ ASCs in IAT. To investigate the ASC clusters that account for higher levels of inflammation and fibrosis in EAT than IAT, I comparatively analyzed ASC clusters in EAT and IAT using combined scRNA-seq datasets from lean and obese

mice. Pseudotime analysis revealed an obese-EAT specific ASC cluster that shows a unique fate and specific expression of SDC1. $SDC1^+$ ASCs are specifically observed in obese EAT and highly express genes related to inflammation and fibrosis. In contrast, IAT ASCs highly express CXCL14 and repress monocyte infiltration, probably by suppressing CXCL12 activity. These findings suggest that in obesity, fat depot-specific ASCs, such as $SDC1^+$ and $CXCL14^+$ cells, modulate fibro-inflammatory features in a depot-specific manner.

Taken together, this thesis shows that ASCs are crucial mediators of the heterogeneity and plasticity of WAT. Depot-specific ASC subpopulations determine the distinct features of EAT and IAT. In addition, ASC subpopulation characteristics are altered in response to metabolic stimuli and mediate the functional plasticity of adipose tissue. This study broadens our understanding of ASCs with new insights into the origin of white fat depot differences.

**Keywords:** adipose tissue, white adipose tissue, visceral adipose tissue, subcutaneous adipose tissue, adipose stem cell, adipogenesis, inflammation, fibrosis

**Student Number:** 2018-23827

# TABLE OF CONTENTS

# LIST OF FIGURES

# LIST OF TABLES

# BACKGROUNDS

## I. Functions of Adipose Tissue

Adipose tissue is one of the central metabolic organs that regulates whole-body energy homeostasis [1, 2]. Adipose tissue has long been considered a simple lipid deposit and classified as a connective tissue. However, this concept had to be revised as numerous studies demonstrated the diverse roles of adipose tissue including energy conservation and supply, hormone secretion, immune regulation, and heat generation [3]. In energy-enriched states, adipose tissue stores surplus nutrients in the form of neutral lipids and provides them as fuel for other organs in energy-depleted conditions [4, 5]. Also, adipose tissue secretes various cytokines (termed adipokines) such as leptin and adiponectin and acts as an endocrine organ via crosstalk with other organs [6-11]. In addition, adipose tissue is an immunologically active organ that contains various tissue-resident or infiltrated innate and adaptive immune cells [12-15]. Further, brown and beige adipocytes can consume energy to generate heat in a process termed non-shivering thermogenesis [16]. These diverse functions emphasize the importance of adipose tissue in the control of systemic energy metabolism.

Functional flexibility is one of the key features of adipose tissue [3, 17]. Adipose tissue is distributed throughout the body in several fat depots that seem to have unique characteristics and functions [18]. The metabolic roles of adipose tissue are varied and dynamically change in response to metabolic stimuli [3]. The plasticity of adipose tissue is important for adaption to environmental changes and maintenance of systemic energy homeostasis.

# 1. White and Brown Adipose Tissue

Adipose tissue is categorized into two types: white adipose tissue (WAT) and brown adipose tissue (BAT), each with distinct locations and functions [19]. WAT is distributed throughout the body and further classified into visceral adipose tissue (VAT), which resides in the abdominal cavity, and subcutaneous adipose tissue (SAT), which resides beneath the skin. BAT is predominantly located in the upper back, localized around the shoulders and ribs [20, 21]. The supraclavicular and cervical regions in humans and the interscapular region in rodents are well-characterized BAT depots. BAT is also found in other body parts, such as perirenal BAT in the visceral region and axillary BAT in the subcutaneous region [20, 21]. Major WAT and BAT depots in humans and rodents are graphically summarized in Figure 1.

WAT and BAT contain adipocytes with distinct morphologies, gene expression patterns, and primary functions [19, 22]. White adipocytes in WAT mostly contain large, unilocular lipid droplets, whereas brown adipocytes in BAT store lipids in small, multilocular lipid droplets. These structures appear to be related to the functions of each adipocyte [23, 24]. White adipocytes are specialized in energy storage whereas brown adipocytes can generate heat by burning lipids and metabolites. Brown adipocytes have high numbers of mitochondria with uncoupling protein 1 (UCP1), which primarily mediates non-shivering thermogenesis [25, 26]. In contrast, white adipocytes have relatively low amounts of mitochondria and nearly undetectable UCP1 levels. Thus, WAT and BAT perform non-overlapping primary functions with distinct types of adipocytes.

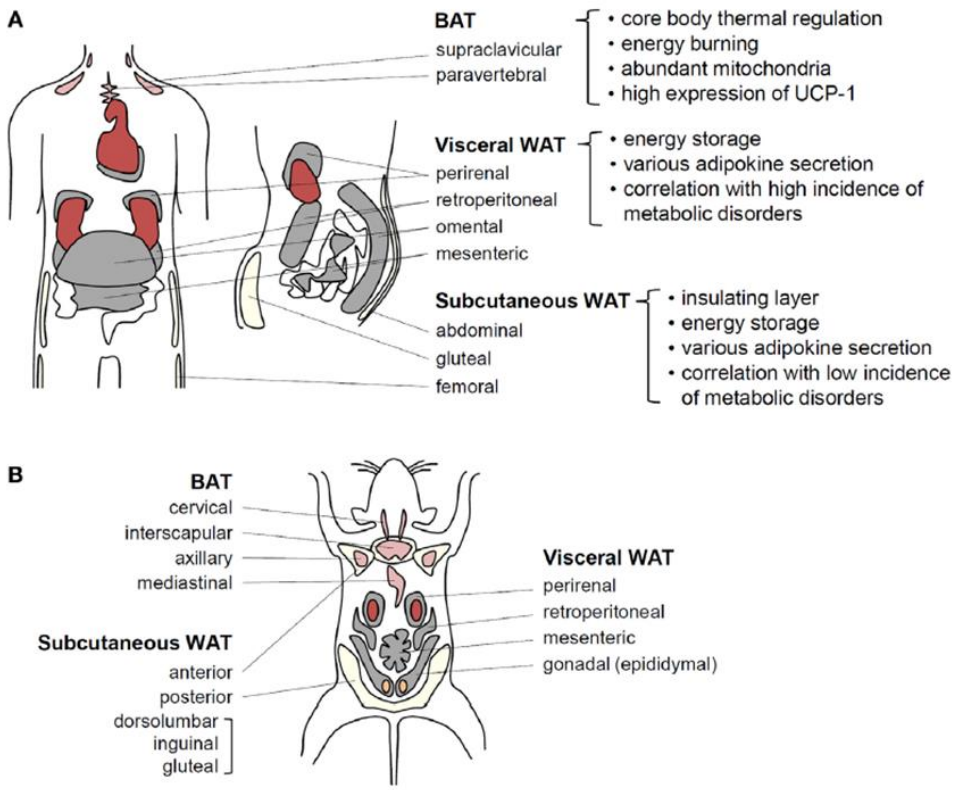


**Figure 1. Fat depots in humans and rodents**

Major fat depots in humans (A) and rodents (B). Images are generously provided by Choe, S. S., *et al*. (2016). "Adipose Tissue Remodeling: Its Role in Energy Metabolism and Metabolic Disorders." Front Endocrinol (Lausanne) 7: 30.

Because of their functional differences, WAT and BAT have distinct roles in the regulation of systemic energy homeostasis, particularly in obesity. Since BAT can consume lipids and various metabolites and act as a metabolic sink, the activation of BAT has been considered as a potential target against metabolic complications [26-28]. In this regard, the discovery of active BAT in adult humans highlighted its possible importance [29, 30]. In contrast, abnormal expansion of WAT in obesity is closely associated with metabolic diseases. Therefore, it is necessary to understand the function of WAT and BAT from different perspectives. This thesis focuses on the metabolic roles of WAT. The functions of BAT have been reviewed in detail elsewhere [19, 22, 31-34].

## 2. Functional Plasticity of WAT

WAT can undergo dynamic functional changes in response to metabolic stimuli, which are essential for whole-body energy homeostasis [3]. For example, environmental cues such as feeding, fasting, cold exposure, and high calorie intake modulate the metabolic roles and morphological features of WAT [1, 5, 19, 35, 36]. To mediate these functional transitions, the characteristics of the various cell types composing WAT including adipocytes, adipose stem cells (ASCs), immune cells, and vascular cells are altered [37, 38]. Therefore, it is likely that metabolic signals and the responses of cells in WAT are key conductors of WAT plasticity.

### Feeding and Fasting

In many animals, maintaining constant levels of systemic energy is essential for survival. WAT senses and manages systemic energy levels via two opposing path-

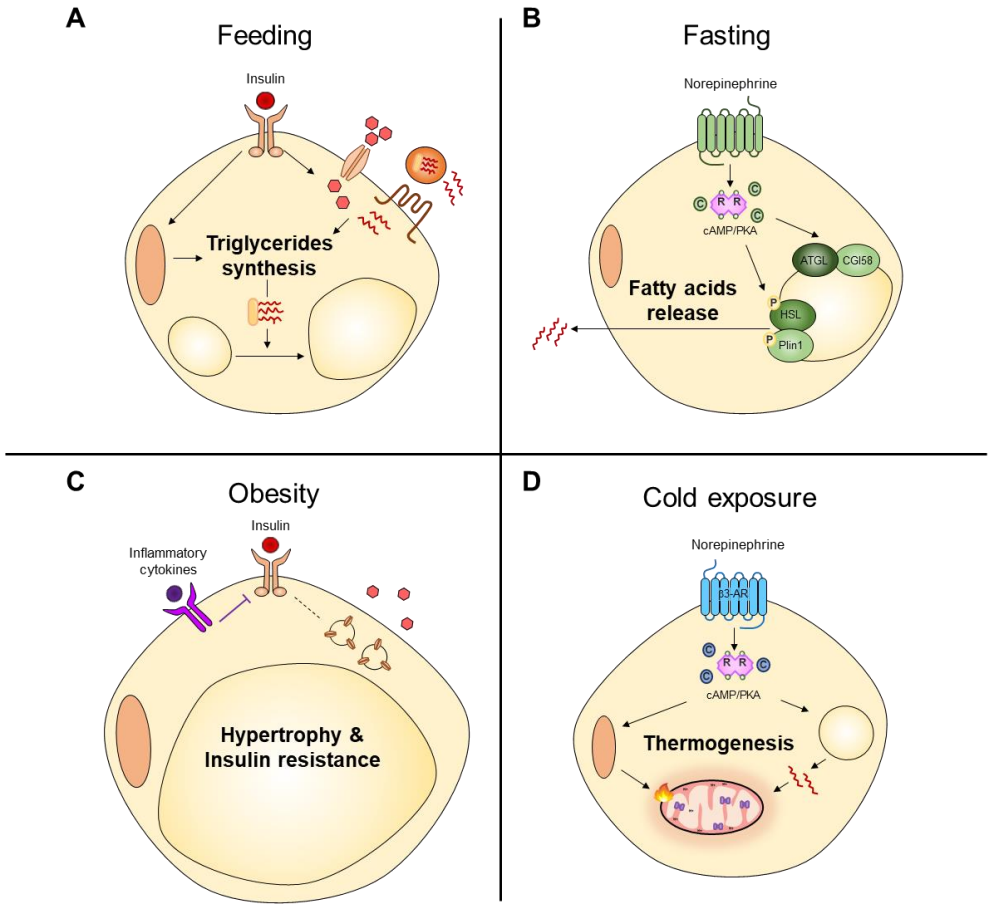


**Figure 2.Functional plasticity of white adipose tissue**

Adipose tissue dynamically changes its properties, including adipocyte number, size, and function, in response to metabolic stimuli. (A) During the fed state, insulin induces adipocytes to uptake excess nutrients, activate lipogenic transcription factors, and store nutrients in the form of triglycerides (B) In the fasted state, PKA signaling induces adipocytes to release fatty acids as fuel for other organs. (C) In obesity, adipocytes become hypertrophic and insulin-resistant. (D) During cold exposure, formation of beige adipocytes mediates heat generation.

ways [5, 35, 36]. Surplus energy states activate the anabolic program in WAT to preserve the excess energy, whereas insufficient energy states activate the catabolic program of WAT to release the stored energy. The anabolic and catabolic pathways in WAT are regulated by different hormones, signaling pathways, and metabolic enzymes [5, 35, 36].

During times of a positive energy balance, such as in the fed state, insulin plays a pivotal role as the key hormone driving the anabolic functions of WAT in several ways (Figure 2A) [39]. Insulin is secreted from beta cells in pancreatic islets in response to elevated blood glucose levels and binds insulin receptors expressed on adipocytes. This binding induces the phosphorylation of the insulin receptor and insulin receptor substrate, activates downstream signaling pathways including AKT and mTOR, and triggers various anabolic programs [39, 40]. Insulin signaling promotes the uptake of glucose and lipids by inducing the translocation of glucose transporter type 4 and fatty acid transporter protein 1 to the plasma membrane and stimulating lipoprotein lipase activity [41-45]. Further, insulin signaling activates several transcription factors involved in lipogenesis, such as sterol regulatory element-binding protein and carbohydrate response element-binding protein, which upregulate lipogenic genes, thereby promoting lipogenesis [46, 47].

In periods of negative energy balance, such as in the fasted state, catecholamines (epinephrine and norepinephrine) are major inducers of catabolic programs in WAT (Figure 2B) [35]. Catecholamines bind to β-adrenoceptors and activate the protein kinase A (PKA) signaling pathway. PKA phosphorylates several targets to mediate lipolysis, the breakdown of triglycerides into fatty acids and glycerol [35, 48]. PKA phosphorylates perilipin 1, the major lipid droplet coating

protein in adipocytes, and facilitates the release of CGI-58 [49, 50]. Released CGI-58 binds to adipose triglyceride lipase and enhances its activity [51]. In addition, PKA phosphorylates hormone-sensitive lipase and increases its activity and translocation onto lipid droplets [52]. Fatty acids and glycerol released from WAT are transported via the circulation and serve as energy sources for other organs.

An imbalance between anabolic and catabolic functions of WAT can induce certain metabolic defects. For example, the deletion of key lipase genes induced expansion of WAT and suppressed the function of other organs, such as muscle, during fasting [53-55]. Selective removal of insulin receptors in adipocytes downregulated amounts of lipids in WAT [56, 57]. Thus, anabolic and catabolic pathways in WAT appear to play complementary roles in maintaining systemic energy levels through opposing functions.

**Obesity**

Chronic energy imbalance resulting from increased energy intake or decreased energy expenditure leads to obesity, which is characterized by excessive adipose tissue accumulation [58]. The obesity epidemic is a global health threat, with more than two billion people worldwide being overweight or obese [59]. Obesity also significantly increases the risk of various metabolic diseases, including non-alcoholic fatty liver disease, cardiovascular disease, and type 2 diabetes [58, 60]. Numerous studies have proposed that obesity-induced adipose tissue remodeling is a causal factor linking obesity and metabolic disease [1, 58].

The most pronounced change in WAT in obesity is an increase in mass. WAT expands in two ways: hypertrophic expansion, which involves an increase in the size

of pre-existing adipocytes, and hyperplastic expansion, which involves the formation of new adipocytes (by adipocyte differentiation of ASC) and an increase in the number of adipocytes. Emerging evidence suggests that hyperplasia contributes to healthy adipose tissue expansion, whereas hypertrophic expansion is associated with detrimental WAT remodeling [61, 62]. It has been proposed that obese patients with small adipocytes often exhibit better metabolic phenotypes than those with large adipocytes [63, 64]. Transgenic mouse models with an increased adipocyte number also show metabolically healthy phenotypes, even in case of severe obesity [65-68]. The formation of new adipocytes through the activation of PPARγ, the master regulator of adipogenesis (differentiation of adipocytes from precursors), induces hyperplastic WAT expansion and improves metabolic phenotypes [69-71]. In contrast, hypertrophic WAT expansion is closely associated with adipose tissue dysfunction. In obesity, hypertrophic adipocytes exhibit insulin resistance, increased basal lipolysis, upregulation of inflammatory genes, and downregulation of lipogenic gene expression (Figure 2C) [72-75]. Thus, the mode of WAT expansion is one of the key factors determining metabolic phenotypes in obesity.

Low-grade, chronic inflammation is one of the key events in obesity-induced adipose tissue remodeling [76-79]. Pioneering studies have shown that TNF-α, a pro-inflammatory cytokine, mediates insulin resistance, and inhibiting TNF-α or its signaling cascade improves insulin sensitivity in animal models [80-84]. In obese animals and human patients, macrophages accumulate in WAT [12, 13]. In particular, pro-inflammatory M1 or M1-like macrophage levels are highly increased in obese adipose tissue and form crown-like structures around dead or stressed adipocytes [85, 86]. Inflammatory cytokines, secreted by M1 macrophages, suppress insulin

signaling through inhibitory phosphorylation of the insulin receptor substrate [87, 88]. The activation of Toll-like receptors by fatty acids, hypoxia, and increased expression of chemokines such as MCP1 is considered as one of the causing factors of obesity-induced adipose tissue inflammation [89-93]. Not only macrophages, but also other immune cells including, T, B, natural killer, and natural killer T cells could regulate adipose tissue inflammation and insulin sensitivity [94-98]. Overall, obesity facilitates the accumulation of pro-inflammatory cells, leading to chronic and low-grade inflammation and insulin resistance [1]. It has been recently reported that immune cells appear to have more diverse roles such as scavenging of dead adipocytes and induction of new adipocyte formation [99-101].

Fibrosis, characterized by the accumulation of excessive collagens and extracellular matrix (ECM) components, is another hallmark of obesity-induced adipose tissue remodeling [102-104]. It has been proposed that fibrosis could contribute to adipose tissue dysfunction. For instance, several mouse models that exhibit decreased levels of WAT fibrosis show improved metabolic phenotypes [105-109]. Mechanistically, a stiffened ECM could impair the expansion capacity and function of adipocytes [110]. As the ECM contains growth factors and signaling molecules, ECM compositional changes could affect various signaling pathways [111]. For example, it has been reported that endotrophin, a cleavage product of collagen type 6, stimulates pro-fibrotic and pro-inflammatory responses [112-114]. In addition, a stiffened ECM could inhibit adipogenesis [108, 115]. Various cell types including ASCs, adipocytes, macrophages, and endothelial cells can secrete and modify ECM components and their abnormal fibrogenic activation might contribute to fibrosis [104, 108, 116, 117].

Obesity-induced WAT remodeling results in the development of metabolic diseases [60]. Obese adipose tissue releases large amounts of fatty acids due to uncontrolled lipolysis, resulting in lipid accumulation in other organs, such as the liver and muscle, deteriorating their function, which is termed “lipotoxicity” and is closely associated with insulin resistance [60, 118, 119]. Further, abnormal adipokine secretion aggravates metabolic phenotypes. For example, serum levels of adiponectin, an insulin-sensitizing hormone, are decreased in obesity [11, 120, 121]. Furthermore, the secretion of inflammatory cytokines, plasminogen activator inhibitor-1, exosomes, and even mitochondria from WAT could be altered in obesity and affect whole-body metabolism [11, 60, 87, 122-125]. Understanding the diverse features of obesity-induced adipose tissue remodeling, including expansion, inflammation, hypoxia, oxidative stress, and fibrosis, would provide promising targets for the development of effective treatment strategies against metabolic diseases [12, 58, 67, 68, 74, 88, 93, 113, 126]

**Cold Exposure**

Temperature, particularly low temperatures in cold environments, is one of the key factors modulating WAT function. In response to acute cold, lipolysis of WAT is induced. Released fatty acids from WAT are used as energy sources for heat generation by other organs [127-129]. BAT and muscle generate heat to block hypothermia through non-shivering and shivering thermogenesis, respectively. Further, during prolonged cold exposure, brown-like adipocytes in WAT, termed beige adipocytes, are generated in certain WAT depots and contribute to heat production (Figure 2D) [22].

Beige adipocyte formation has been suggested to be mediated by two mechanisms: (1) the differentiation of ASCs into beige adipocytes and (2) the thermogenic activation of white adipocytes [32, 130, 131]. Beige adipocytes differentiate from unique precursors that have distinct properties and molecular markers compared to typical white adipocyte precursors [132, 133]. β3-adrenergic receptor activation in white adipocytes mediates thermogenic activation and beige adipocyte formation. The relative contributions of *de novo* beige adipogenesis and thermogenic activation of pre-existing adipocytes vary with stimuli, housing conditions, and fat depots [131, 134]. Therefore, beige adipocytes are likely generated by diverse routes and mechanisms.

Several key signals and transcriptional regulators of beige adipocyte formation have been identified [31, 32]. Sympathetic nerve activity is a key determinant of beige adipocyte formation in WAT [135, 136]. Catecholamines from sympathetic nerves activate PKA signaling and phosphorylate and activate various factors including PGC1-α [137]. PGC1-α and PRDM16 are key transcription cofactors in beige adipocyte formation [19, 22, 138]. These factors facilitate thermogenic gene expression and promote mitochondria biogenesis through modulating other transcription factors such as PPARγ and PPARα [137, 139, 140]. Besides catecholamines, it has been reported that certain secreted factors from immune cells such as type 2 innate lymphoid cells and hormones regulate beige adipocyte differentiation [130, 141-147].

Beige adipocytes could generate heat via various mechanisms. Electron transport through mitochondrial UCP1 appears to be the major mechanism of heat production in beige adipocytes [148]. In addition, it has been proposed that UCP1-

independent mechanisms such as SERCA-mediated calcium cycling, creatine cycling, and TAG-fatty acid cycling could also contribute to thermogenesis [32, 149-153]. However, the detailed molecular mechanism and relative contribution of each pathway in the thermogenesis of beige adipocytes remain to be elucidated.

Under warm conditions, beige adipocytes lose their characteristics and transform into white adipocytes. During this process, mitochondria are degraded by mitophagy and thermogenic gene expression is downregulated [154, 155]. Interestingly, it has been shown that beige adipocytes retain thermogenic memory through epigenetic mechanisms [155, 156]. These dormant beige adipocytes could rapidly reactivate thermogenic programs in response to repetitive cold exposure [131]. Together, these findings highlight the plasticity of WAT in terms of thermogenesis.

## 3. Heterogeneity of WAT

In mammals, WAT is distributed throughout the body and anatomically classified into VAT and SAT. VAT and SAT are further categorized into fat depots, located at specific areas [157]. In humans, omental, mesenteric, perirenal, and retroperitoneal fat depots are examples of VAT, whereas abdominal superficial, gluteal, and femoral fat depots are examples of SAT [1, 157]. In rodents, perigonadal (epididymal fat in males and parametrial fat in females), mesenteric, perirenal, and retroperitoneal fat depots are parts of VAT and suprascapular, anterior, and inguinal fat depots are parts of SAT (Figure 1) [21, 157]. Among them, epididymal adipose tissue (EAT) and inguinal adipose tissue (IAT) are representative models of VAT and SAT, respectively. However, as humans lack perigonadal adipose tissue such as EAT, extrapolating

research findings in rodents to humans requires cautious interpretation.

**Distinct Properties of VAT and SAT**

In the basal state, VAT and SAT are morphologically similar. Therefore, it has been assumed that VAT and SAT share common functions. However, accumulating evidence shows that VAT and SAT not only differ in their locations but also play unique roles [157, 158]. Epidemiological research in humans has shed light on the differences between VAT and SAT. Measurements of the distribution of VAT and SAT based on the waist-to-hip ratio or computed tomography imaging have shown that VAT and SAT have different relationships with metabolic parameters. Individuals with excess VAT (termed visceral obesity) exhibit worsened metabolic phenotypes and an increased incidence of metabolic diseases when compared with individuals with a similar body mass index but low VAT levels [159-164]. The notion that VAT and SAT would have distinct roles in obesity-associated complications has been further strengthened. For example, treatment of thiazolidinediones, PPARγ agonist and anti-diabetic drugs, induces a shift in fat distribution from VAT to SAT [70, 165, 166]. Several mouse models of obesity that have a high proportion of SAT, exhibit metabolically healthy phenotypes [66, 68, 166-168]. These results indicate that VAT and SAT have distinct metabolic functions.

VAT and SAT may play distinct metabolic roles according to their anatomical locations. VAT is located close to internal organs such as the liver and gut and communicates with them [169-174]. In contrast, SAT protects and insulates the body from physical stress and cold [175]. The differences between VAT and SAT appear to be more obvious in response to various stimuli including feeding, fasting,

cold exposure, and an obesogenic diet [176]. It has been reported that VAT and SAT exhibit different profiles of adipokine secretion and fatty acid release during feeding and fasting [160, 177-180].

In obesity-induced adipose tissue remodeling, VAT and SAT show remarkable differences in expansion, adipogenesis, inflammation, and fibrosis. As described above, hyperplasia facilitates the healthy expansion of adipose tissue as compared to hypertrophy. It has been speculated that SAT might preferentially expand through hyperplasia, whereas VAT might expand through hypertrophy. In metabolically healthy obese models, SAT is greatly expanded but displays hyperplastic features, with small and numerous adipocytes [66, 68, 167]. In addition, preadipocytes from SAT show higher *in vitro* adipogenic potential than preadipocytes from VAT [181-184]. However, several mouse model studies have reported contradictory outcomes. In high-fat diet (HFD)-induced obesity, *de novo* adipogenesis is preferentially stimulated in EAT, not in IAT [134, 185]. It seems that the hyperplastic potential of VAT and SAT appears to vary according to the genetic background and variation, sex, and age [186-190]. For example, IAT in female mice exhibits a higher capacity of HFD-induced adipogenesis compared to IAT in male mice [186]. Further studies in various experimental models and settings are required to clarify the differences in adipogenesis between VAT and SAT.

Inflammation and fibrosis in response to obesogenic stimuli also noticeably differ between VAT and SAT. In obesity, VAT often exhibits an elevated inflammatory response, characterized by the accumulation of immune cells and formation of CLS, whereas SAT maintains a relatively low degree of inflammation [12, 191-193]. Additionally, obesity induces high levels of fibrosis and aberrant

ECM accumulation in VAT but not SAT, at least in mouse models [108]. Therefore, obesity-induced inflammation and fibrosis appear to participate in fat-depot specific characters in obesity and metabolic complications [176].

VAT and SAT also show different features in response to a cold environment. In mice, beige adipocyte formation in response to cold exposure primarily occurs in IAT, not EAT [21, 132, 134]. It has been reported that ablation of PRDM16, a key transcription cofactor in beige adipocyte formation, induces phenotypic switch from IAT to EAT, including decreased expression of thermogenic genes and increased obesity-induced inflammatory responses. These results indicate that thermogenesis is key difference between EAT and IAT [140]. In humans, VAT exhibits a higher degree of thermogenic gene expressions than SAT. Therefore, species differences in the thermogenic features of VAT and SAT require further investigation [194].

**Mechanisms Underlying Fat Depot Differences**

Tremendous efforts have been made to elucidate the mechanisms underlying the differences between VAT and SAT. Initially, the distinct anatomical locations of VAT and SAT received attention. VAT is connected to the liver through the portal veins. Therefore, free fatty acids and cytokines derived from VAT could have a significant effect on the liver, a concept known as “the portal theory” [169-171]. Furthermore, VAT and SAT not only differ in their locations but also have unique intrinsic characteristics [157, 176]. Tran *et al*. investigated the cause of differences between VAT and SAT using fat transplantation [195]. They transplanted VAT and SAT into both visceral and subcutaneous regions and examined metabolic phenotypes in mice. Interestingly, transplanted VAT did not improve metabolic parameters regardless of

location, whereas transplanted SAT did. Moreover, the beneficial effects of SAT transplantation were more robust when transplanted in the visceral region than when transplanted in the subcutaneous region. These findings suggest that VAT and SAT are intrinsically different. Other studies using fat transplantation have supported this notion and revealed distinct intrinsic properties of VAT and SAT [193, 196-200].

To identify the intrinsic factors of VAT and SAT, many groups have comparatively analyzed their transcription profiles and revealed unique expression patterns of developmental marker genes [158, 201-204]. Also, studies using lineage tracing models reported distinct developmental origins of VAT and SAT. For example, EAT develops from the $Wt1^{+}$ $Prrx1^{-}$ lineage between postnatal days 7 and day 28, whereas IAT develops from the $Prrx1^{+}$ $Wt1^{-}$ lineage between embryonic days 14 and 18. [134, 205-207]. These results suggest that intrinsic factors from different precursors would mediate the differences between VAT and SAT.

Given that VAT and SAT appear to have distinct developmental origins, it has been suggested that ASCs and adipocytes differentiated from unique ASCs would mediate fat depot-specific features. Several studies that compared adipocytes and ASCs from different fat depots support this hypothesis [176, 184]. For instance, adipocytes derived from VAT and SAT ASCs differ in functions such as lipolysis, adipokine secretion, and thermogenesis [132, 181, 183, 184, 208]. In addition, ASCs from VAT and SAT exhibit differences in adipogenic potential and inflammatory properties [181, 182, 193, 209, 210]. Furthermore, VAT and SAT-specific factors that could mediate the different functions of the two fat depots have been reported [211-226]. Collectively, these findings suggest that intrinsic developmental features could contribute to the differences between VAT and SAT.

# II. ASCs

Compared to other organs, WAT shows high plasticity and heterogeneity. Adipocytes and various cell types including immune cells, vascular cells, and ASCs play essential roles in the unique functions of WAT. Several clues have highlighted the importance of ASCs in the plasticity and heterogeneity of WAT [3, 227]. ASCs contribute to adipose tissue plasticity by forming new adipocytes and secreting various cytokines and ECM components [3, 227-229]. Additionally, because VAT and SAT comprise ASCs of different origins, it is plausible that ASCs are involved in adipose tissue heterogeneity. Figure 3 graphically summarizes the various functions of ASCs in WAT based on recent studies [61, 230-235].

## 1. Characteristics and Nomenclature of ASCs

Anatomical observations of adipose tissue have raised questions regarding the origin of adipocytes [227, 236]. It has been suggested that fibroblast or fibroblast-like cells would differentiate into adipocytes because adipose tissue is a type of loose connective tissue. The establishment of a highly adipogenic 3T3-L1 subclonal cell line derived from 3T3 mouse embryonic fibroblasts supported this idea [237, 238]. In addition, it has been suggested that perivascular cells could differentiate into adipocytes because the development of adipose tissue and angiogenesis appear to be spatially and temporally linked [207, 239]. Although certain plate-adherent cells extracted from WAT have shown high adipogenic potential, precise markers and tissue location of these cells had not been identified [230, 240].

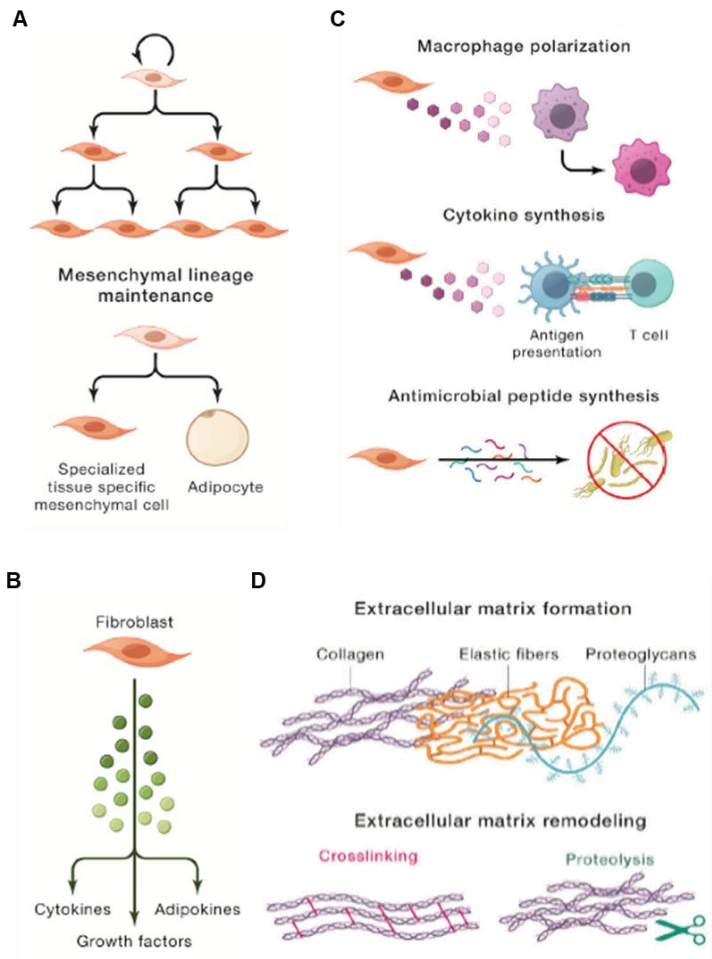


**Figure 3. Characteristics and functions of ASCs**

ASCs maintain their number by proliferation and differentiate into adipocyte (A), secrete various cytokines and growh factors (B), regulate immune cell functions (C), and synthesize, degrade, modify ECM (D). The images are modified from Plikus, M. V., *et al*. (2021). "Fibroblasts: Origins, definitions, and functions in health and disease." Cell 184(15): 3852-3872.

Two studies identified ASCs in WAT using different approaches. Rodeheffer *et al*. reported that ASCs are not immune cells ($CD45^+$) or endothelial cells ($CD31^+$), but fibroblast-like cells expressing markers such as CD29, CD34, and Sca1 [241]. Tang *et al*. demonstrated that ASCs express PDGFRβ and reside in the mural cell compartment of the adipose tissue vasculature [242]. In addition, it has been suggested that PDGFRα, Pref-1 (Dlk1), and ZFP423 would be ASC markers [243-247]. The key characteristics of ASCs are self-renewal and the capacity to differentiate into adipocytes when exposed to appropriate stimuli. However, not all ASCs equally possess these proliferation and differentiation capacities. For example, it has been shown that transplantation of $CD24^+$ ASCs, which are rare, induces the formation of normal-sized adipose tissue when transplanted into lipodystrophy A-ZIP mice [241, 244, 248]. In contrast, $CD24^-$ ASCs could not form normal-sized fat pads, although they could divide and differentiate into adipocytes *in vitro* [241, 244]. Furthermore, the division rate and adipogenic potential of ASCs appear to vary based on markers such as Pref-1, DPP4, and ICAM1 [246, 247, 249].

Because of the heterogeneity, defining an appropriate term for ASCs has been a complex and ambiguous problem. Despite the numerous studies on ASCs, more research and discussions are required to define these cell types [231, 250]. Nevertheless, it is likely that ASCs are not endothelial or hematopoietic cells [244, 250]. Moreover, several studies have shown that ASCs are not smooth muscle cells, pericytes, and mesothelial cells [133, 250-255]. Various terms, including stem cell, progenitor, precursor, preadipocyte, stromal cell, and fibroblast have been used to define these cells, each having its advantages and limitations [227-229, 250, 256-258]. Establishing a suitable term will require a deepening of our understanding of

ASCs. In this thesis, the term “adipose stem cell” (“ASC”) is used to emphasize that at least some of these cells can differentiate into several mesenchymal lineage cells such as adipocytes and osteoblasts with different intrinsic characteristics depending on their developmental origins.

## 2. Developmental Origins of ASCs

The major role of ASCs is to form functional fat cells, particularly during development. Although adipocytes and ASCs originate from the mesoderm, the developmental origin of adipose tissue and ASCs varies among fat depots [234]. For example, WAT and BAT have distinct developmental origins. BAT is derived from the $Myf5^{+}$ lineage, indicating that BAT has a closer lineage relationship to muscle than WAT [22, 138, 158]. Recent single-cell RNA-seq (scRNA-seq) studies have revealed the detailed developmental hierarchy of BAT, from the dermomyotome to brown adipocytes [259, 260].

WAT is developmentally derived from the mesoderm [211, 261]. As discussed above, VAT and SAT have different developmental origins [205, 206, 234, 261]. Sebo *et al*. reported a mesodermal fat map of certain VAT and SAT depots [261]. They combined three markers to establish the WAT lineage: Pax7 for the central dermomyotome, Meox1 for the somitic mesoderm, and HoxB6 for the posterior lateral plate mesoderm. Based on their findings, they suggested that IAT originates from the somatic region of the posterior lateral plate mesoderm whereas a significant proportion of EAT originates from the somitic mesoderm [234, 261]. Further, they proposed that each VAT and SAT depot might differ in developmental origin [234, 261]. Therefore, it is plausible that each VAT and SAT depot might harbor ASCs of

different lineages. Although the WAT lineages have not been fully characterized, analysis of scRNA-seq or spatial-sequencing data from developing mice would facilitate developmental mapping of various fat depots composing VAT and SAT [259, 260, 262, 263].

## 3. Functions of ASCs: Adipogenesis

Adipogenesis is a differentiation process of ASCs into mature adipocytes [61, 264, 265]. Adipogenesis is largely divided into two steps. In the first step, ASCs lose the multipotent differentiation potential of mesenchymal lineage cells and committed preadipocytes. In the second step, preadipocytes terminally differentiate into adipocytes. [230]. Studies using adipogenic cell lines such as 3T3-L1 and mouse models have unraveled numerous signaling pathways, transcriptional rewiring, and epigenetic regulatory mechanisms that control adipogenesis [266]. In addition, lineage tracing studies of adipocytes and ASCs have shown the activation of adipogenesis in response to certain metabolic stimuli [134]. These studies have revealed the roles and regulatory mechanisms of the differentiation of ASCs into adipocytes.

Adipogenesis occurs in various conditions including development, obesogenic diet intake, cold exposure, and even the basal state. During developmental periods, adipogenesis occurs actively to generate adipose tissue [207, 267, 268]. In the basal state, adipogenesis continuously occurs to compensate for adipocyte death [269, 270]. In adults, metabolic stimuli such as HFD feeding or cold exposure facilitate the differentiation of ASCs into new adipocytes [61, 62]. Studies using HFD-induced obesity models have suggested that obesity could trigger the

generation of new adipocytes [134, 185, 270, 271]. Also, cold exposure or treatment of cold-mimicking compounds such as CL-316,243, a β3-adrenergic receptor agonist, could induce beige adipocyte differentiation of ASCs [131, 134, 243, 271-273].

Adipogenesis of ASCs is governed by diverse factors. The commitment step to preadipocytes is regulated by signaling molecules such as WNT, BMP, and TGFβ [116, 249, 274-280]. Canonical WNT signaling inhibits adipogenesis, whereas TGFβ and BMP play complex roles. These signaling factors can be secreted from various cell types, including adipocytes, immune cells, and ASCs [281-287]. Studies using adipogenic cell lines have suggested that at least two waves of transcription factor activation occur during adipogenesis [266]. In the first wave, transcription factors such as C/EBPβ and C/EBPδ are activated and upregulate target genes that mediate the second wave [187, 288-292]. In the second wave, C/EBPα, PPARγ, and SREBP1c are activated, upregulate each other, induce lipogenesis, and form mature adipocytes [293-299]. Among them, PPARγ is known as the master regulator of adipogenesis [266, 298]. The coordinated action of these factors determines the adipogenic capacity of ASCs [61, 265].

Adipogenesis has an essential role in the maintenance and plasticity of adipose tissue. It seems that continuous adipocyte differentiation of ASCs is required to maintain adipocyte numbers [269, 270]. Also, obesity-induced adipogenesis could replace dead adipocytes and mediate hyperplastic expansion of WAT [71, 100]. Further, beige adipogenesis upon cold exposure mediates heat generation [145]. In line with this, inhibiting the adipogenic capacity of ASCs declines metabolic functions of adipose tissue, implying the importance of adipogenesis [71, 145].

## 4. Functions of ASCs: Inflammation and Fibrosis

Inflammation and fibrosis are key features of pathological WAT expansion. ASCs can modulate these processes by secreting various factors. It has been reported that ASCs contribute to the production of certain cytokines, modulate immune cell function, and produce a significant portion of adipose tissue ECM components [108, 115, 227, 228, 300-307].

ASCs interact with diverse immune cells and could play both pro-inflammatory and anti-inflammatory roles. ASCs regulate monocyte infiltration by expressing chemokines such as CCL2 and macrophage polarization by expressing cytokines such as IL6 [115, 307-309]. In addition, ASCs are a major source of IL33 in WAT. ASC-derived IL33 regulates the migration, survival, and activity of regulatory T cells and type 2 innate lymphoid cells. [94, 141, 142, 144, 303-305, 310-315]. Thus, ASCs would regulate the numbers and activity of certain types of immune cells.

Besides these immune cell regulation, ASCs could play a pivotal role in adipose tissue fibrosis. ASCs highly express type I and III collagens and fibronectin compared to other cells, such as adipocytes, macrophages, and endothelial cells [108]. Moreover, ASCs could acquire characteristics of myofibroblasts which are scar-forming cells that exist in fibrotic regions [108, 115, 117, 316, 317]. In particular, $CD9^+$ $PDGFR\alpha^+$ cells exhibit a higher fibrogenic capacity than $CD9^-$ compartments which have high adipogenic potential [108, 115]. Myofibroblasts produce aberrant amounts of ECM components, form scar-like regions, and act as key effector cells in fibrosis [316, 318]. These findings suggest that fibrogenic ASC activation might be a key event in the onset of WAT fibrosis.

The immunomodulatory and fibrogenic roles of ASCs vary depending on the fat depot and conditions [176, 227]. It has been reported that IAT ASCs, but not EAT ASCs, suppress obesity-induced macrophage accumulation in response to gamma-aminobutyric acid [193]. Obesogenic stimuli could induce fibrotic features of ASCs via PDGF signaling activation [108, 317, 318]. In addition, it has been suggested that immune cells would induce the formation of fibrogenic ASCs [105, 319]. However, the fat depot- and condition-specific roles of ASCs in inflammation and fibrosis are not completely understood.

## 5. Heterogeneity of ASCs

ASCs are involved in various aspects of adipose tissue remodeling including white and beige adipogenesis, local immune responses, and ECM production. These functions are likely not shared equally among different ASC types. Instead, ASCs are composed of heterogeneous subpopulations that could perform specialized functions. [108, 132, 241, 244, 320]. The application of scRNA-seq has greatly enhanced our understanding of the heterogeneity, subpopulations, and functions of ASCs (Table 1) [3, 38, 227, 231].

Different ASC subpopulations have different adipogenic potential [241, 244, 245, 247]. Recent studies using scRNA-seq have revealed the heterogeneity of ASCs [227, 231]. It has been suggested that IAT ASCs can be divided into $DPP4^+$ ASCs with low adipogenic capacity and $ICAM1^+$ ASCs with high adipogenic capacity [249]. Similarly, EAT ASCs could be categorized into low adipogenic cells termed fibro-inflammatory progenitors (FIPs) and high adipogenic cells termed adipocyte precursor cells (APCs) [115]. Collectively, these findings propose that

ASCs are composed of subpopulations with different adipogenic potential.

Secretory functions of cytokines and ECM components might also differ among ASC subpopulations. It has been reported that some ASC clusters can suppress the adipogenesis of other ASCs by secreting certain factors [321, 322]. Further, it has been suggested that FIPs secrete higher amounts of pro-inflammatory cytokines and collagens than APCs [115]. Further, ASC subsets that highly express IL33 have been reported [323]. Thus, ASC subpopulations appear to have unique secretory profiles and play different roles in the regulation of inflammation and fibrosis.

Many ASC subpopulations have been recently discovered and the underlying mechanisms of ASC heterogeneity are not fully understood. It has been suggested that TGFβ signaling and NR4A nuclear receptors could participate in the low-adipogenic properties of $DPP4^+$ ASCs and FIPs, respectively [115, 249]. However, the signaling pathways and transcription factors that regulate ASC heterogeneity require further research.

Table 1. Heterogeneity, subpopulations, and markers of ASC

| Sample | Technique | Markers | Major Findings | Ref |
|---|---|---|---|---|
| SVFs from subcutaneous and parametrial WAT | FACS | CD29 CD34 SCA1 CD24 | Identification of white adipocyte precursor *in vivo* | [241, 244] |
| Inguinal and retroperitoneal WAT | PPARγ tracing mice | PPARγ PDGFRβ | Adipocyte progenitors reside in the mural cell compartment of the adipose vasculature, | [242] |
| BAT, IAT, and EAT | Clonal cell | Tmem26, CD137, Tbx1 | Identification of beige adipocyte precursor | [132] |
| BAT, IAT, and EAT in cold-exposed and HFD-fed condition | PDGFRα tracing mice | PDGFRα | PDGFRα cells contribute to both beige and white adipogenesis | [243] |
| IAT and EAT | FACS and Zfp423 tracing mice | PDGFRβ Zfp423 | $Zfp423^+$ cells exhibit high adipogenic potential compare to $Zfp423^-$ cells | [245] |
| IAT and EAT | FACS and Pref-1 tracing mice | Pref-1 (Dlk1) | Pref-1 marks very early mesenchymal precursors | [247] |
| BAT, IAT and EAT | TRAP and Myh11 tracing mice | Myh11, Acta2, Tagln | Beige adipocytes have unique smooth-muscle like origin | [133] |
| IAT and EAT in NCD- and HFD-fed mice | FACS | CD9 | $CD9^+$ $PDGFR\alpha^+$ cells are fibrogenic, low-adipogenic cells | [108] |
| $Lin^-$ cells from IAT and EAT in control and CL-treated mice | scRNA-seq | Pi16, Dpp4, Icam1, Col4a2 | CL specifically induce beige adipogenesis in EAT but not in IAT | [273] |
| $PDGFR\beta^+$ cells from EAT | scRNA-seq | PDGFRβ LY6C, CD9 | $LY6C^-$ $CD9^-$ $PDGFR\beta^+$ cells: adipocyte precursor cells (‘APCs’) $LY6C^+$ $PDGFR\beta^+$ cells: fibro-inflammatory progenitors (‘FIPs’). | [115] |
| $Lin^-$ cells from IAT | scRNA-seq | CD142 | $CD142^+$ adipogenesis-regulatory cells can suppress adipogenesis | [321] |
| Human visceral and subcutaneous fat | FACS | MSCA1, CD271 | $MSCA1^+$ adipogenic subset enriched in stroma $MSCA1^-$ less adipogenic subset enriched in septa | [324] |
| Peri-vascular adipose tissue | scRNA-seq | CD36, TGFbr2 | PV-ADSCs participate in vascular remodeling *in vivo* notably through SMC differentiation. | [325] |
| IAT and EAT | Clonal cell | Wt1, Tagln, Mx1 | Investigate functional heterogeneity of white adipocytes within a single fat depot | [326] |
| $Lin^-$ cells from IAT | scRNA-seq | DPP4, ICAM1 | Identification of hierarchy of ASCs | [249] |
| Human subcutaneous fat | Clonal cell | | Identification of diverse subtypes of ASC and adipocyte | [320] |
| IAT SVFs from control and CL-treated mice | scRNA-seq | | Identification of ASC clusters (APC 1~4) | [327] |
| $PDGFR\alpha^+$ $Sca\text{-}1^+$ cells from EAT, lymph node, and muscle | scRNA-seq | Thy1, CD55, PPARγ | Identified the major IL-33 producingmesenchymal stromal cell subtypes | [313] |

| | | | | |
|---|---|---|---|---|
| IAT and EAT | Lineage tracing mice | PDGFRα, Tle2, Tbx18 | Mural and endothelial cells have no significant adipogenic potential | [252] |
| BAT, IAT, and EAT | scRNA-seq | CD81 | CD81 controls proliferation of beige fat progenitor cell | [145] |
| Human SAT and VAT | scRNA-seq | CFD, MSLN, etc | VAT and SAT contains distinct progenitors (SP1~5 in SAT, VP1~6 in VAT) | [328] |
| Bone marrow | scRNA-seq | Adipoq | Identified cell type that expresses adipocyte markers but contains no lipid droplets, termed marrow adipogenic lineage precursors (MALPs) | [329] |
| Perivasular adipsoe tissue | scRNA-seq | PDGFRα, Ly6a, Myh11 | Identified adipogenic smooth muscle cells that contribute to perivascular adipocyte formation. | [254] |
| BAT | scRNA-seq | Trpv1 | $Trpv1^+$ vascular smooth muscle cells are previously unidentified thermogenic adipocyte progenitors | [255] |
| Across 17 tissues including adipose tissue | scRNA-seq | Dpt, Pi16, Col15a1 | Identified Universal fibroblast subpopulation ($Dpt^+$ cluster composed of $Pi16^+$ cluster and $Col15a1^+$ cluster) and specialized fibroblast subtypes | [257] |
| Muscle from diabetic and non-diabetic patients | scRNA-seq | CD34, CD90 | $CD90^+$ fibro-adipogenic progenitors have high proliferative activity, clonogenicity, and production of ECM | [330] |
| IAT from young and aged mice | scRNA-seq | Lgals3, CD36, Pu.1 | Identification of aging-dependent regulatory cell (ARC) | [322] |
| EAT from NCD- and HFD-fed mice | snRNA-seq | | FAP1~4 clustering, FAP2, which highly express Pparg and Lpl, is increased in obesity | [75] |
| SAT from lean and obese humans | scRNA-seq | DKK1, Pi16, CXCL14, GPC3 | APCs are positively correlated with BMI whereas pADs has a negative correlation | [331] |
| Lin- cells from BAT in RT and Cold-exposed mice | scRNA-seq | Col5a3, Pi16, Gdf10 | Identify three ASC subpopulation with distinct tissue location and adipogenci potential | [332] |
| IAT and EAT in NCD and HFD-fed mice and VAT and SAT from human | snRNA-seq and scRNA-seq | | provide cellular atlases of human and mouse SAT and VAT at single-cell resolution across a range of body weight | [250] |
| EAT in adult and pup | scRNA-seq | Ly6c, CD9 | Identified distinct properties of perinatal and adults ASCs | [268] |
| Various fats in human | scRNA-seq and snRNA-seq | | Investigated commitment, cell-cell interaction, and location of ASCs | [333] |
| Developing BAT | scRNA-seq | GATA6 | Identified of embryonic brown fat progenitors and importance of GATA6 | [259, 260] |
| Various fats in humans | scRNA-seq | | Identify Wnt-regulated adipose tissue-resident (SWAT) cells. | [334, 335] |

# III. Purpose of This Study

Recent studies have greatly enhanced our understanding of the markers, heterogeneity, and functions of ASCs in WAT. However, the roles and features of ASCs have not been fully explored. For instance, while ASCs in VAT and SAT exhibit distinct gene expression and characteristics, their heterogeneity has not been comparatively explored. Furthermore, the responses of ASC subpopulations to metabolic stimuli, including alterations in cell state or subtype, remain largely unknown. In addition, intrinsic and environmental factors that determine the heterogeneity of ASCs have not been thoroughly examined.

In this thesis, I aimed to identify fat-depot specific ASC subpopulations, their roles, and their responses to metabolic stimuli. In addition, I investigated the intrinsic and extrinsic factors that mediate the formation of ASC subpopulations. In Chapter I, I comparatively analyzed white and beige adipogenesis in EAT and IAT with fat depot-specific ASC clusters. Through this, I elucidated the underlying mechanisms of HFD-induced adipogenesis in EAT and beige adipogenesis in IAT. In Chapter II, I discussed obese EAT-specific pro-inflammatory and fibrotic $SDC1^+$ ASCs and IAT-specific anti-inflammatory $CXCL14^+$ ASCs. Taken together, this study provided a comprehensive map of ASC clusters in EAT and IAT and proposed the potential roles of the different ASC clusters to clarify the distinct features of EAT and IAT.

# CHAPTER ONE:

# Comparative Analysis of White and Beige Adipogenesis in VAT and SAT

# 1. Abstract

In mammals, white adipose tissues are largely divided into VAT such as EAT and SAT such as IAT with distinct metabolic properties. Although emerging evidence suggests that subpopulations of ASC would be important to explain fat depot differences, ASCs of two fat depots have not been comparatively investigated. Here, I characterized heterogeneous ASCs and examined the effects of intrinsic and tissue micro-environmental factors on distinct ASC features. I demonstrated that ASC subpopulations in EAT and IAT were divided into three adipogenic stages with different molecular features. The majority of EAT ASCs were stage 2 and 3 with high adipogenic potential, while IAT ASCs were mostly stage 1 cells with low adipogenic potential. Furthermore, ASC transplantation experiments revealed that intrinsic ASC features primarily determined their adipogenic potential. Upon obesogenic stimuli, secreted factors from EAT adipocytes induced the proliferation of ASCs and stimulated adipogenesis. On the other hand, IAT-specific $BST2^{high}$ ASCs exhibited a high potential to differentiate into beige adipocytes. Together, these data propose that distinct properties of ASC subpopulation would regulate white and beige adipogenesis in a fat depot-specific manner.

# 2. Introduction

Adipose tissues store excess energy and secrete various adipokines and lipid metabolites to regulate systemic energy homeostasis [336, 337]. In mammals, adipose tissues are largely divided into WAT, which is specialized in energy storage, and BAT, which produces heat to maintain body temperature. WATs are anatomically categorized into two major fat depots, VAT and SAT. In mice, EAT and IAT are representative models of VAT and SAT, respectively.

EAT and IAT differ in their developmental origin, anatomical location, and response to metabolic stimuli [157, 176]. EAT arises postnatally from *Wt1*$^{+}$ and *Pax3*$^{+}$ lineages, whereas IAT arises embryonically from the *Prrx1*$^{+}$ lineage [205, 206]. EAT interacts with intra-abdominal organs, such as the gut, whereas IAT protects the body from physical stress and cold environments [157, 158]. Furthermore, EAT and IAT exhibit different features in response to metabolic stimuli. At the onset of obesity, EAT expands rapidly by increasing adipocyte size (hypertrophy) and *de novo* adipogenesis (hyperplasia), whereas IAT expansion mainly depends on adipocyte hypertrophy in mice [134, 185]. Moreover, upon exposure to cold stimuli, thermogenic beige adipocytes are produced in IAT, but not in EAT [134].

Accumulating evidence suggests that distinct properties of ASCs would mediate different characteristics of EAT and IAT. For instance, studies using adipocytes derived from EAT or IAT ASCs have shown that these cells functionally differ in lipolysis, adipogenic potential, and thermogenic activity [132, 184]. In obesity, ASC proliferation and *de novo* adipogenesis are enhanced selectively in EAT [134, 185]. Upon cold exposure, CD81-expressing ASCs in IAT can differentiate into

thermogenic beige adipocytes [145].

Recently developed single-cell RNA sequencing analysis is able to deconstruct heterogeneous subpopulations, to provide molecular markers, and to project potential differentiation trajectories [338-340]. With these advantages, scRNA-seq analysis has been adopted to identify adipogenic lineage and markers to deconstruct ASC heterogeneity. [75, 115, 145, 231, 249, 273, 321, 325, 327, 328]. Nonetheless, as the heterogeneity and hierarchy of ASC in EAT and IAT have not been comparatively explored in a side-by-side manner, fat depot-specific ASC clusters and their properties in adipogenesis are incompletely understood.

In this study, I employed scRNA-seq analysis to comparatively characterize heterogeneous ASCs in EAT and IAT from lean and obese mice. I found that fat depot-specific ASC clusters are important for the regulation of white and beige adipocyte biogenesis. In addition, I investigated how metabolic stimuli, such as HFD feeding and cold exposure, could alter ASC subpopulations that regulate depot-selective *de novo* adipogenesis. Further, I examined whether intrinsic or tissue micro-environmental factors would drive the distinct features of fat depot-specific ASC clusters using ASC transplantation and lymph node (LN) dissection experiments. Together, this study provides a comprehensive map of ASC clusters in EAT and IAT, presenting the clues to explain key features of EAT and IAT upon metabolic stimuli.

# 3. Materials and Methods

### Animals

Eight-to-ten-week-old C57BL/6 mice were purchased from Central Lab Animal Incorporation (Seoul, Korea). $GFP^+$ transgenic (Tg) mice were generously gifted by Gou Young Koh (KAIST, Daejeon, South Korea). The mice were housed in a specific pathogen-free, temperature- and humidity-controlled animal facility at 22 °C under a 12-h/12-h light/dark cycle. High-fat diet feeding experiments were performed using 8-week-old mice fed a diet consisting of 60% calories from fat (D12492, Research Diets). BrdU (559619, BD Biosciences) was administered in the drinking water at 0.8 mg/ml for one week. The animal study was approved by the Institutional Animal Care and Use Committee of the Seoul National University.

### Human Subjects

Human adipose tissue samples were obtained during weight reduction laparoscopic bypass surgery at the Metabolic Surgery Center in Seoul National University Bundang Hospital (SNUBH). This study was conducted in accordance with the Declaration of Helsinki and was approved by the Ethics Committee of the SNUBH (IRB No. B-1801445301 & B-1812513302). All subjects agreed to provide their written informed consent. Tissue samples consisted of 25-mg tissue blocks. The tissues were processed within 3 hours of removal from the patients.

### scRNA-seq Library Preparation

scRNA-seq libraries were generated using the Chromium Single Cell 3' Library & Gel Bead Kit (PN-1000092, 10X Genomics), Chromium Single Cell B Chip kit (PN-

1000074, 10X Genomics), and Chromium i7 Multiplex Kit (PN-120262, 10X Genomics). Cells were resuspended in reverse transcription enzyme mix and loaded onto the Chromium Single Cell B Chip to generate gel beads-in-emulsion of 6,000 cells per channel. Reverse transcription was performed using a Bio-Rad C1000 Thermal Cycler. cDNA purification and library generation were performed according to the manufacturer's instructions. Libraries were sequenced on an Illumina NovaSeq 6000 instrument (paired-end 100-bp reads), with an average of 50,000 read pairs per cell.

**scRNA-seq Data Processing**

Raw reads were mapped to a mouse reference genome (GRCm38) using the Ensembl GRCm38.95 GTF file and the Cell Ranger software (v3.0.2). For each sample, a gene-by-cell count matrix was generated with default parameters, except for expected cells = 6000. Using the emptyDrops function of the DropletUtils (v1.6.1) R package (Lun et al., 2019) with a false discovery rate (FDR) < 0.01, empty droplets were removed. To filter out low-quality cells, cells with >5% (EAT NCD, EAT 10-week HFD, and IAT NCD) or >3% (EAT 2-week HFD, IAT 2-week HFD, IAT 10-week HFD) of unique molecular identifiers (UMIs) assigned to mitochondrial genes, <1,000 total UMI counts, or <1,000 detected genes were excluded using the calculateQCMetrics function of the scater (v1.14.6) R package (McCarthy et al., 2017). To normalize cell-specific biases, cells were clustered using the quickCluster function of the scran (v1.14.6) R package (Lun et al., 2016). Then, cell-level size factors were calculated using the computeSumFactors function of the same package. Raw UMI counts were normalized by size factors and then log2-transformed with a

pseudocount of 1. Highly variable genes (HVGs) were identified using the modelGeneVar function of the scran package, with FDR < 0.05 for biological variability. All cells across the fat depot and diet conditions were clustered into 17 clusters using the FindClusters function of the Seurat (v3.2.3) R package (Stuart et al., 2019) on the first 15 principal components (PCs) of HVGs with resolution = 0.8. Cells were visualized in a two-dimensional UMAP plot using the RunUMAP function of the same package. Two clusters (clusters 14 and 16) annotated as immune cells and mesothelial cells were removed. Cells from EAT samples were further clustered using the method described above with the top 10 PCs. Cluster 12, annotated as testis cells, was removed. All remaining cells were visualized in the UMAP plot from the top 15 PCs. Cells in the normal chow diet were grouped into 11 clusters and visualized in the UMAP plot using the above method, with the top 25 PCs of 1,000 HVGs.

**scRNA-seq Data Analysis**

Stage-specific marker genes were identified using the FindAllMarkers function of the Seurat package, with default parameters. Pseudotime analysis was performed for each condition using the run_palantir function of the Palantir (v0.2.6) python package (Setty et al., 2019). For Palantir t-SNE plots in EAT or IAT NCD, diffusion components (DCs) were computed using the run_diffusion_maps function with the first 200 PCs for EAT NCD and the first 100 PCs for IAT NCD. Then, a k-nearest neighbor (k-NN) graph (k = 30) was constructed from the first 10 DCs. The coordinates for the t-SNE plots were computed using the run_tsne function with perplexity = 300 (for EAT NCD) or 200 (for IAT NCD). Gene ontology analysis

was performed using the runTest function of the topGO (v2.38.1) R package. To project EAT NCD cells onto IAT NCD cells, k-NNs (k = 10) of each EAT NCD cell were obtained from IAT NCD cells with respect to the Pearson correlation coefficients of normalized expression profiles of HVGs between EAT and IAT NCD cells, by applying the knn.index.dist function of the KernelKnn (v 1.0.8) R package. For every EAT NCD cell, two-dimensional coordinates of 10-NNs in the t-SNE plot of IAT NCD cells were averaged to obtain the projection of the EAT NCD cell. Cells from IAT and EAT NCD samples were also integrated using the RunHarmony function of the harmony (v1.0) R package on the top 15 PCs of HVGs. The corrected PCs were used as inputs for clustering and visualization.

**Adipose Tissue Fractionation**

EAT and IAT were obtained from age-matched NCD-fed and 2- or 10-week HFD-fed mice. Adipose tissues were fractionated as described previously (Jeon et al., 2020). Briefly, adipose tissues were minced and digested with collagenase buffer [0.1 M HEPES, 0.125 M NaCl, 5 mM KCl, 1.3 mM CaCl2, 5 mM glucose, 1.5% (w/v) bovine serum albumin, and 0.1% (w/v) collagenase I (Worthington, 49A18993)] in a shaking water bath at 37 °C for 30–60 min. After centrifugation at 200 × g, room temperature (RT) for 5 min, the pelleted stromal vascular fraction (SVF) was collected. The SVF was incubated in red blood cell lysis buffer (1.7 M Tris, pH 7.65, and 0.16 M NH4Cl) for 15 min. Then, the SVFs were washed with phosphate-buffered saline (PBS) several times, passed through a 100 μm filter (93100, SPL), and collected by centrifugation at 200 × g for 5 min.

**Fluorescence-Activated Cell Sorting (FACS)**

FACS was carried out as previously described with minor modifications [193]. SVFs were stained with anti-CD31 (1:100, 102405, 102409 and, 102419 BioLegend), anti-CD45 (1:100, 103107, 103111, and 103131, BioLegend), anti-DPP4 (1:100, 137809, BioLegend), anti-ICAM1 (1:100, 116107, BioLegend), and anti-BST2 (1:100, 127015, BioLegend) for 30 min. To detect $Ki67^{+}$ cells, the SVFs were co-stained with anti-Ki67 (1:100, 151211, BioLegend). The cells were analyzed using a FACS Canto II instrument (BD Biosciences).

**Isolation of SVFs from Human Adipose Tissue**

Human adipose tissues were rinsed in PBS twice, manually minced, and digested with collagenase buffer [0.1 M HEPES, 0.125 M NaCl, 5 mM KCl, 1.3 mM CaCl2, 5 mM glucose, 1.5% (w/v) bovine serum albumin, and 0.1% (w/v) collagenase I (Worthington, 49A18993)] in a shaking water bath at 37°C for 30–60 min. The subsequent steps were the same as those for preparing mouse adipose tissue fractionation.

**Immunocytochemistry and Immunohistochemistry**

Samples were incubated with fluorescently labeled Hoechst 33342 (ab228551, Abcam) and stained with fluorescein isothiocyanate-conjugated BODIPY 493/503 (D3922; Thermo Fisher Scientific). BODIPY staining was performed as previously with minor modifications [341]. Adipogenesis was assessed by staining with BODIPY 493/503 (D3922, Invitrogen) for lipid droplet accumulation and by staining with Hoechst 33342 for nucleus number at 8 days post induction (mouse

cells) and 2 weeks post induction (human cells) in individual wells of a 384-well plate (37384, SPL). The cells were imaged using a CQ1 microscope (Yokogawa). Coherent anti-Stokes Raman scattering was used to measure lipids [342].

Whole-mount imaging was carried out as previously with minor modifications (Park et al., 2019). A small fraction of fat tissue was fixed in 4% paraformaldehyde for 10 min and permeabilized with 0.5% Triton X-100 in PBS for 5 min. The fixed tissues were incubated with a primary antibody against UCP1 (14670; Cell Signaling, 1:300) and a primary antibody against tyrosine hydroxylase (818007, BioLegend, 1:500) overnight. The tissues were then washed three times for 10 min each, incubated with secondary antibody for 1 h, washed three times for 5 min each, and mounted on slides in 8-well plates (155409, Nunc Lab-Tek II) with Hoechst 33342. Tissues were observed and imaged using a CQ1 microscope (Yokogawa).

For immunohistochemistry, small fractions of fat tissues were isolated from mice, fixed in 4% paraformaldehyde, and embedded in paraffin. The paraffin blocks were cut into 5-μm sections and stained with hematoxylin and eosin. Tissues were imaged using a digital slide scanner (Axio Scan Z1, Carl Zeiss).

**Isolation of Adipocyte Nuclei**

BrdU (559619, BD Biosciences) was administered in the drinking water at 0.8 mg/ml for one week. Adipocytes were fractioned using collagenase treatment. Floating adipocyte fractions were washed with collagenase buffer three times and centrifuged at 200 × g for 10 min. Isolation of intact adipocytes was verified by quantitative reverse transcription (RT-q)PCR analysis of adipocyte marker genes (Adipoq, Plin1),

and endothelial cell marker gene (Pecam1/CD31), and a immune cell marker gene (Ptprc/CD45). CD31 and CD45 were expressed in the SVF, but not in the adipocyte fraction. Nuclei isolated from The adipocyte fractions were processed using the FITC BrdU Flow Kit (559619, BD Biosciences) according to the manufacturer's instructions. Following antibody incubation, the samples were washed and analyzed using a FACS Aria II instrument (BD Biosciences). The proportion of BrdU+ nuclei among total nuclei (7-AAD$^{+}$) was measured.

**Cell Culture**

ASCs were seeded in 96-well plates at 3,000 cells/well and cultured in DMEM containing 10% FBS for two days until confluence. For adipogenic differentiation, the cells were incubated in adipogenic media (1 μM dexamethasone, 520 μM IMBX, 850 nM insulin, and 1 μM rosiglitazone). Two days after adipogenic induction, the culture medium was replaced with FI medium (850 nM insulin and 1 μM rosiglitazone), and the cells were analyzed after 8–10 days of differentiation. For osteogenic differentiation, cells were cultured in DMEM with 10% FBS, 50 μM ascorbic acid, and 10 mM β-glycerophosphate for 10 days. For beige adipocyte differentiation, the cells were incubated in beige adipogenic media (1 μM dexamethasone, 520 μM IBMX, 850 nM insulin, 1 nM T3, 125 μM indomethacin, and 1 μM rosiglitazone). After adipogenic induction for two days, the culture medium was replaced with FI medium (850 nM insulin, 1 nM T3, and 1 μM rosiglitazone), and the cells were analyzed after 8–10 days of differentiation.

**Cell Proliferation Assay**

Cell proliferation was assayed as described previously [343] with minor modifications. Briefly, cells were seeded in 96-well plates at 100 cells/well. CCK-8 (Dojindo, CK04) assays were performed according to the manufacturer's instructions. For cell proliferation assay using CM, adipocytes and SVFs were isolated from IAT and EAT of NCD- and 3-day HFD-fed mice. Adipocytes and SVFs were incubated in DMEM containing 10% FBS for 24 h and CM was collected. Both adipocytes CM and SVF CM were normalized by fat mass (5 ml of media per adipocytes and SVFs from 1 g of fat tissue).

**siRNA Treatment**

siRNAs were purchased from Bioneer Inc. (Daejeon, South Korea). Cells were mixed with siRNA or vectors and transfected with a single pulse of 1100 V for 30 ms using a Microporator MP-100 (Digital Bio, Seoul, Korea) according to the manufacturer's instructions.

**RT-qPCR**

Total RNA was isolated using Direct-zol™ RNA MiniPrep (Zymo Research). The RNA was reverse-transcribed using the ReverTra Ace qPCR RT Kit (Toyobo). RT-qPCRs were run using SYBR Green master mix (DQ384-40h, Biofact). Target gene expression levels were normalized to Tbp expression.

**Transplantation and Lymph Node (LN) Dissection**

$DPP4^{+}/GFP^{+}$ ES1 and IS1 ASCs were purified (donor cells) by FACS from EAT and

IAT of GFP-Tg adult male mice. $GFP^+$ and $DPP4^+$ S1 cells were concentrated to ~5,000 cells/μl by centrifugation and then mixed 1:1 with Matrigel (356230, Corning) on ice. Donor cells (10-20 μl) were injected into the fat pads of WT C57BL/6 adult male mice. Donor GFP+ cells were harvested from the recipient animals 3 hours or 10 days after transplantation and subjected to FACS analysis.

For the LN dissection experiment, the skin near the IAT was incised, and the LN was removed. One week after LN removal, the mice were exposed to a cold environment (6 °C) for 4 or 7 days or treated with a dose of 1 mg/kg body weight of CL316,243 compound for 7 days.

**Statistical Analysis**

Data are presented as the mean ± standard deviation (SD). n-Values indicated in the figures refer to biological replicates. Means of two groups were compared using a two-tailed Student's t-test. Means of multiple groups were compared using one-way ANOVA followed by Tukey's post-hoc test. Two independent variables were compared using two-way ANOVA followed by Sidak's multiple comparisons test. Statistical analyzes were performed using GraphPad Prism (GraphPad Software).

Table 2. Primer sequences in Chapter I

| Primers for qRT-PCR | | | |
|---|---|---|---|
| Species | Gene | Forward | Reverse |
| Mouse | *Adipoq* | GGCAGGAAAGGAGAACCTGG | AGCCTTGTCCTTCTTGAAGAG |
| | *Bst2* | CAATCTACTTCGCCGTCACA | TCTTCTCCAGGGACTCCTGA |
| | *Ccnd1* | AGAAGTGCGAAGAGGAGGTC | TTCTCGGCAGTCAAGGGAAT |
| | *Cd81* | TCTACGTGGGCATCTACATTCT | ATCCTTGGCGATCTGGTCTTT |
| | *Cxcl13* | AGGCCACGGTATTCTGGAAG | AGCTTGGGGAGTTGAAGACA |
| | *Fabp4* | AAGAAGTGGGAGTGGGCTTT | GCTCTTCACCTTCCTGTCGT |
| | *Il33* | GGTCCCGCCTTGCAAAATAA | CCGTGGATAGGCAGAGAAGT |
| | *Irf4* | GCAGCTCACTTTGGATGACA | CCAAACGTCACAGGACATTG |
| | *Irf7* | GAAGACCCTGATCCTGGTGA | CCAGGTCCATGAGGAAGTGT |
| | *Ocn (Bglap)* | AAGCAGGAGGGCAATAAGGT | TTTGTAGGCGGTCTTCAAGC |
| | *Opn (Spp1)* | TGCACCCAGATCCTATAGCC | CTCCATCGTCATCATCATCG |
| | *Pi16* | TGGATCTTCACAACCAGTACCG | CAGCTCGTCATCCCACCTC |
| | *Pparg2* | GCATGGTGCCTTCGCTGA | TGGCATCTCTGTGTCAACCATG |
| | *Scg3* | ACGTGGAAGACGCTGATTCAA | TGGCAATCTTATGGACGATGTC |
| | *Tbp* | GGGAGAATCATGGACCAGAA | CCGTAAGGCATCATTGGACT |
| | *Tmem26* | GAAACCAGTATTGCAGCACCCAAT | AATATTAGCAGGAGTGTTTGGTGG |
| | *Ucp1* | TCTGCATGGGATCAAACCCC | ACAGTAAATGGCAGGGGACG |
| | *Wnt2* | CGTGCCTTTGTAGATGCCAA | CCTCCAGAGATAGTCGCCTG |

# 4. Results

**In EAT and IAT, ASC clusters exhibit different molecular properties and comprise three adipogenic stages**

To characterize ASCs in two white fat depots, $Lin^-$ ($CD31^-/CD45^-$) stromal vascular fractions (SVFs) from normal chow diet (NCD)-fed mice were subjected to scRNA-seq analysis. *Msln*$^+$ mesothelial cells were removed from the downstream analysis to focus ASCs. Unsupervised clustering analysis of 11,225 quality control-positive cells revealed ASCs from NCD mice were divided into four ASC clusters in EAT ($E_N1$–$E_N4$, N denotes NCD) and seven ASC clusters in IAT ($I_N1$–$I_N7$) (Figure 4A). It is likely that molecular features of ASC clusters in EAT and IAT were distinct, partly, due to fat depot-specific genes such as *Wt1* and *Col6a5* in EAT, and *Tbx5* and *Prrx1* in IAT (Figure 4B).

As ASCs are a heterogeneous population of cells with different adipogenic potentials [241, 244, 249, 265, 344] I inferred differentiation trajectories of the ASC clusters using Palantir with collaborators [345]. As shown in Figures 4C and 4D, EAT ASC clusters were largely divided into three stages: stage 1 (S1) multipotent ASCs in EAT expressing BMPs (ES1: cluster $E_N1$); stage 2 (S2) early committed preadipocytes in EAT highly expressing early adipogenic markers, such as *Cebpd* (ES2: clusters $E_N2$–$E_N3$); and stage 3 (S3) late committed preadipocytes in EAT expressing late adipogenic markers, such as *Fabp4* (ES3: cluster $E_N4$). Similarly, IAT ASC clusters were grouped into three stages: IS1 (clusters $I_N1$–$I_N4$), IS2 (cluster $I_N5$), and IS3 (clusters $I_N6$–$I_N7$) ASCs. To affirm these *in silico* adipogenic hierarchy of ASC stages, I aimed to isolate and characterize ASCs in EAT and IAT by FACS. Among several surface markers, DPP4 was highly expressed in S1 and S2 ASCs,

while ICAM1 was abundantly expressed in S2 and S3 ASCs in EAT and IAT (Figures 4E and 4F)

Sorted $DPP4^+$, $DPP4^+/ICAM1^+$, and $ICAM1^+$ ASCs from the two fat depots expressed S1, S2, and S3 markers (Figures 4F, 5A, and 5F), respectively, validating that DPP4 and ICAM1 seemed to be suitable markers for the isolation of S1, S2, and S3 ASCs. As expected, the extents of lipid droplet formation and adipocyte marker gene expression were higher in ES2 and ES3 ASCs than in ES1 ASCs cultured with adipogenic cocktails, whereas cell proliferation activity and osteogenic potential were higher in ES1 ASCs (Figures 5B–5E). Similarly, IS1, IS2, and IS3 ASCs exhibited different adipogenic and osteogenic potentials (Figures 5G–5J). Nonetheless, the gene expression profiles of the clusters comprising EAT and IAT ASCs of the three adipogenic stages were significantly different (Figure 4B), implying that the EAT and IAT ASCs in the different subpopulations may have different biological features.

One of the notable differences between EAT and IAT was that *de novo* adipogenesis appears to be more active in EAT than IAT in lean mice (Figures 6A and 6B). Further, the percentage of committed preadipocytes in EAT (ES2 and ES3) was significantly higher than that IAT (IS2 and IS3) (Figures 4F and 6C). Thus, I hypothesized that the proportion of committed preadipocytes (S2 and S3) in ASCs might be positively correlated with *de novo* adipogenesis. To address this, I decided to examine pups and adult female mice, which have an enhanced capacity of *de novo* adipogenesis compared to adult male mice [186, 249]. The proportions of S2 and S3 ASCs were higher in pups and adult female mice than adult male mice (Figure 6D), implying that the high proportions of ES2 and ES3 ASCs would indeed reflect active

*de novo* adipogenesis in EAT.

Then, I explored whether analogous ASCs might be conserved in human VAT from patients with obesity. Similar to the findings in mouse EAT, the proportion of $DPP4^+/ICAM1^+$ S2 (40.5%) and $ICAM1^+$ S3 (38.4%) ASCs was higher than that of $DPP4^+$ S1 ASCs (12.1%) (Figure 7A). Also, S2 and S3 ASCs in human VAT showed higher adipogenic potential and lower proliferative activity than S1 ASCs (Figures 7B–7D), indicating that human ASCs might be also divided into three adipogenic stages analogous to those in mice. Collectively, these data suggested that the distinct molecular properties of ASC clusters and the different proportions of ASCs in EAT and IAT would be involved in their adipogenic capacity.

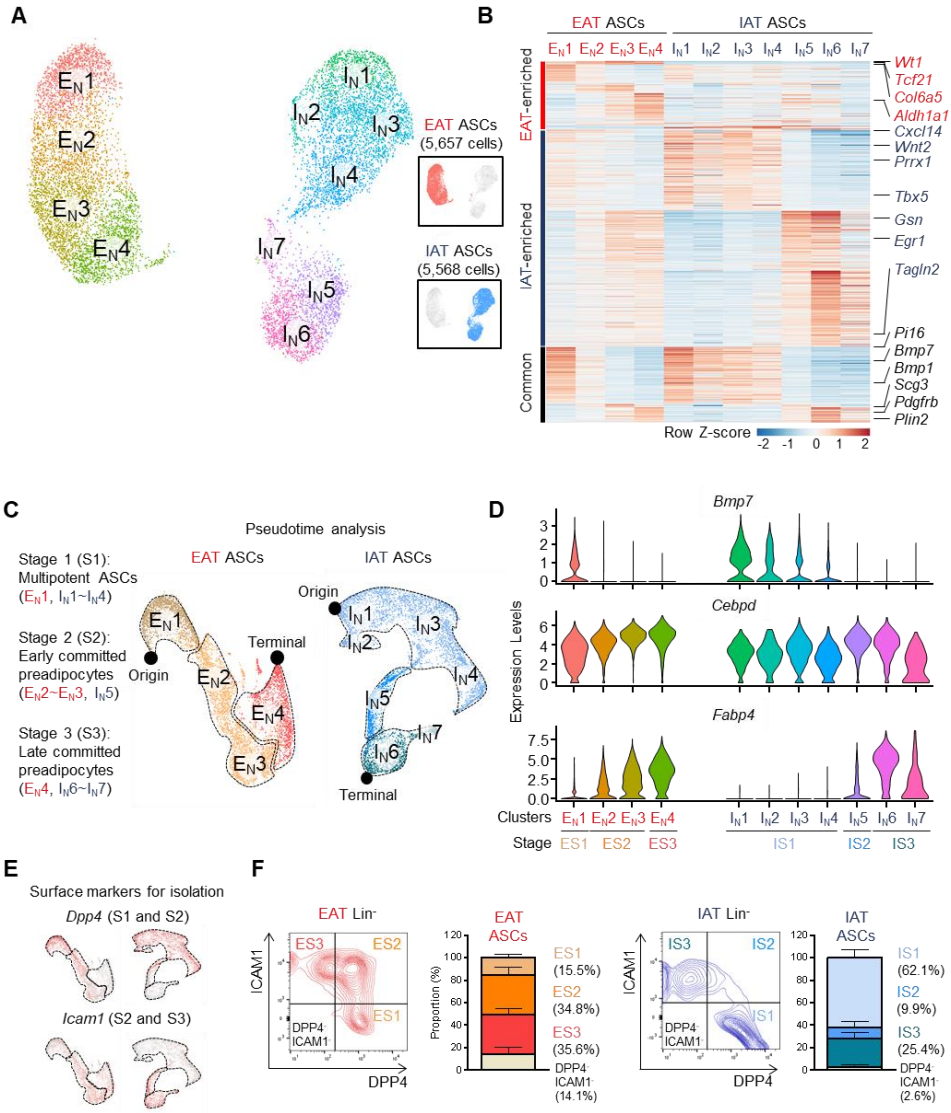


**Figure 4. In EAT and IAT, ASC clusters exhibit different molecular properties and comprise three adipogenic stages**

(A) Unsupervised clustering of CD31$^{-}$/CD45$^{-}$ 5,657 cells from EAT and 5,568 cells from IAT of male adult mice on a UMAP plot. Each color means separated clusters (4 clusters in EAT and 7 clusters in IAT).

(B) Heatmap showing the expression levels of fat-depot specific and common gene

(C) *In silico* pseudotime analysis of ASCs along differentiation trajectories.

(D) Expression levels of stage-enriched genes.

(E) Gene expression levels of *Dpp4* and *Icam1* in EAT and IAT ASCs.

(F) Representative FACS plots and FACS-based ASC stage proportion in EAT and IAT.

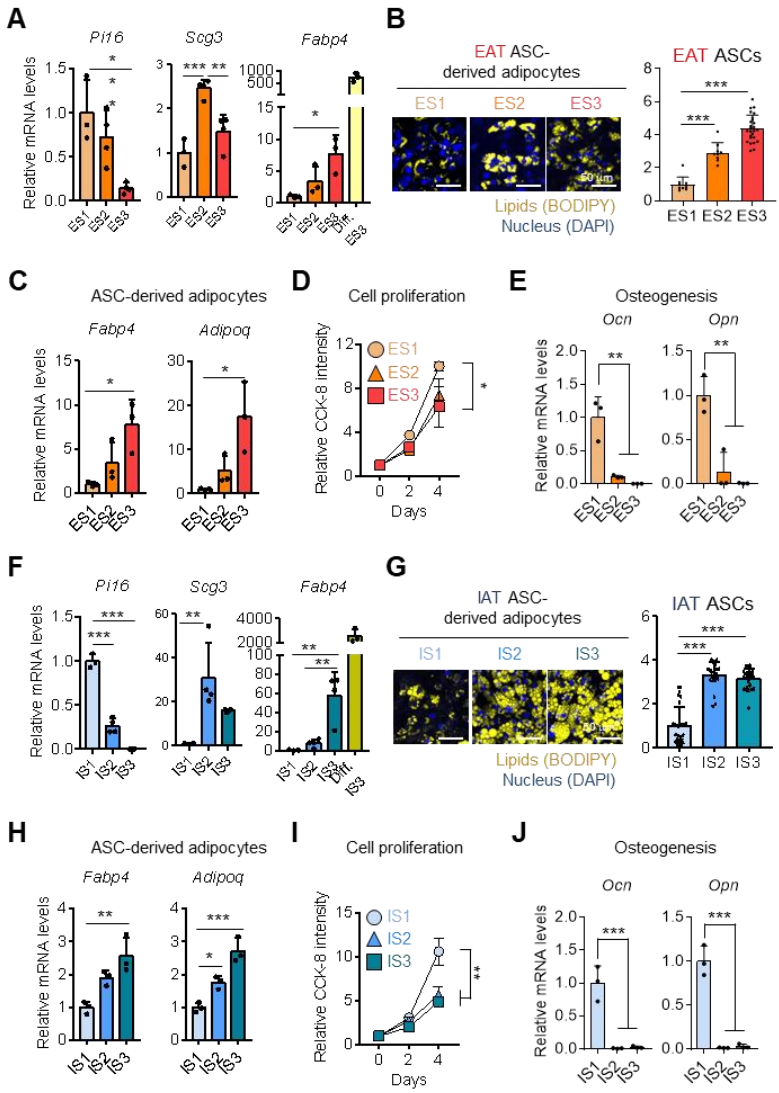


**Figure 5. Characterization of three adipogenic stages in EAT and IAT**

(A and F) mRNA levels of stage markers of S1~S3, and differentiated adipocytes from S3 ASCs in the sorted cells.

(B and G) Representative image of BODIPY lipid staining of differentiated cells. Cells were differentiated for 8 days under an adipogenic condition. Scale bar: 50 mm.

(C and H) mRNA levels of Fabp4 and Adipoq in the differentiated cells. n = 3.

(D and I) Quantification of cell proliferation. n = 3.

(E and J) mRNA levels of osteogenic markers in cells with osteogenic cocktail for 2 weeks. n = 3.

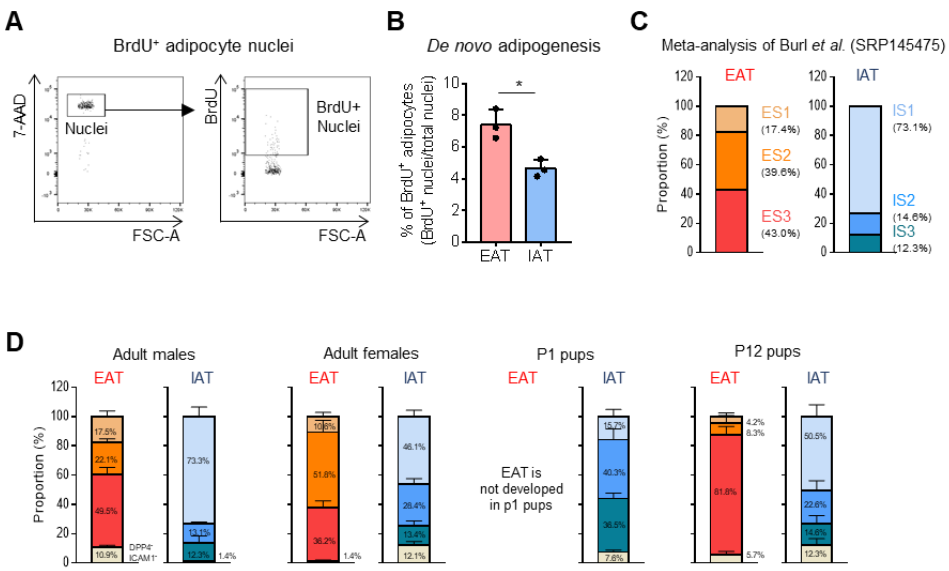


**Figure 6. EAT exhibits more active *de novo* adipogenesis and a higher proportion of committed preadipocytes than IAT**

(A) Representative FACS plots of BrdU$^{+}$ adipocyte nuclei.

(B) Quantification of BrdU incorporation into adipocyte nuclei after pulse from the first week and nine-week chase upon NCD. n = 3.

(C) Meta-analysis of scRNA-seq data (SRP145475) from Burl et al. Quantification of ASC proportion from scRNA-seq data based on stage marker expressions.

(D) Quantification of ASC proportion according to stage from p1 pups, p12 mice, adult female, and adult male mice. n = 2~6. EAT is not developed in p1 pups.

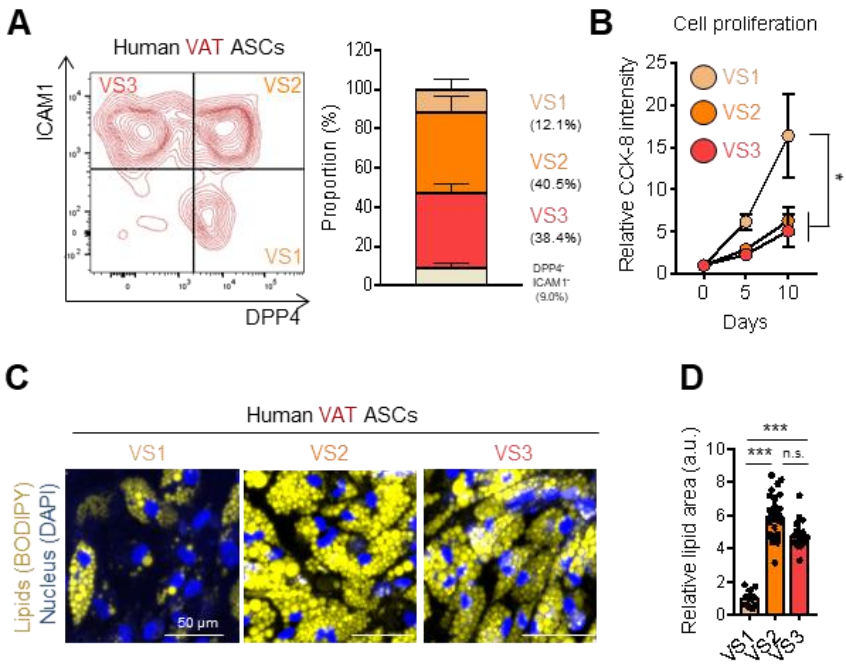


**Figure 7. Characterization of three adipogenic stages in human visceral adipose tissue**
(A) Representative FACS plot of ASC from human visceral adipose tissue (VAT) and quantification of the proportion of stages 1, 2, and 3 in VAT (VS1, VS2, and VS3).
(B) Quantification of cell proliferation in human VAT ASC. n = 3.
(C) BODIPY lipid staining of differentiated S1, S2, and S3 cells from human VAT. ASCs were differentiated for two weeks under an adipogenic condition. Scale bars, 50 mm.
(D) Quantification of adipogenesis by measuring lipid area. n = 3

**Intrinsic factors of ES1 and IS1 ASCs drive adipogenic potential**

The finding that committed preadipocytes were more abundant in EAT than in IAT raised the idea that a commitment step towards preadipocytes might be differentially regulated in EAT and IAT. To address this, I isolated $GFP^+/DPP4^+$ ES1 and IS1 ASCs from GFP-transgenic mice and transplanted them into EAT and IAT, respectively, of wild-type mice (Figures 8A and 8B). When donor ES1 ASCs were examined, 65% of $GFP^+$ cells were found in the ES2 and ES3 populations after transplantation (Figure 8C). In contrast, 14.3% of donor IS1 ASCs were found in the IS2 and IS3 populations (Figure 8D). To investigate whether cell-intrinsic features or tissue micro-environmental factors would determine the fat depot-specific regulation of adipogenic potential, I crossly transplanted donor ES1 and IS1 ASCs into the opposite fat depot (Figure 8A). 52.2% of $DPP4^+$ donor ES1 ASCs transplanted into IAT were found in the ES2 and ES3 populations after transplantation (Figure 8E), whereas 24.3% of donor IS1 ASCs transplanted into EAT were found in the IS2 and IS3 populations (Figure 8F). These data indicated that intrinsic features of ES1 and IS1 ASCs would primarily drive commitment towards preadipocytes, whereas the fat tissue microenvironment might have a minor effect.

To identify the cell-intrinsic factors that regulate adipogenic potential in ES1 and IS1 ASCs, I analyzed differentially expressed genes in these cells. Gene ontology analysis showed that genes enriched in ES1 ASCs, such as *Tle3* and *Egr2* (*Krox20*), were associated with fat cell differentiation [346, 347], whereas genes enriched in IS1 ASCs were related to cold-induced thermogenesis and canonical WNT signaling (Figures 9A-9E). As WNT signaling inhibits adipogenesis of mesenchymal stem cells [274, 275], I decided to evaluate whether *Wnt2*, the most

strongly expressed WNT family gene in IS1 ASCs (Figure 9F), might suppress commitment to preadipocytes in IAT. When *Wnt2* expression was suppressed in IS1 ASCs using siRNA, lipid content and adipogenic marker gene expression were greatly enhanced in differentiated adipocytes (Figures 10A–10C). In contrast, suppression of *Wnt2* in ES1 ASCs did not significantly affect adipogenic potential (Figures 10D–10F), implying that expression of *Wnt2* in ASC would affect adipogenesis in a depot-specific manner. In this regard, expression quantitative trait loci related to the waist-to-hip ratio, a surrogate of VAT versus SAT expansion in humans, were found to exist in the promoter/enhancer regions of *WNT2* and *CCND1* (Figure 10G). Taken together, these results suggested that intrinsic features would predominantly regulate the adipogenic potential of ES1 and IS1 ASCs, and WNT signaling in IS1 ASCs would restrain commitment towards preadipocytes.

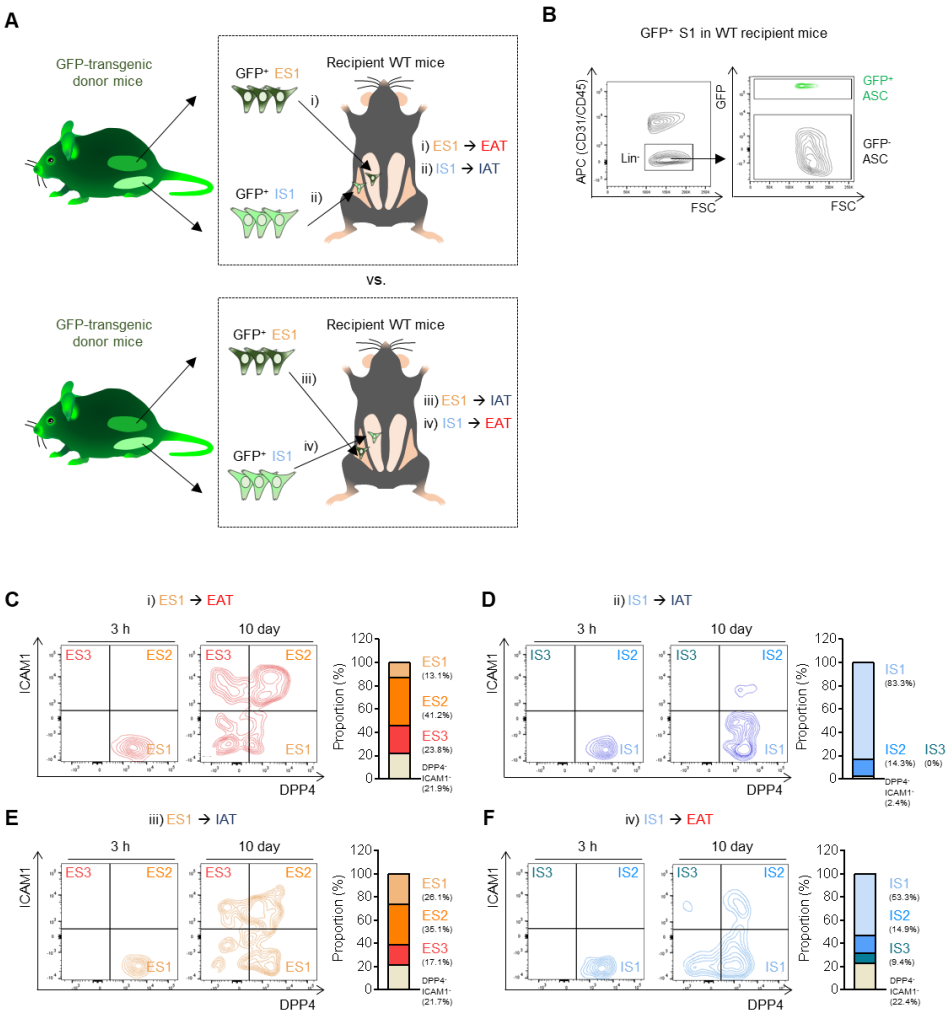


**Figure 8. Intrinsic factors of ES1 and IS1 drive adipogenic potential**

(A) Experimental design for ASC transplant experiments. Sorted GFP$^+$/DPP4$^+$ ES1 and IS1 ASCs were transplanted into EAT or IAT.

(B) Representative FACS plot of GFP$^+$ cells demonstrating engraftment of donor-derived GFP$^+$ ASCs in the recipient mice.

(C–F) Representative FACS plots and proportion of transplanted GFP$^+$/DPP4$^+$ donor cells in recipient WT mice.

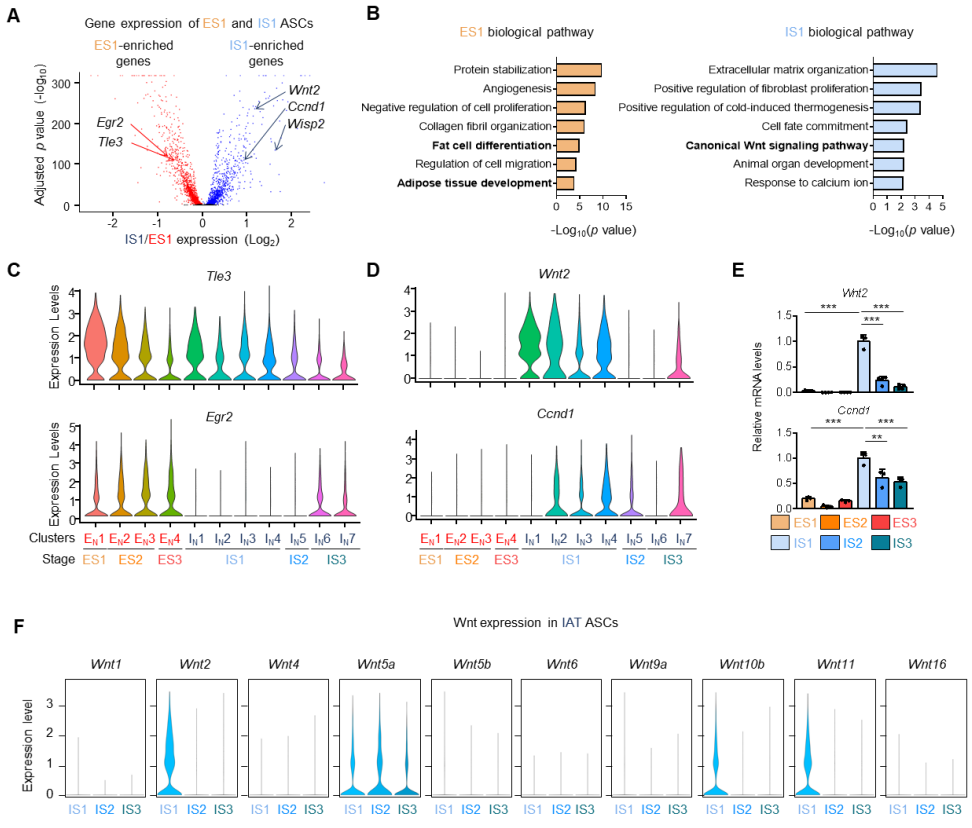


**Figure 9. Differentially expressed genes between ES1 and IS1**

(A) A volcano plot of ES1 and IS1-enriched genes.

(B) Gene ontology of ES1- and IS1-enriched genes.

(C) Expression levels of Tle3 and Egr2 in EAT and IAT ASC clusters.

(D) Expression levels of Wnt2 and Ccnd1 in IAT and EAT ASC clusters.

(E) mRNA levels of Wnt2 and Ccnd1 in EAT and IAT ASC stages. n = 3.

(F) Expression levels of WNT family in IAT ASCs.

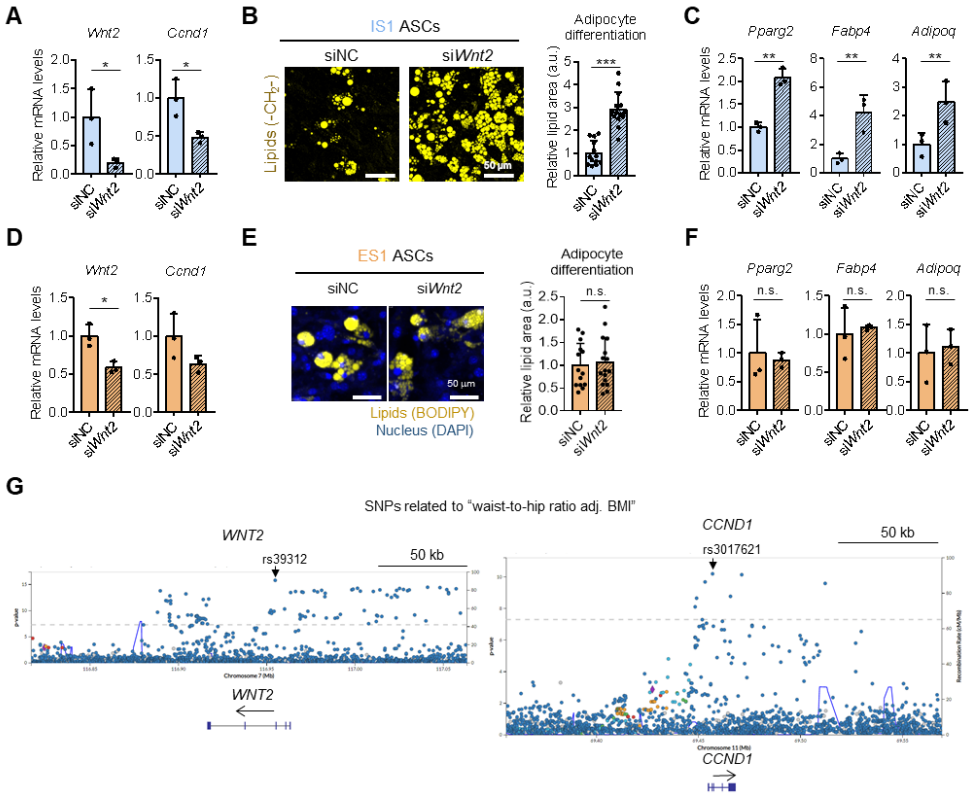


**Figure 10. IS1 ASC specific Wnt2 suppress adipogenesis**

(A) mRNA levels of Wnt2 and Ccnd1 of IS1 ASCs with siRNA for negative control (NC) or Wnt2. n = 3.

(B) (Left) Representative images of differentiated adipocytes from IS1 ASCs with siRNA for negative control (NC) or Wnt2. (Right) Quantification of lipid area in differentiated adipocytes. Scale bar: 50 μm.

(C) mRNA levels of adipocyte markers in differentiated adipocytes from IS1 ASCs. n = 3.

(D) mRNA levels of Wnt2 and Ccnd1 of ES1 ASCs with siRNA for negative control (NC) or Wnt2. n = 3.

(E) (Left) Representative images of differentiated adipocytes from ES1 ASCs with siRNA for negative control (NC) or Wnt2. (Right) Quantification of lipid area in differentiated adipocytes. Scale bar: 50 μm.

(F) mRNA levels of adipocyte markers in differentiated adipocytes from ES1 ASCs. n = 3.

(G) Single nucleotide polymorphisms (SNPs) related to the waist-to-hip ratio in human WNT2 and CCND1 locus. Data from T2D Knowledge Portal (https://t2d.hugeamp.org/).

**In EAT, obesogenic stimuli promote ES1 ASC proliferation via FGF and TGFβ signaling to induce *de novo* adipogenesis**

It has been recently demonstrated that ASCs contribute to the fat depot-selective remodeling process in obesity [157, 193]. Upon HFD, *de novo* adipogenesis was stimulated in EAT (Figures 11A and 11B), consistent with previous findings [134, 185]. However, the key ASC cluster(s) and underlying molecular mechanisms mediating EAT-selective *de novo* adipogenesis in obesity are largely unknown. To tackle these issues, I characterized and compared ASC clusters in EAT and IAT using combined scRNA-seq datasets from NCD-fed, 2-week HFD-fed, and 10-week HFD-fed mice (Figure 11C). As I used unsupervised analysis, the exact cluster corresponding to the previously defined clusters $E_N1$–4 and $I_N1$–7 could not be annotated in combined scRNA-seq datasets; however, most cells of the $E_N1$ cluster were found in cluster $E_{NH}1$ (NH denotes merged NCD and HFD datasets), $E_N2$–3 clusters in $E_{NH}2$, $E_N4$ cluster in $E_{NH}3$, $I_N1$–4 clusters in $I_{NH}1$, $I_N5$ cluster in $I_{NH}2$, and $I_N6$–7 clusters in $I_{NH}3$ cluster. Upon HFD, 8 ASC clusters in EAT ($E_{NH}4$–11) and 10 clusters in IAT ($I_{NH}4$–13) newly emerged (Figure 11C). With regard to adipogenesis, cells in the new clusters $E_{NH}4$–6 expressed ES1 markers, cells in $E_{NH}7$–9 expressed ES2 markers, and cells in $E_{NH}10$–11 expressed ES3 markers (Figure 11C). Similarly, clusters $I_{NH}4$–9 were classified as IS1, clusters $I_{NH}10$–11 as IS2, and clusters $I_{NH}12$–13 as IS3 (Figure 11C). Although the expression of several genes was altered by HFD feeding (Figure 12A), there were no significant differences in adipogenic gene expression and *ex vivo* adipogenic potential of S1, S2, and S3 ASCs in both fat depots in obesity (Figures 12B-12E).

Notably, the proportion of ES1 ASCs was increased at the onset of obesity,

and ES3 ASCs were sequentially expanded after 10-week HFD (Figures 13A and 13E). Also, after a 3-day or 7-day HFD, the total number of ES1 ASCs was significantly elevated, probably due to cell proliferation (Figures 13B and 13C). Unlike in EAT, I found no significant proportion changes in IS1, IS2, or IS3 during HFD feeding periods or in the proliferation of IAT ASCs upon a 3-day HFD (Figures 13D-13F).

To examine how ES1 ASCs would be proliferated by HFD, ES1 ASCs were incubated with conditioned media (CM) from EAT adipocytes or SVFs from mice of the NCD and 3-day HFD groups (Figure 14A). ES1 ASC proliferation was promoted by HFD-CM from adipocytes, but not SVFs, containing heat-sensitive molecules, such as growth factors (Figures 14B and 14C). Transcriptome analyses of adipocytes from mice fed a NCD or a 3-day HFD [74] indicated that the expression of several growth factors, including FGFs, TGFβ, BMPs, GDFs, and PDGFs would be increased upon 3-day HFD (Figure 14D). To identify potential signaling molecule(s) contributing to the ES1-specific proliferation at the onset of obesity, we sought the 'ligand-receptor' relationships between ligands from obese adipocytes and receptors enriched in ES1 ASCs. The results suggested that FGF and TGFβ signaling(s) may mediate the proliferation of ES1 ASCs after 3 days of HFD, which was validated using *Fgfr1* and *Tgfbr2* knockdown in ES1 ASCs (Figure 14E).

Next, I investigated whether the responsiveness of ASCs or micro-environmental factors would determine the fat depot-specific ASC proliferation upon HFD. In this regard, ES1 and IS1 ASCs were treated with CM from EAT or IAT adipocytes (Figure 15A). CM from EAT adipocytes with HFD enhanced proliferation of ES1 and IS1 ASCs, in which receptors for FGFs and TGFβ were

highly expressed (Figures 15B and 15C). On the contrary, IAT adipocytes with HFD did not enhance proliferation of both ES1 and IS1 ASCs (Figure 15B), implying that tissue micro-environmental factors including FGFs and TGFβ secreted from EAT adipocytes might upregulate ASC proliferation at the onset of obesity. Together, these data propose that EAT-specific adipogenesis upon HFD would be potentiated by proliferation of ES1 ASCs mediated, at least in part, by FGF and TGFβ signaling cascades.

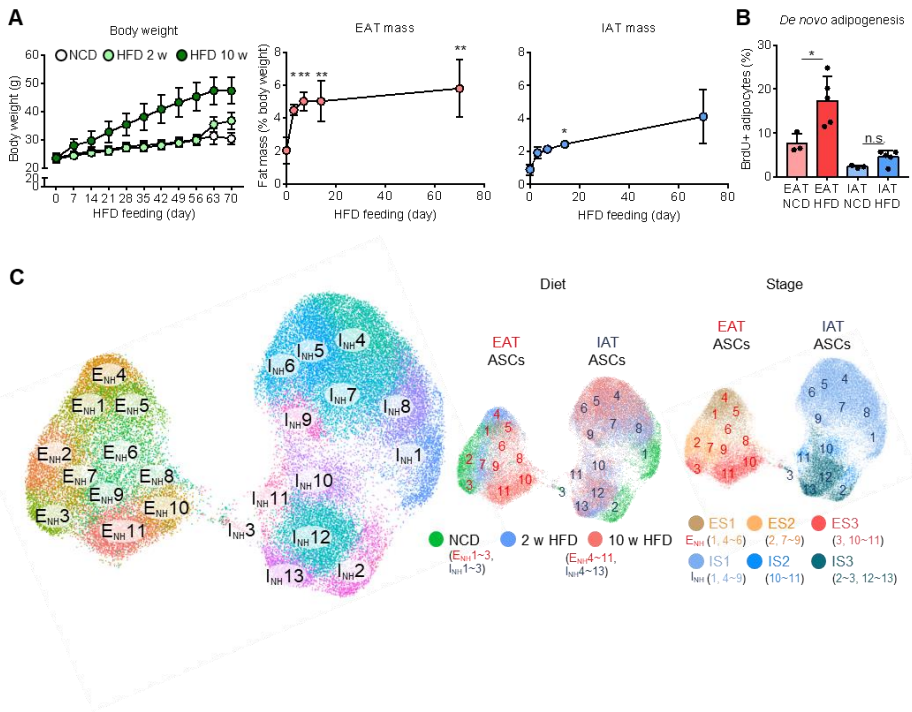


**Figure 11. Clustering of EAT and IAT ASCs from lean and obese mice**

(A) Body weight and EAT and IAT mass per body weight during HFD feeding. n = 3~14.

(B) Quantification of BrdU incorporation into adipocyte nuclei after pulse from the first week of diet feeding and nine-week chase upon NCD or HFD. n = 3~5.

(C) Unsupervised clustering of $CD31^{-}/CD45^{-}$ ASCs from EAT and IAT of NCD-, 2-week or 10-week HFD-fed mice.

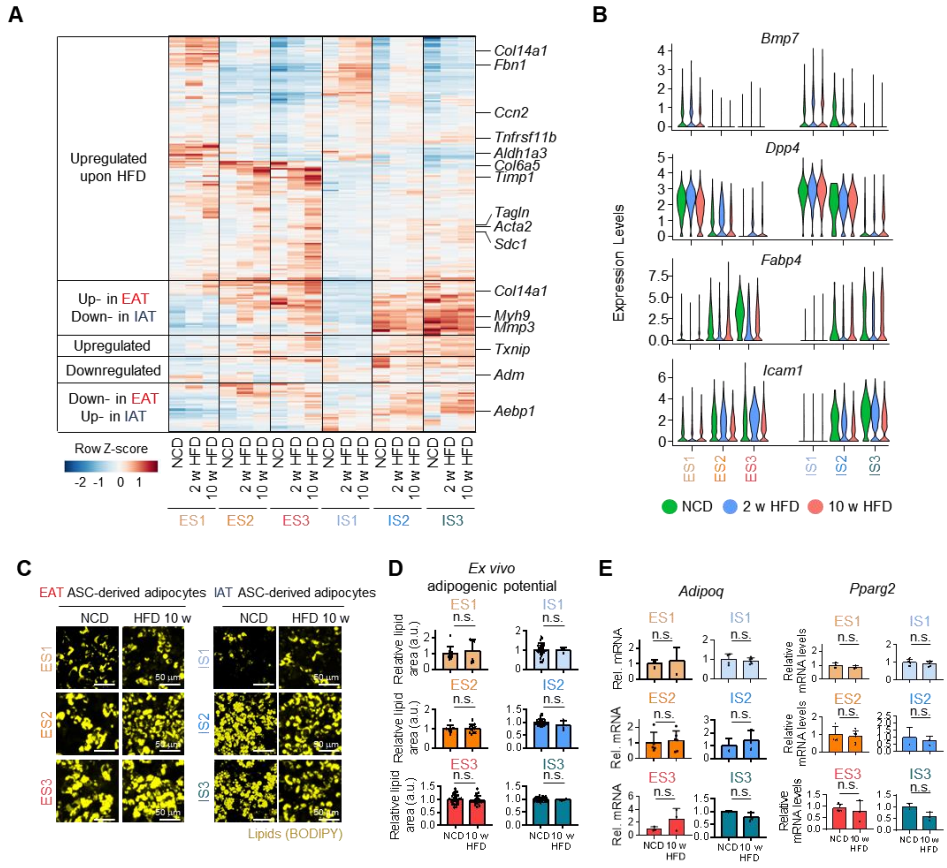


**Figure 12. Adipogenic potential of S1, S2, and S3 EAT and IAT ASCs from lean and obese mice**

(A) Representative genes that are differentially expressed in ASCs of HFD-fed mice compared to NCD-fed mice.

(B) Gene expression levels of Bmp7, Dpp4, Fabp4, and Icam1 in EAT and IAT ASC stages.

(C) BODIPY lipid staining of differentiated S1, S2, and S3 cells from EAT or IAT ASC from NCD or 10-week HFD-fed mice. Scale bar: 50 mm.

(D) Quantification of lipid area in differentiated adipocytes. ASCs were differentiated for 8 days under an adipogenic condition.

(E) mRNA levels of Adipoq and Pparg2 in differentiated adipocytes of ASCs from NCD- and 10-week HFD-fed mice. n = 2~6.

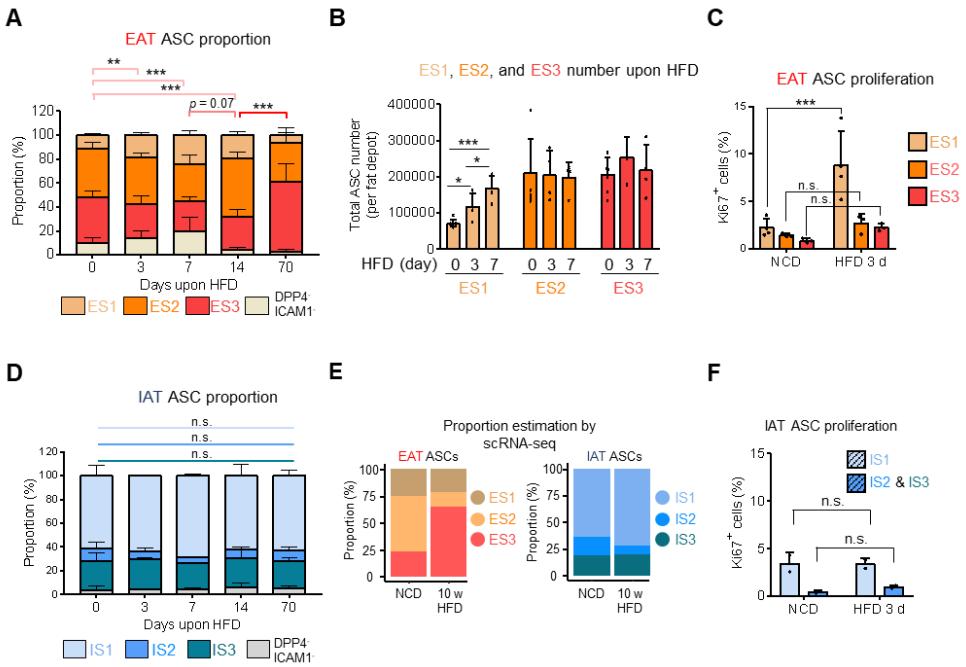


**Figure 13. In EAT, obesogenic stimuli promote ES1 proliferation to induce *de novo* adipogenesis**

(A) Proportion of ES1, ES2, and ES3 ASCs. Brackets with different colors indicate the statistical differences between ES1, ES2, and ES3 ASCs. n = 4~7.

(B) Total ES1, ES2, and ES3 cell numbers from NCD, 3- and 7-day HFD-fed mice. n = 4~7.

(C) Quantification of Ki67-positive cells in ASC in EAT of NCD and 3-day HFD-fed mice. n = 3.

(D) Proportion of IS1, IS2, and IS3 ASCs. Brackets with different colors indicate the statistical differences between IS1, IS2, and IS3 ASCs. n = 2~16.

(E) scRNA-seq based ASC stage proportion in EAT and IAT.

(F) Quantification of Ki67-positive cells in ASC in IAT of NCD and 3-day HFD-fed mice. n

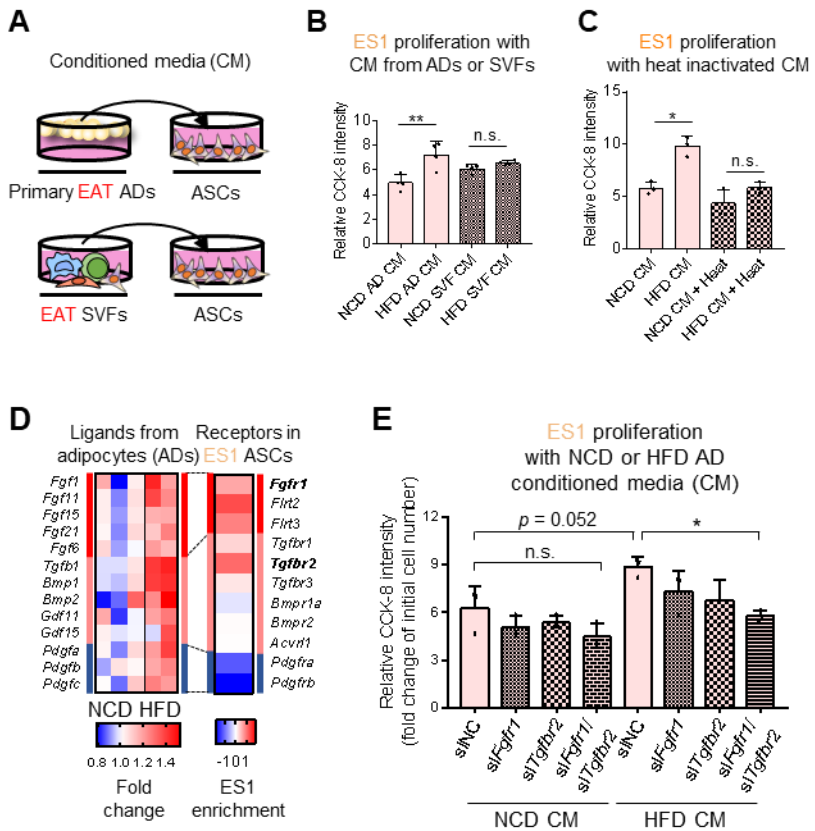


**Figure 14. FGF and TGFβ from EAT adipocytes promote ES1 proliferation**

(A) Experimental scheme for cell proliferation assay cultured with CM from primary EAT adipocytes or EAT SVFs.

(B) Quantification of cell proliferation of ES1 ASCs cultured with CM of primary EAT adipocytes or SVFs from EAT of NCD and 3-day HFD-fed mice. n = 3.

(C) Quantification of cell proliferation of ES1 ASCs cultured with CM of primary EAT adipocytes from EAT of NCD and 3-day HFD-fed mice. CM was heat-inactivated by incubating at 70℃ for 10 min. n = 3.

(D) The ligand-receptor relationship between EAT adipocyte and ES1. Expression levels of ligands were analyzed from NCD and 3-day HFD-fed mice (GSE65557). ES1 enrichment score was calculated as a fold of ES1 expression level compared to ES2 and ES3.

(E) Quantification of cell proliferation of ES1 cultured with conditioned media from primary EAT adipocytes. ES1 was transfected with siRNA for Fgfr1 and Tgfbr2 before CM treatment. n = 3.

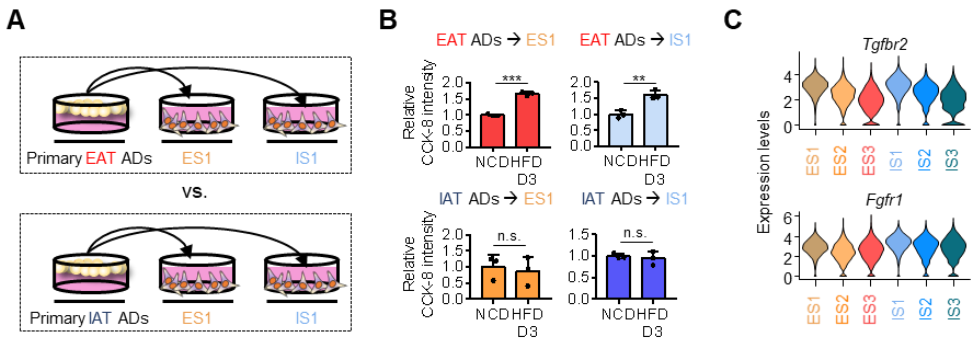


**Figure 15. Tissue micro-environmental factors regulate ASC proliferation at the onset of obesity**

(A) Experimental scheme for cell proliferation assay cultured with CM from primary EAT or IAT adipocytes from NCD- or 3-day HFD-fed mice.

(B) Quantification of relative cell proliferation of ES1 or IS1 ASCs cultured with CM from primary EAT or IAT adipocytes from NCD- or 3-day HFD-fed mice. n = 3.

(C) Expression levels of Fgfr1 and Tgfbr2 in EAT and IAT ASCs.

**IAT-specific BST2$^{high}$ ASCs are beige adipocyte precursors, whose biogenesis is regulated by LNs**

It has been suggested that beige adipocyte precursors in IAT appear to be different from classical white adipocyte precursors [19, 31, 132, 348-350]. Given that beige adipocytes are hardly observed in EAT, I postulated that beige adipocyte precursors would be rarely present in EAT ASCs, and differentiation pathways of beige adipocyte precursors might differ from canonical white adipocyte differentiation. To identify IAT-specific beige adipocyte precursors, I conducted a projection analysis in which EAT ASCs were projected onto similar IAT ASCs (Figure 16A). This comparative analysis showed that cluster $E_N1$ was projected onto clusters $I_N1$–3, clusters $E_N2$–3 were projected onto cluster $I_N5$, and cluster $E_N4$ was projected onto clusters $I_N6$–7 (Figure 16A). Notably, there appeared to be no EAT clusters that could be projected onto cluster $I_N4$ (Figure 16A). An independent analysis using batch correction corroborated that cluster $I_N4$ was distinct from the other IAT and EAT clusters (Figure 16B). Cells in the IAT-specific $I_N4$ cluster highly expressed *Tmem26* and *Il33,* which are associated with beige adipocytes [132, 142] (Figures 16C and 16D). In addition, cells in cluster $I_N4$ seemed to have a differentiation fate distinct from that of other IAT ASCs (Figure 16E).

To affirm that IAT-specific cluster $I_N4$ would exhibit beige adipocyte precursor features, I tried to isolate and characterize these ASCs by FACS. The IAT-specific cluster $I_N4$ highly expressed the surface marker *Bst2* (Figure 17A). Consistent with the scRNA-seq data, BST2$^{high}$ ASCs were abundantly detected in IAT, whereas BST2$^{high}$ ASCs were barely observed in EAT (Figures 17B and 17C). As BST2$^{high}$ ASCs largely expressed cluster $I_N4$ markers such as *Il33* and *Tmem26*

(Figure 17D), it seemed that BST2 would be a suitable marker for isolating cluster $I_N4$. Although differentiated adipocytes from $BST2^{high}$ ASCs highly expressed *Ucp1* and *Dio2* compared to those from $BST2^{low}$ ASCs, the mRNA level of adipocyte marker genes and lipid accumulation were comparable between differentiated adipocytes from $BST2^{high}$ and $BST2^{low}$ ASCs (Figures 17E-17G). Moreover, the proportion of $BST2^{high}$ ASCs was increased by cold exposure, whereas that of $BST2^{high}$ ASCs was downregulated in HFD-fed mice in which *Ucp1* expression was dampened (Figures 17H-17K), implying that $BST2^{high}$ ASCs might be important to modulate *in vivo* beige fat formation in IAT upon metabolic stimuli. Together, these data proposed that IAT-specific ASC subpopulations, distinct from EAT and other IAT ASCs with the high expression of cell surface marker BST2, could differentiate into beige adipocytes.

Notably, I found that *Cxcl13* and *Pdpn,* associated with the development of ASCs into LN fibroblastic reticular cells [351, 352], were also highly expressed in $I_N4$ cells (Figure 18A). As LN was found in IAT, but not EAT, I asked whether IAT-specific $I_N4$ cells might be abundant near LN. To test this, I anatomically divided IAT into peri-LN IAT (PL-IAT) and distal-LN IAT (DL-IAT) (Figure 18B). As shown in Figure 18C, the proportion of $BST2^{high}$ ASCs in total ASCs was significantly higher in PL-IAT than in DL-IAT. *Ucp1* mRNA expression was also higher in PL-IAT, accompanied by an enrichment of multilocular adipocytes, at room temperature and after cold exposure (Figures 18D-18G). The spatial relationship between $BST2^{high}$ ASCs and LN raised the issue to investigate the roles of LN in biogenesis of $BST2^{high}$ beige adipocyte precursors, using LN dissection (Figure 19A). LN removal decreased the proportion of $BST2^{high}$ ASCs in IAT (Figure 19B), implying that the

LN would be involved in the formation of beige adipocyte precursors. Accordingly, UCP1 expression in PL-IAT was decreased and the induction of $UCP1^{+}$ beige adipocytes was dampened in PL-IAT at room temperature and upon exposure to cold as well as upon β3-adrenergic agonist CL316,243 treatment (Figures 19C-19G), but not in DL-IAT (Figures 19H-19J). Although it is still possible that LN dissection might induce surgical damage in IAT, it seemed that LN dissection did not significantly affect sympathetic nerve innervation in PL-IAT (Figure 19K).

In humans, it has been reported that UCP1 and thermogenic gene expression levels were, unexpectedly, high in VAT [194], in which lymphatic vessels are highly developed, compared to SAT [353]. In line with these, my analysis of human VAT and SAT showed that *UCP1* expression was high in human VAT compared to SAT, accompanied by relatively high expression of *TMEM26*, *IL33, BST2*, *CXCL13,* and *PDPN* in VAT compared to SAT (Figure 20). Taken together, these data propose that IAT-specific $BST2^{high}$ ASCs would give rise to beige adipocytes and that LN might regulate the thermogenic features of IAT through, at least in part, biogenesis of IAT-specific $BST2^{high}$ beige adipocyte precursors.

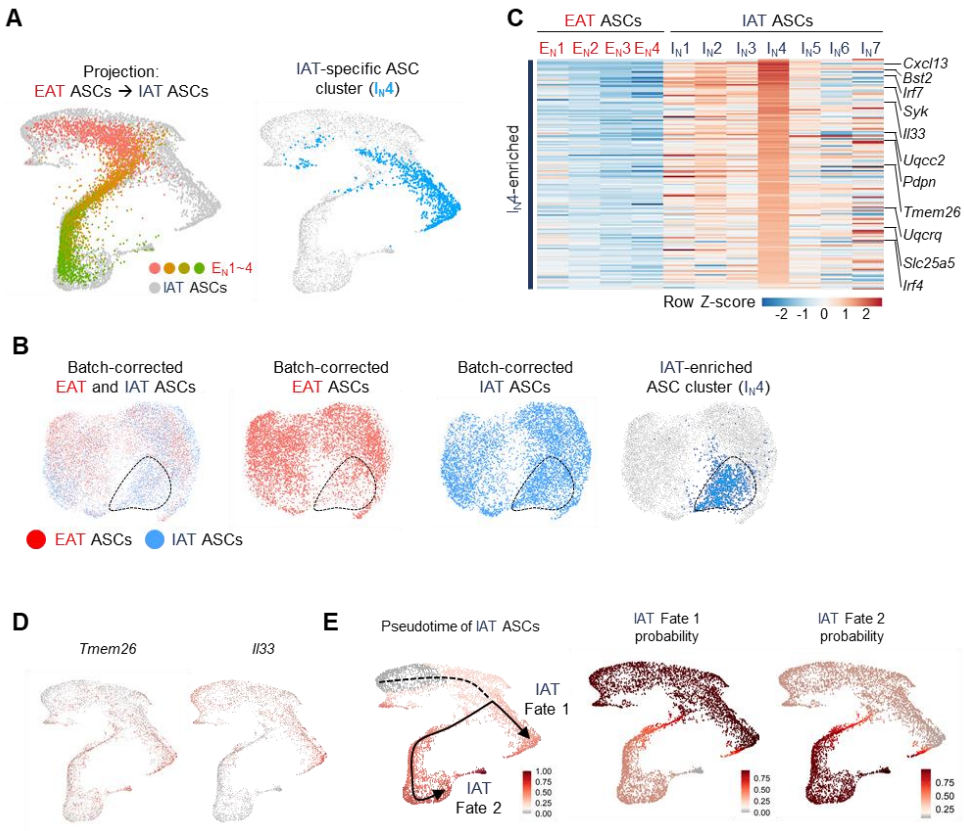


**Figure 16. Identification of IAT-specific ASC clusters with unique differentiation fate**
(A) Projection plot of EAT ASCs to IAT ASCs. EAT ASC clusters are projected to most similar IAT ASCs. IAT ASC is shown in gray, and EAT ASC clusters are shown in color. $I_N4$ cluster marked by blue.
(B) $I_N4$ clusters in batch-corrected plot marked by blue.
(C) Heatmap showing $I_N4$ cluster-specific genes.
(D) Expression levels of Tmem26 and Il33.
(E) In silico pseudotime analysis and IAT Fate 1 and Fate 2 probabilistic analysis of IAT ASCs from NCD-fed mice.

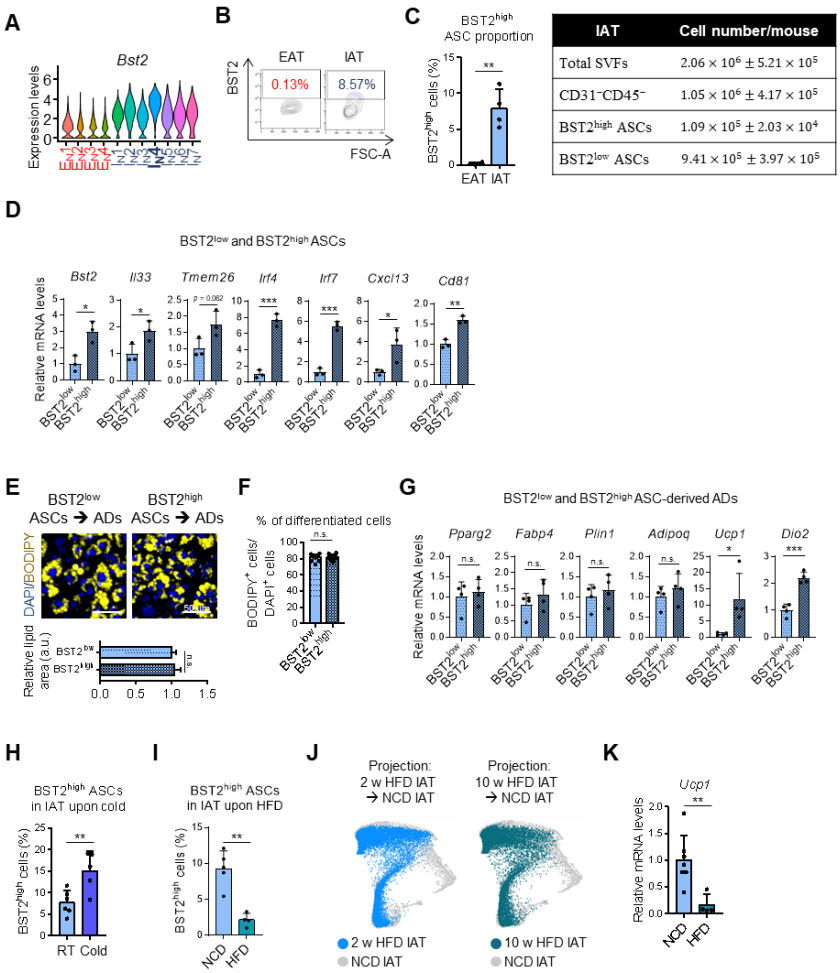


**Figure 17. IAT-specific BST2$^{high}$ ASCs are beige fat precursors**

(A) Expression levels of Bst2 in ASCs.

(B and C) Representative FACS plots and proportion of BST2$^{high}$ cells from ASCs in EAT and IAT. n = 4.

(D) mRNA levels of cluster $I_N4$ markers in BST2$^{high}$ and BST2$^{low}$ ASCs. n = 3.

(E) (Top) Representative image of BODIPY lipid staining of differentiated BST2$^{high}$ and BST2$^{low}$ ASCs. (Bottom) Quantification of BODIPY$^{+}$ area in differentiated cells from BST2$^{high}$ and BST2$^{low}$ ASCs. Scale bar: 50 mm.

(F) Proportion of the differentiated cells. The proportion of BODIPY$^{+}$ cells to DAPI$^{+}$ cells was calculated.

(G) mRNA levels of Pparg2, Fabp4, Plin1, and Dio2 in differentiated BST2$^{high}$ and BST2$^{low}$ ASCs. n = 4.

(H) Proportion of BST2$^{high}$ ASCs from mice at room temperature (RT) and upon cold exposure for 3 days. n = 5~6.

(I) Proportion of BST2$^{high}$ ASCs from NCD- and 8-week HFD-fed mice. n = 4.

(J) Projection plot of 2 week HFD IAT ASCs and 10 week HFD to NCD ASCs.

(K) mRNA levels of Ucp1 in IAT from NCD and 8 week HFD-fed mice. n = 4~7.

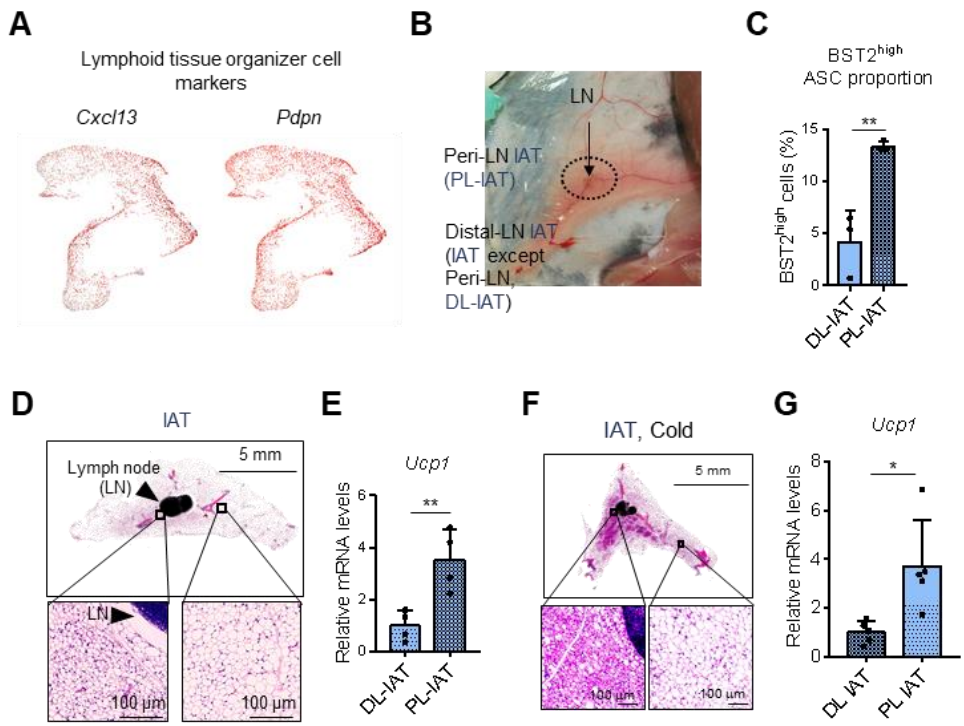


**Figure 18. BST2$^{high}$ ASCs are enriched near lymph node**

(A) Expression levels of genes related to lymphoid tissue organizer cell markers Cxcl13 and Pdpn.

(B) A representative macroscopic image of IAT. Lymph node (LN), peri-LN IAT (PL-IAT), and distal-LN IAT (DL-IAT) are represented. DL-IAT means IAT excluding the PL-IAT region.

(C) FACS analysis of BST2high cells from DL-IAT and PL-IAT ASCs. n = 3.

(D) Representative H&E staining in PL-IAT and DL-IAT. Scale bar: 5 mm or 100 μm.

(E) mRNA levels of UCP1 in PL-IAT and DL-IAT. n = 4.

(F) Representative H&E staining in PL-IAT and DL-IAT. Mice were exposed to cold environment (6℃) for 7 days. Scale bar: 5 mm or 100 μm.

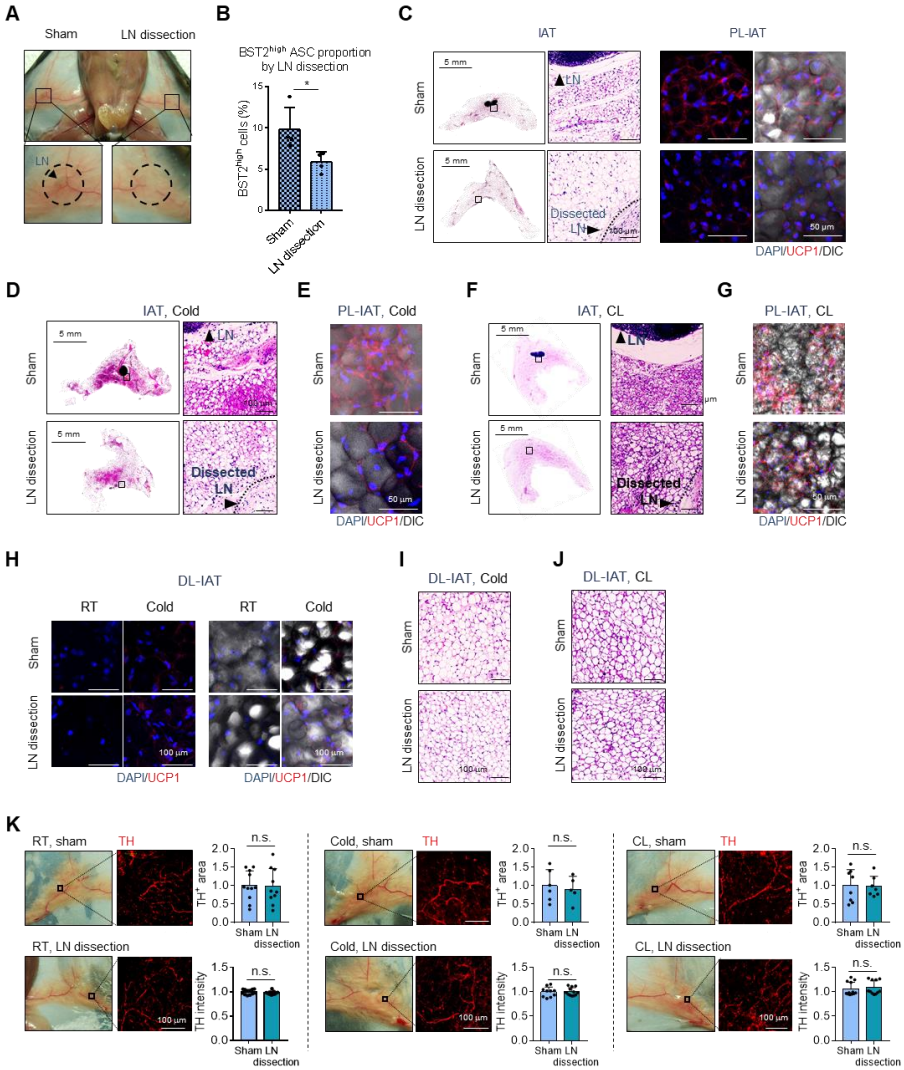


**Figure 19. Lymph nodes regulate biogenesis of IAT-specific BST2$^{high}$ ASCs**

(A) A representative macroscopic image of IAT. IAT of sham operation and LN dissection were presented. An arrow indicates LN.

(B) FACS analysis of BST2$^{high}$ cells from sham and LN dissection IAT. n = 4.

(C) Representative macroscopic images and whole-mount microscopic images of sham and LN dissection experiments two week after surgery at RT.

(D-J) Representative macroscopic and whole-mount microscopic images of PL-IAT and DL-IAT from sham control and LN dissected condition. For cold exposure, mice were kept in a cold environment (6℃) for 4 days. For CL316,243 (CL) treatment, CL was administrated daily with a dose of 1 mg/kg body weight for 7 days. Scale bar: 100 μm.

(K) Representative TH staining images of PL-IAT from sham control and LN dissected region.

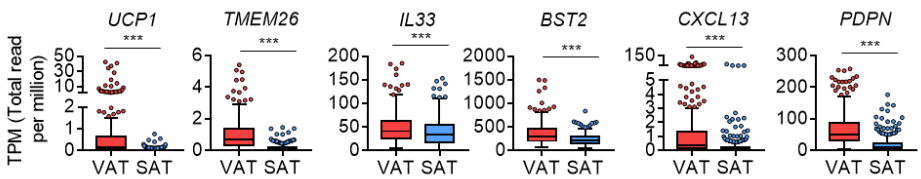


**Figure 20. Expression of markers of BST2$^{high}$ ASCs and thermogenic genes in human VAT and SAT**

Expression levels of UCP1, TMEM26, IL33, BST2, CXCL13, and PDPN in human VAT and SAT. Data from GTEx Portal (www.gtexportal.org).

# 5. Discussion

Basically, mouse EAT and IAT exhibit a similar appearance with lipid storage function under room temperature. However, emerging evidence suggests that EAT and IAT have distinct features in the regulation of energy homeostasis under certain metabolic stimuli [157, 158, 176]. Further, human epidemiological studies have shown that anatomical distribution of fat tissues, rather than whole-body fat mass, appears to be critical in metabolic diseases [354, 355].

In this study, I analyzed white and beige adipogenesis of EAT and IAT ASCs in response to metabolic stimuli at the single-cell resolution. Several lines of evidence suggest that the distinct properties of ASC subpopulations would determine fat depot-specific adipogenesis. First, side-by-side comparison and transplantation experiments revealed that the intrinsic features of $DPP4^{+}$ ES1 and IS1 ASCs would primarily determine their adipogenic potential. Second, at the onset of obesity, $DPP4^{+}$ ES1-specific proliferation stimulated by FGF and TGFβ signaling would induce EAT-selective *de novo* adipogenesis. Consistent with these, it has been reported that *Fgf1* whole-body knockout mice exhibit dysregulated fat expansion in obesity [356]. Lastly, IAT-specific $BST2^{high}$ ASCs appeared to be pivotal in IAT-selective beige adipocyte biogenesis. Collectively, these data suggest that the distinct properties of ASC clusters from EAT and IAT would determine the fat depot-specific adipogenesis and metabolic features.

Notably, ASC hierarchy is important to understand the regulatory mechanisms of *de novo* adipogenesis in WAT. Although recent reports have shown the ASC hierarchy in either EAT or IAT [75, 273, 321, 357, 358], comparative analysis of EAT and IAT ASC hierarchy and analysis of fat depot-specific regulatory

mechanisms of ASC hierarchy have not been attempted. In this study, current data showed that mouse EAT and IAT ASCs and their human counterparts seemed to be largely categorized into three adipogenic stages. Nevertheless, gene expression profiles and cell populations in ASC clusters of each stage of EAT and IAT ASCs were strikingly different. ES1 ASCs consisted of about 15% of EAT ASCs, whereas IS1 ASCs were composed of more than 60% IAT ASCs, implying that regulatory mechanisms of ASC maintenance and differentiation, including preadipocyte commitment, might be differently regulated in EAT and IAT ASCs. Transplantation experiments revealed that ES1 ASCs were innately prone to differentiation into ES2 and ES3 committed preadipocytes, whereas IS1 ASCs would be less likely to differentiate into IS2 and IS3 committed preadipocytes, probably due to intrinsic factors such as WNT signaling in IS1 ASCs. In line herewith, a genome-wide association study showed that single nucleotide polymorphisms in the promoter and enhancers of the *Wnt2* gene were related to the waist-to-hip ratio in humans. Together, these data suggest that the intrinsic features of ASC clusters in EAT and IAT would be primary drivers of fat depot-selective ASC hierarchy and *de novo* adipogenesis.

Thermogenic beige adipocyte precursors in IAT would be distinct from white adipocyte precursors in EAT [19, 31, 132, 348-350, 359]. I found that IAT-specific BST2$^{high}$ ASCs would serve as beige adipocyte precursors. IAT-specific BST2$^{high}$ ASCs had distinct molecular profiles and progressed into different cell fates from other IAT ASCs. IAT-specific BST2$^{high}$ ASCs highly expressed *Cxcl13*, *Il33*, and beige adipocyte precursor marker genes, including *Tmem26* [132]. It is noteworthy that BST2$^{high}$ ASCs were enriched near LNs. Through LN dissection experiments, I showed that IAT LN would potentiate BST2$^{high}$ ASC biogenesis. It is

plausible to speculate that IAT-specific BST2$^{high}$ ASCs might recruit immune cells such as type 2 innate lymphoid cells through IL33 secretion, which is important for beige fat formation [142, 144, 360-362]. In accordance with these, human thermogenic beige adipocytes are abundant in the neck and supraclavicular regions, where LNs are rich [30]. Given that human LNs are abundant in VAT, but rare in SAT, human LNs near fat depots might also contribute to beige adipocyte biogenesis upon cold exposure [353]. Thus, these data proposed that IAT-specific BST2$^{high}$ ASCs would be important for the formation of IAT-specific thermogenic adipocytes and that IAT LN would be involved in thermogenesis through enrichment of IAT-specific BST2$^{high}$ beige precursors. Nonetheless, further studies are clearly needed to elucidate the detailed mechanism(s) by which LN could influence BST2$^{high}$ ASCs in IAT.

In conclusion, I examined and scrutinized heterogeneous ASCs in two white fat depots and elucidated specific ASC clusters that contribute to fat depot-selective white and beige adipogenesis. I found that the distinct features of fat depot-specific ASC clusters would be pivotal to pathophysiological features of EAT and IAT upon metabolic stimuli.

**Limitation of study**

The primary goal of this study was to identify and characterize fat depot-specific ASC clusters through comparative analyses. Although I extensively analyzed white and beige adipogenesis in EAT and IAT, exclusive investigations of these ASC clusters-such as selective removal or *in vivo* lineage tracing until the formation of adipocytes-were not performed. In addition, I could not exclude the possibility that

surgical interventions, such as transplantation or LN dissection, might damage or affect the features of adipose tissue. Also, investigations using genetically modified animal models will be informative to uncover the pathophysiological significance of each ASC cluster in systemic energy homeostasis.

# CHAPTER TWO:

# Identification of Fibrotic SDC1$^{+}$ ASCs in VAT and Anti-Inflammatory CXCL14$^{+}$ ASCs in SAT

# 1. Abstract

In obese mice, expanded EAT exhibits chronic low-grade inflammation and fibrosis, whereas these phenomena are not largely manifested in IAT. Although heterogeneous ASCs could play key roles to confer fat depot-specific characteristics, it is largely unknown which ASC subpopulations would mediate distinct fibro-inflammatory features of EAT and IAT. In this study, I identified fat depot-selective ASC subpopulations and investigated their roles in adipose tissue inflammation and fibrosis. In obese EAT, scRNA-seq analysis revealed a certain ASC cluster showing fibrotic fate with high expression of *Sdc1*. EAT-specific SDC1$^{+}$ ASCs expressed numerous fibrotic genes and myofibroblast markers and they enriched in CLS, implying that obese EAT-specific cell-to-cell interaction would mediate the formation of SDC1$^{+}$ ASC. On the contrary, IAT-specific CXCL14$^{+}$ ASCs suppressed inflammation and macrophage accumulation, probably, by suppressing CXCL12 activity. Taken together, these data suggest that EAT-specific SDC1$^{+}$ ASCs and IAT-specific CXCL14$^{+}$ ASCs would modulate fibro-inflammatory features in a fat depot-specific manner in obesity.

# 2. Introduction

In mammals, WAT is a major energy storage site and has tremendous expansion capacity compared to other organs. Prolonged energy surplus state greatly increases the size of WAT. During obesity-induced expansion, WAT undergoes various remodeling processes including low-grade, chronic inflammation, hypoxia, oxidative stress, and fibrosis, which are key mediators linking obesity to systemic insulin resistance and metabolic complications [1, 193]. In obesity, accumulated pro-inflammatory immune cells such as M1-like macrophages in WAT can repress insulin action by secreting cytokines such as TNFα [87]. In addition, it has been suggested that fibrotic activation of ASC could promote ECM deposition, alter mechanical cues, and impair adipocyte function [227].

Detrimental features of obese WAT including inflammation and fibrosis obviously appear in VAT such as EAT, whereas these are not largely occurred in SAT such as IAT [1, 76, 126, 363]. In this regard, accumulation of VAT is a high-risk factor of metabolic diseases, whereas SAT would have metabolically beneficial roles [157]. Thus, a proper understanding of the differences in inflammatory and fibrotic responses between VAT and SAT has been one of the major aims in obesity research.

Various cell types including adipocytes, immune cells, and ASCs could modulate inflammation and fibrosis in WAT. Among them, it has been suggested that distinct properties of ASCs would contribute to distinct degrees of obesity-induced inflammatory and fibrotic features of EAT and IAT. IAT ASCs seem to actively repress macrophage infiltration and inflammatory responses via secreted molecules, while EAT ASCs in obese mice could secrete pro-inflammatory cytokines and aberrant ECM molecules such as collagen, thereby upregulating inflammation and

fibrosis [108, 115, 193].

Recent studies have proposed that ASCs are composed of several subpopulations with distinct fibro-inflammatory features. It has been reported that $CD9^+$ ASCs are increased in obesity and highly express genes related to fibrosis [108, 115]. In addition, certain ASC subpopulations seem to secrete high amounts of IL-33 and participate in $T_{reg}$ maintenance [313]. Nevertheless, the heterogeneity of ASCs in the aspect of fat depots and obesity has not been thoroughly examined.

In this study, by adopting scRNA-seq, I was able to identify fat depot-specific ASC clusters that were important for WAT inflammation and fibrosis in obesity. Obesogenic stimuli induced the formation of EAT-specific $SDC1^+$ ASC in EAT, which could promote inflammation and fibrosis. On the contrary, IAT-specific $CXCL14^+$ ASCs suppressed inflammation and macrophage infiltration, probably, by suppressing CXCL12 activity. Collectively, this study proposes the significance of ASC subpopulations in determining fat depot-selective regulation of inflammatory and fibrogenic responses in obesity.

# 3. Materials and Methods

### Animals

Eight-to-ten-week-old C57BL/6 mice were purchased from Central Lab Animal Incorporation (Seoul, Korea). The mice were housed in a specific pathogen-free, temperature- and humidity-controlled animal facility at 22 °C under a 12-h/12-h light/dark cycle. High-fat diet feeding experiments were performed using 8-week-old mice fed a diet consisting of 60% calories from fat (D12492, Research Diets). For *in vivo* Cxcl14 suppression, NCD- and 10-week HFD-fed mice received a dose of 20 μg/single IAT pad of control siRNA (siNC) or siCxcl14 complexed with *in vivo*-jetPEI (Polyplus Transfection, Cat# 201-50G) every 3 days for 2 weeks [322]. Control siRNA was injected into IAT in the left flanks and siCxcl14 was injected into IAT in the right flanks. 2 weeks after siRNA injection, $GFP^+$ blood mononuclear cells were intravenously injected into mice and sacrificed on the following day. The animal study was approved by the Institutional Animal Care and Use Committee of the Seoul National University.

### scRNA-seq Library Preparation

scRNA-seq libraries were generated using the Chromium Single Cell 3' Library & Gel Bead Kit (PN-1000092, 10X Genomics), Chromium Single Cell B Chip kit (PN-1000074, 10X Genomics), and Chromium i7 Multiplex Kit (PN-120262, 10X Genomics). Cells were resuspended in reverse transcription enzyme mix and loaded onto the Chromium Single Cell B Chip to generate gel beads-in-emulsion of 6,000 cells per channel. Reverse transcription was performed using a Bio-Rad C1000 Thermal Cycler. cDNA purification and library generation were performed

according to the manufacturer's instructions. Libraries were sequenced on an Illumina NovaSeq 6000 instrument (paired-end 100-bp reads), with an average of 50,000 read pairs per cell.

**scRNA-seq Data Processing**

Raw reads were mapped to a mouse reference genome (GRCm38) using the Ensembl GRCm38.95 GTF file and the Cell Ranger software (v3.0.2). For each sample, a gene-by-cell count matrix was generated with default parameters, except for expected cells = 6000. Using the emptyDrops function of the DropletUtils (v1.6.1) R package (Lun et al., 2019) with a false discovery rate (FDR) < 0.01, empty droplets were removed. To filter out low-quality cells, cells with >5% (EAT NCD, EAT 10-week HFD, and IAT NCD) or >3% (EAT 2-week HFD, IAT 2-week HFD, IAT 10-week HFD) of unique molecular identifiers (UMIs) assigned to mitochondrial genes, <1,000 total UMI counts, or <1,000 detected genes were excluded using the calculateQCMetrics function of the scater (v1.14.6) R package (McCarthy et al., 2017). To normalize cell-specific biases, cells were clustered using the quickCluster function of the scran (v1.14.6) R package (Lun et al., 2016). Then, cell-level size factors were calculated using the computeSumFactors function of the same package. Raw UMI counts were normalized by size factors and then log2-transformed with a pseudocount of 1. Highly variable genes (HVGs) were identified using the modelGeneVar function of the scran package, with FDR < 0.05 for biological variability. All cells across the fat depot and diet conditions were clustered into 17 clusters using the FindClusters function of the Seurat (v3.2.3) R package (Stuart et al., 2019) on the first 15 principal components (PCs) of HVGs with resolution = 0.8.

Cells were visualized in a two-dimensional UMAP plot using the RunUMAP function of the same package. Two clusters (clusters 14 and 16) annotated as immune cells and mesothelial cells were removed. Cells from EAT samples were further clustered using the method described above with the top 10 PCs. Cluster 12, annotated as testis cells, was removed. All remaining cells were visualized in the UMAP plot from the top 15 PCs. Cells in the normal chow diet were grouped into 11 clusters and visualized in the UMAP plot using the above method, with the top 25 PCs of 1,000 HVGs.

**scRNA-seq Data Analysis**

Stage-specific marker genes were identified using the FindAllMarkers function of the Seurat package, with default parameters. Pseudotime analysis was performed for each condition using the run_palantir function of the Palantir (v0.2.6) python package (Setty et al., 2019). For Palantir t-SNE plots in the EAT and IAT samples, batch effects across diet conditions were corrected using the run_harmony function of the Harmonypy (v0.0.4) Python package on 300 PCs (Korsunsky et al., 2019). Then, a k-NN graph (k = 30) was constructed from the first 10 DCs. The coordinates for the t-SNE plots were computed using the run_tsne function with perplexity = 400 (for EAT) or 300 (for IAT). To identify differentially expressed genes (DEGs) between the two fates, cells from EAT samples were grouped into early (0–0.35), intermediate (0.35–0.75), or late (0.75–1), according to their pseudotime. Cells were assigned into one of two differentiation fates by binomial sampling based on branch probabilities, which were calculated for each cell using the run_palantir function. DEGs between the two fates were identified for each pseudotime stage (early,

intermediate, and late) using the FindAllMarkers function of the Seurat package. Signaling pathway activity for each cluster was inferred using the progeny function of the progeny (v1.12.0) R package (Schubert et al., 2018). For Monocle2 trajectory analysis, batch effects across diet conditions were corrected using the reduceDimension function of the monocle2 (v2.14.0) R package (Qiu et al., 2017), regressing out the number of total UMIs and detected genes.

**Adipose Tissue Fractionation**

EAT and IAT were obtained from age-matched NCD-fed and 2- or 10-week HFD-fed mice. Adipose tissues were fractionated as described previously (Jeon et al., 2020). Briefly, adipose tissues were minced and digested with collagenase buffer [0.1 M HEPES, 0.125 M NaCl, 5 mM KCl, 1.3 mM CaCl2, 5 mM glucose, 1.5% (w/v) bovine serum albumin, and 0.1% (w/v) collagenase I (Worthington, 49A18993)] in a shaking water bath at 37 °C for 30–60 min. After centrifugation at 200 × g, room temperature (RT) for 5 min, the pelleted stromal vascular fraction (SVF) was collected. The SVF was incubated in red blood cell lysis buffer (1.7 M Tris, pH 7.65, and 0.16 M NH4Cl) for 15 min. Then, the SVFs were washed with phosphate-buffered saline (PBS) several times, passed through a 100 μm filter (93100, SPL), and collected by centrifugation at 200 × g for 5 min.

**Fluorescence-Activated Cell Sorting (FACS)**

FACS was carried out as previously described with minor modifications [193]. SVFs were stained with anti-CD31 (1:100, 102405, 102409 and, 102419 BioLegend), anti-CD45 (1:100, 103107, 103111, and 103131, BioLegend), anti-DPP4 (1:100, 137809,

BioLegend), anti-ICAM1 (1:100, 116107, BioLegend), anti-SDC1 (1:100, MA5-23527, Thermo Fisher), anti-CD9 (1:100, 124811, BioLegend) for 30 min. The cells were analyzed using a FACS Canto II instrument (BD Biosciences).

**Immunocytochemistry and Immunohistochemistry**

Samples were incubated with fluorescently labeled Hoechst 33342 (ab228551, Abcam) and stained with fluorescein isothiocyanate-conjugated BODIPY 493/503 (D3922; Thermo Fisher Scientific). BODIPY staining was performed as previously with minor modifications [341]. Adipogenesis was assessed by staining with BODIPY 493/503 (D3922, Invitrogen) for lipid droplet accumulation and by staining with Hoechst 33342 for nucleus number at 8 days post induction (mouse cells) and 2 weeks post induction (human cells) in individual wells. The cells were imaged using a CQ1 microscope (Yokogawa).

Whole-mount imaging was carried out as previously with minor modifications [100]. A small fraction of fat tissue was fixed in 4% paraformaldehyde for 30 ~ 60 min and permeabilized with 0.1% Triton X-100 in PBS for 5 min. The fixed tissues were incubated with a primary antibody against SDC1 (112502; Biolegend, 1:200~1:500), PDGFRα (135902; Biolegend, 1:200~1:500), and F4/80 (157301; Biolegend, 1:200~1:500) overnight. The tissues were then washed three times for 10 min each, incubated with secondary antibody for 1 h, washed three times for 5 min each, and stained Hoechst 33342. Tissues were observed and imaged using a CQ1 microscope (Yokogawa). Immunohistochemistry imaging of formalin-fixed, paraffin-embedded tissue section was carried out as previously with minor modifications [364]. Fat tissue was fixed in 4% paraformaldehyde for several days

and embedded in a paraffin block. Slices cut from paraffin-embedded fat tissues were deparaffinized in xylene and rehydrated in a graded series of ethanol solutions, and stained with (1) hematoxylin and eosin (2) Masson's trichrome (3) primary antibodies. Sections were blocked with 3% horse serum. Sections were incubated with a primary antibody against SDC1 (112502; Biolegend, 1:200~1:500), ACTA2(14-9760-82; Invitrogen, 1:200~1:500), and PDGFRα (135902; Biolegend, 1:200~1:500) overnight. The tissues were then washed three times for 30 min each, incubated with secondary antibody for 4 h, washed three times for 10 min each, and mounted with cover glass. Tissues were observed and imaged using a CQ1 microscope (Yokogawa). H&E and Trichrome stained sections were imaged using a digital slide scanner (Axio Scan Z1, Carl Zeiss).

**Cell Culture**

ASCs were seeded in 96-well plates at 3,000 cells/well and cultured in DMEM containing 10% FBS for two days until confluence. For adipogenic differentiation, the cells were incubated in adipogenic media (1 μM dexamethasone, 520 μM IMBX, 850 nM insulin, and 1 μM rosiglitazone). Two days after adipogenic induction, the culture medium was replaced with FI medium (850 nM insulin and 1 μM rosiglitazone), and the cells were analyzed after 8–10 days of differentiation.

**siRNA Treatment**

siRNAs were purchased from Bioneer Inc. (Daejeon, South Korea). Cells were mixed with siRNA or vectors and transfected with a single pulse of 1100 V for 30 ms using a Microporator MP-100 (Digital Bio, Seoul, Korea) according to the

manufacturer's instructions.

**RT-qPCR**

Total RNA was isolated using Direct-zol™ RNA MiniPrep (Zymo Research). The RNA was reverse-transcribed using the ReverTra Ace qPCR RT Kit (Toyobo). RT-qPCRs were run using SYBR Green master mix (DQ384-40h, Biofact). Target gene expression levels were normalized to Tbp expression.

**Conditioned media treatment to SVFs**

For preparation of CM, adipocytes and SVFs were isolated from IAT and EAT of HFD-fed mice. Adipocytes and SVFs were incubated in DMEM containing 10% FBS for 24 h and CM was collected. Both adipocytes CM and SVF CM were normalized by fat mass (5 ml of media per adipocytes and SVFs from 1 g of fat tissue). Conditioned media was treated to SVFs were isolated from and EAT of NCD mice and exrpessio of *Sdc1* and *Tnc* was analazed by RT-Qpcr.

**Monocyte Migration Assay**

*In vitro* monocyte migration was performed using THP-1 monocytes. For CM preparation, chopped fat tissues or IAT ASCs were incubated in serum-free DMEM for 24 h and CM was harvested. CM from fat tissue was normalized by fat mass (5 ml of media per 1 g of fat tissue). Synthetic CXCL12 or CXCL14 peptides were dissolved in serum-free DMEM. In CM experiments. THP-1 cells were pre-stained with 2 μM of CellTrackerTM-Red CMTPX (C34552; Thermo Fisher Scientific) to distinguish THP-1 cells and cells from CM. In each sample group, 2 x 10^5 (per well

of the 6-well culture plate) or 5 x 10^4 (per well of the 24-well culture plate) THP-1 cells were loaded on the surface of the upper layer of Trans-well insert. 4 ~ 12 hours after incubation, the upper layer and Trans-well insert were carefully removed. Migrated THP-1 cells were stained with Hoechst dye (H3570; Thermo Fisher Scientific) and quantified using the CQ1 confocal microscope.

*In vivo* monocyte infiltration was performed using $GFP^+$ blood mononuclear cells. To isolate blood mononuclear cells from GFP-Tg mice, blood was collected by heart puncture and mixed with 20 μL of 0.5 M EDTA. Blood samples were pooled in a Greiner Leucosep tube (GN163290, Sigma Aldrich) pre-equilibrated with 3 mL of NycoPrep 1.077 (1114550, Axis-Shield PoC AS). After centrifugation at 2,500 rpm for 10 min, the middle layer was carefully isolated and washed with RoboSep buffer (20104, STEMCELL Technologies). Mononuclear cells in RoboSep buffer were intravenously injected into mice. 1 day after GFP+ blood mononuclear cell injection, fat tissues were subjected to FACS analysis.

**Statistical Analysis**

Data are presented as the mean ± standard deviation (SD). n-Values indicated in the figures refer to biological replicates. Means of two groups were compared using a two-tailed Student's t-test. Means of multiple groups were compared using one-way ANOVA followed by Tukey's post-hoc test. Two independent variables were compared using two-way ANOVA followed by Sidak's multiple comparisons test. Statistical analyzes were performed using GraphPad Prism (GraphPad Software).

Table 3. Primer sequences in Chapter II

| Primers for qRT-PCR | | | |
|---|---|---|---|
| Species | Gene | Forward | Reverse |
| Mouse | *Tbp* | GGGAGAATCATGGACCAGAA | CCGTAAGGCATCATTGGACT |
| | *Sdc1* | CAAGGAAAAGGAGGTCACCA | CTGATTGGCAGTTCCATCCT |
| | *Acta2* | GTCCCAGACATCAGGGAGTAA | TCGGATACTTCAGCGTCAGGA |
| | *Col1a1* | GAGCGGAGAGTACTGGATCG | GCTTCTTTTCCTTGGGGTTC |
| | *Col8a1* | TGAGATGCCTGCGTTTACTG | TGTGTACATCATGGGCTCGT |
| | *Tgfb1* | CTTCAATACGTCAGACATTCGGG | GTAACGCCAGGAATTGTTGCTA |
| | *Tnc* | ACGGCTACCACAGAAGCTG | ATGGCTGTTGTTGCTATGGCA |
| | *Adipoq* | GGCAGGAAAGGAGAACCTGG | AGCCTTGTCCTTCTTGAAGAG |
| | *Pparg2* | GCATGGTGCCTTCGCTGA | TGGCATCTCTGTGTCAACCATG |
| | *Plin1* | GATCGCCTCTGAACTGAAGG | CTTCTCGATGCTTCCCAGAG |
| | *Cxcl12* | TGCATCAGTGACGGTAAACCA | TTCTTCAGCCGTGCAACAATC |
| | *Cxcl14* | GAAGATGGTTATCGTCACCACC | CGTTCCAGGCATTGTACCACT |
| Human | *CXCR4* | GAAGCTGTTGGCTGAAAAGG | TGGAGTGTGACAGCTTGGAG |
| | *GAPDH* | CCACTCCTCCACCTTT | ACCACCCTGTTGCTGT |

# 4. Results

**In obesity, EAT-specific SDC1$^+$ ASCs regulate inflammation and fibrosis**

In obesity, high levels of inflammation and fibrosis were observed in EAT but not in IAT (Figure 21A). Given that ASCs highly expressed fibrotic genes such as collagens compared to other WAT composing cells such as adipocytes, immune cells, and endothelial cells (Figures 21B-D), I attempted to identify EAT ASC subpopulations that would mediate fibro-inflammatory features in obesity. Two independent pseudotime analyses showed that there appeared to be two different fates of EAT ASCs in obesity (Figures 22A and 22B). The terminal of EAT Fate 1 with the $E_{NH}10$ cluster, was observed only after a 10-week HFD. $E_{NH}10$ cluster highly expressed genes related to extracellular matrix organization and inflammation, such as *Col1a1*, *Ccn2* (*CTGF*), and *Ccl2* (*MCP1*) (Figures 22C and 22D). Pathway analysis showed that TGFβ signaling would be enhanced in EAT Fate 1 (Figure 22E). At the end of EAT Fate 2, with clusters $E_{NH}3$ and $E_{NH}11$, adipocyte differentiation-related genes, such as Cebpd, Igf1, and type IV collagens [286, 365], were enriched (Figures 22C and 22F), indicating that EAT Fate 2 would reflect the adipogenic pathway. In contrast to EAT, pseudotime analysis shows that IAT ASCs did not branch into different fates upon obesogenic stimuli (Figure 22F). Rationally, it seemed that the fate of IAT ASC would be closer to EAT Fate 2 compared to EAT Fate 1 as adipogenesis could occur in both EAT and IAT.

In $E_{NH}10$ fibro-inflammatory cluster, I identified that surface marker syndecan 1 (*Sdc1*) was abundantly expressed (Figure 23A). Consistent with scRNA-seq data, FACS analysis showed that SDC1$^+$ ASCs were predominant in EAT upon HFD feeding (Figure 23B). SDC1$^+$ ASCs expressed higher levels of fibrogenic genes

compared to SDC1$^-$ ASCs (Figure 23C). Previously, it has been reported that CD9$^+$ ASCs are pro-fibrogenic cells in EAT [108, 115]. In this regard, I decided to investigate the relationship between CD9$^+$ ASCs and SDC1$^+$ ASCs. As shown in Figures 23D and 23E, SDC1$^+$ ASCs were part of CD9$^+$ ASCs, implying that SDC1$^+$ ASCs might mediate the fibro-inflammatory features of CD9$^+$ ASCs as a subpopulation. Further, I found that SDC1$^+$ ASCs exhibited lower adipogenic potential compared to SDC1$^-$ ASCs (ICAM1$^+$ DPP4$^-$ ES3) (Figure 23F). These data suggested that EAT-specific SDC1$^+$ fibro-inflammatory ASCs would contribute to EAT-selective fibro-inflammatory remodeling in obesity.

CLS is a key histological feature of obesity-induced adipose tissue inflammation and fibrosis [105, 106] (Figures 24A and 24B). To test whether SDC1$^+$ ASCs might be located in CLS, histological experiments were adopted. In both whole-mount staining and immunohistochemistry of the formalin-fixed, paraffin-embedded section, SDC1$^+$ ASCs were detected in CLS (Figures 24C and 24D). These results suggested that SDC1$^+$ ASC might be involved in obesity-induced inflammation and fibrosis of WAT.

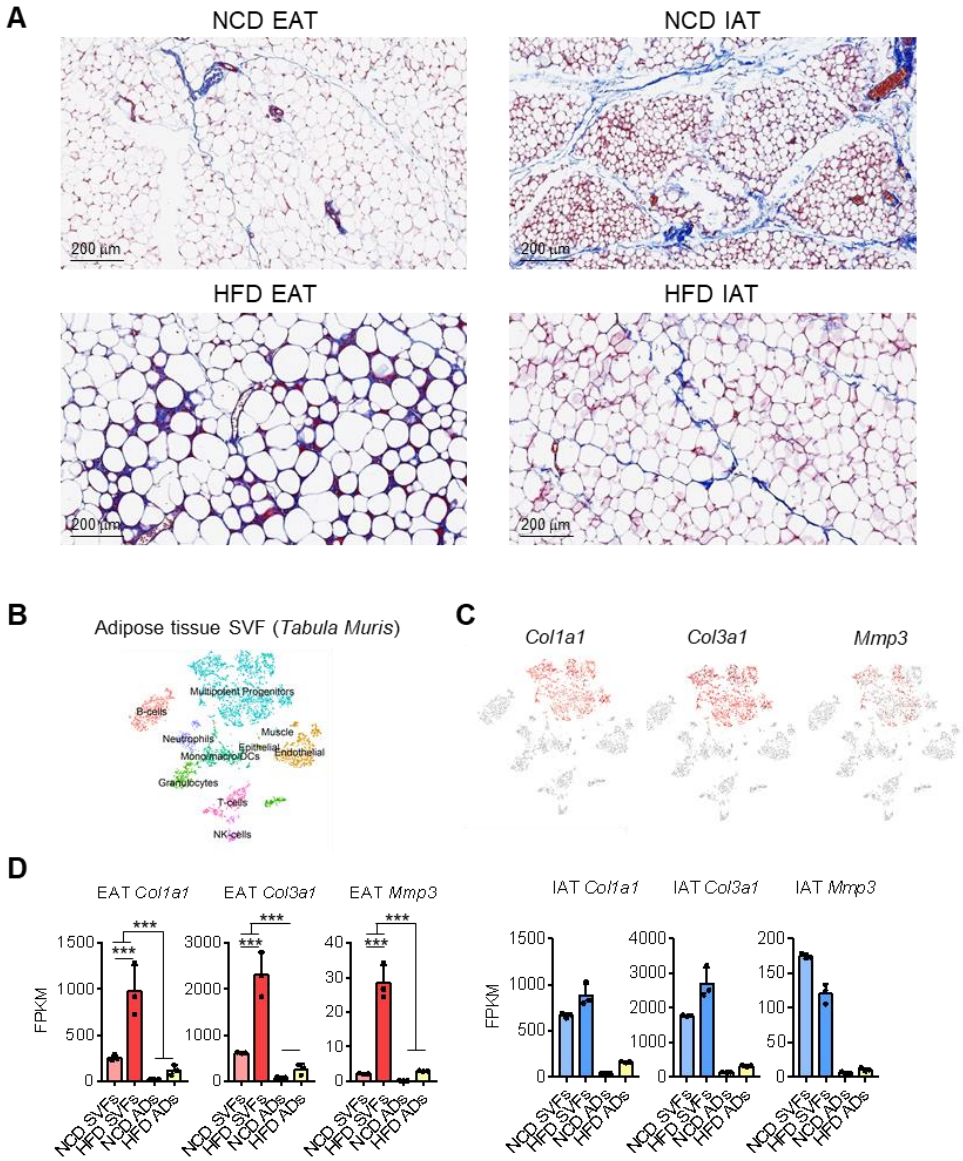


**Figure 21. Obesity induces high levels of fibrosis in EAT, but not in IAT**

(A) Trichrome staing of EAT and IAT in 16 week HFD-fed mice

(B) UMAP plot of adipose tissue SVFs. Data from Tabula Muris compendium.

(C) Expression levels of Col1a1, Col3a1, and Mmp3 on a UMAP plot. These genes are enriched in multipotent progenitors.

(D) FPKM value of Col1a1, Col3a1, and Mmp3 in SVFs and adipocytes (ADs) of NCD or 10 week HFD-fed mice. n = 3.

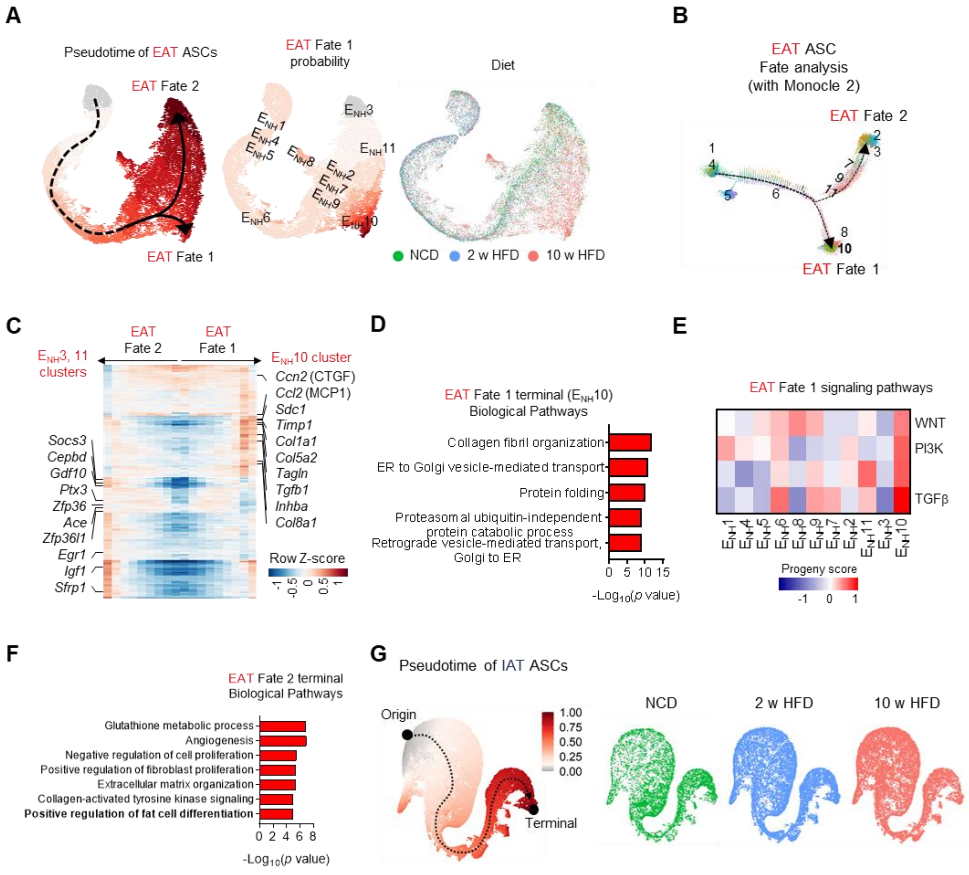


**Figure 22. Obesity induces new fate of ASCs in EAT but not in IAT**

(A) In silico pseudotime analysis and EAT Fate 1 probabilistic analysis of EAT ASC from NCD, 2 w HFD and 10 w HFD-fed mice. Pseudotime (arbitrary units) is depicted from white to red.

(B) In silico pseudotime analysis of EAT ASCs from NCD, 2 w HFD and 10 w HFD-fed mice by Monocle 2.

(C) Split heatmap of upregulated genes along EAT Fate 1 or Fate 2.

(D) Gene ontology of EAT Fate 1 enriched genes.

(E) Pathway analysis of upregulated genes along with EAT Fate 1.

(F) Gene ontology of EAT Fate 2 enriched genes.

(G) In silico probabilistic fate analysis on IAT ASC from NCD, 2 w HFD and 10 w HFD-fed mice. A single fate existed.

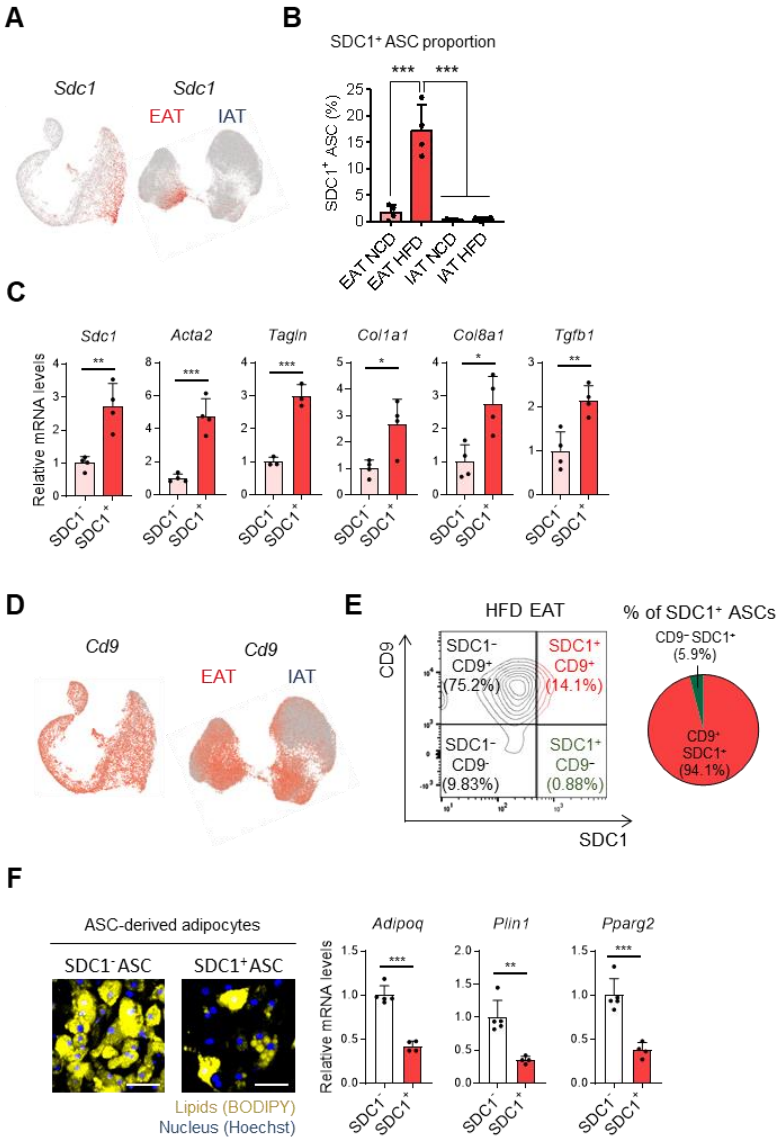


**Figure 23. In obesity, EAT-specific SDC1$^+$ ASCs mediate fibrosis**

(A) Gene expression levels of Sdc1.

(B) Proportion of SDC1+ cells from NCD and 15 w HFD-fed mice. n = 3~4.

(C) mRNA levels of fibrotic genes in SDC1$^+$ and SDC1$^-$ ASCs. n = 3.

(D) Expression levels of Cd9.

(E) (Left) Representative FACS plots of CD9 and SDC1 expression of EAT ASCs in 10 week HFD-fed mice. (Right) FACS-based proportion of CD9-SDC1+ (5.9%) and CD9+SDC1+ (94.1%) of total SDC1+ ASCs.

(F) (Left) Representative image of BODIPY lipid staining of differentiated SDC1$^+$ and SDC1$^-$ (DPP4$^-$ ICAM1$^+$) ASCs. (Right) mRNA levels of *Adipoq*, *Plin1*, and *Pparg2* genes in differentiated SDC1$^+$ and SDC1$^-$ ASCs. n = 3.

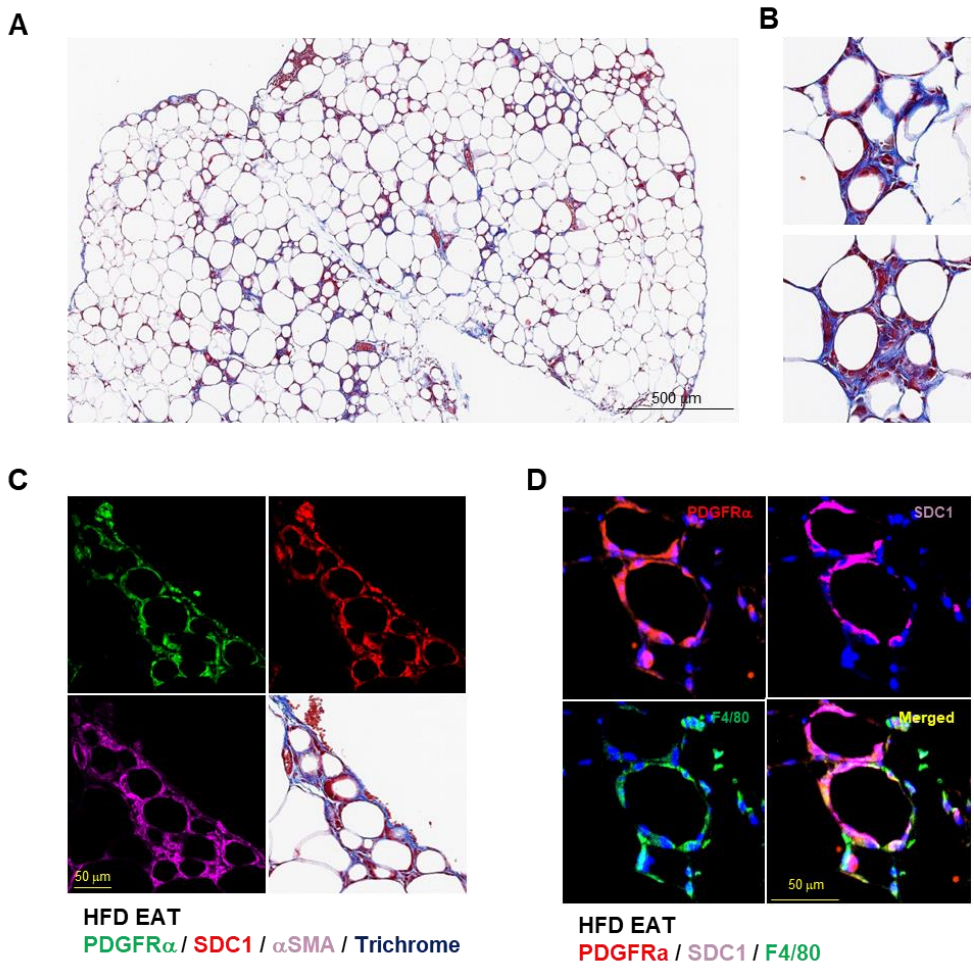


**Figure 24. SDC1$^+$ ASCs are observed in the fibrotic region near crown-like structure**
(A) Trichrome staining images of EAT upon 16 week HFD.
(B) Representative images of crown-like structure.
(C) Representative trichrome staining and immunohistochemistry images of EAT upon 16 week HFD, stained with PDGFRα, SDC1, and αSMA.
(D) Representative immunohistochemistry images of EAT upon 16 week HFD, stained with PDGFRα, SDC1, and F4/80.

**Inflammation induces the formation of SDC1$^+$ ASC**

Next, I investigated the underlying mechanism by which SDC1$^+$ ASCs could be generated in obese EAT. To test the possibility that SDC1$^-$ ASCs might be the source of SDC1$^+$ ASCs, trajectory analysis was performed on the ASCs from 10w HFD EAT. Through this, SDC1$^+$ ASC cluster ($E_H5$, H denotes HFD), and transitional cell types of SDC1$^+$ ASC ($E_H4$) cluster were identified (Figure 25A and 25B). Transcription factor activity analysis using SCENIC showed that several transcription factors, including Nfatc1 and Runx1, exhibited high activity in $E_H4$ and $E_H5$ (SDC1$^+$ ASCs) clusters (Figure 25A and 25B). Consistently, it has been reported that Nfatc1 and Runx1 could induce fibrosis, implying that activation of transcription factors such as Nfatc1 and Runx1 might contribute to the formation of SDC1$^+$ ASCs in obese EAT [366-368].

Inflammation is the most well-known inducer of fibrosis in various organs and diseases [318]. As SDC1$^+$ ASCs were localized in CLS, which contains various inflammatory immune cells (Figures 24C and 24D), I raised the question that enhanced inflammation might be linked to the formation of SDC1$^+$ ASC. To address this, I investigated the temporal kinetics of SDC1$^+$ ASC appearance in obesity. While inflammation rapidly occurs in EAT, even in the early stages of HFD feeding, SDC1$^+$ ASCs were observed after 10w HFD, relatively late stages of HFD (Figure 26A and B) [369]. Next, I investigated the roles of immune cells in the formation of SDC1$^+$ ASC in obese EAT. To resolve this, CM from adipocytes and SVFs in EAT and IAT of HFD-fed mice were treated to plate-attached SVFs from EAT of NCD-fed mice (Figure 26C). Secreted factors from HFD EAT SVFs increased marker genes of SDC1$^+$ ASCs (Figure 26D), which was not observed in other conditions (Figure 26D).

These findings suggest that adipose tissue inflammation might mediate the formation of $SDC1^+$ ASC in EAT.

To examine cell types and signaling molecules to recruit $SDC1^+$ ASC in EAT, I performed scRNA-seq of SVFs of EAT and IAT from NCD- and 16-week HFD-fed mice (Figure 27A). Clustering data revealed the formation of $SDC1^+$ ASCs in obese EAT but not in IAT (Figure 27B). Further, as immune cells such as macrophages were increased in obese EAT, it seemed that elevated macrophages could induce the formation of $SDC1^+$ ASC in EAT (Figure 27C). To test this idea, cell-to-cell interaction analysis was performed. As a result, there were enhanced interactions between ASCs and macrophages, with obese EAT-specific ligands (Figure 27D). Particularly, it appeared that SPP1-CD44 interaction was enhanced in obesity and could induce fibrosis in obese EAT (Figure 27D) [370, 371], implying that obesity-induced inflammation and altered immune cell characteristics might mediate the formation of $SDC1^+$ ASCs and fibrosis, probably through ligand-receptor interactions.

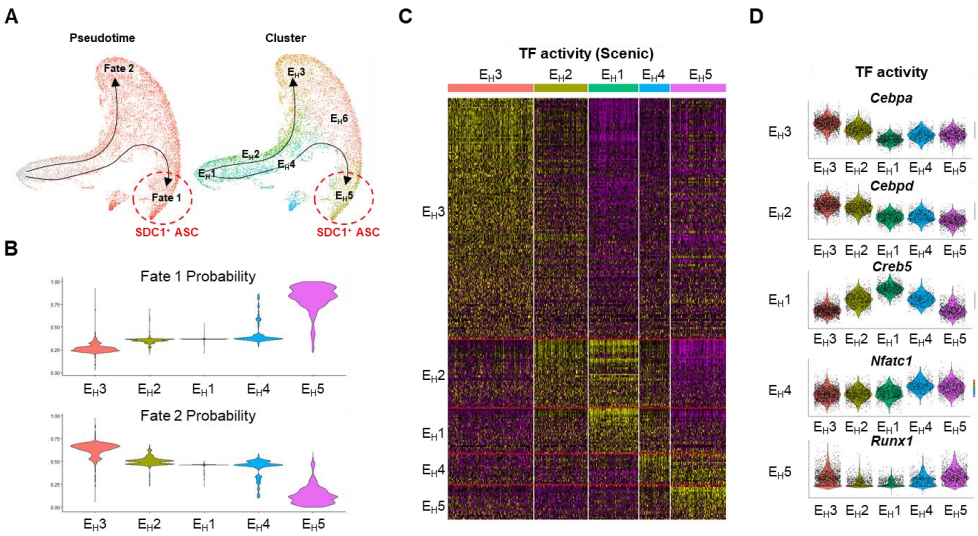


**Figure 25. Trajectory analysis reveals transcription factors that could mediate the formation of SDC1$^+$ ASC**

(A) In silico pseudotime analysis of EAT ASC from 10w HFD-fed mice. Pseudotime (arbitrary units) is depicted from white to red.

(B) Probability of Fate 1 and 2 in each cluster.

(C) Transcription factor (TF) activity analysis of EAT ASC from 10w HFD-fed mice.

(D) Representative TFs with differential acitivty

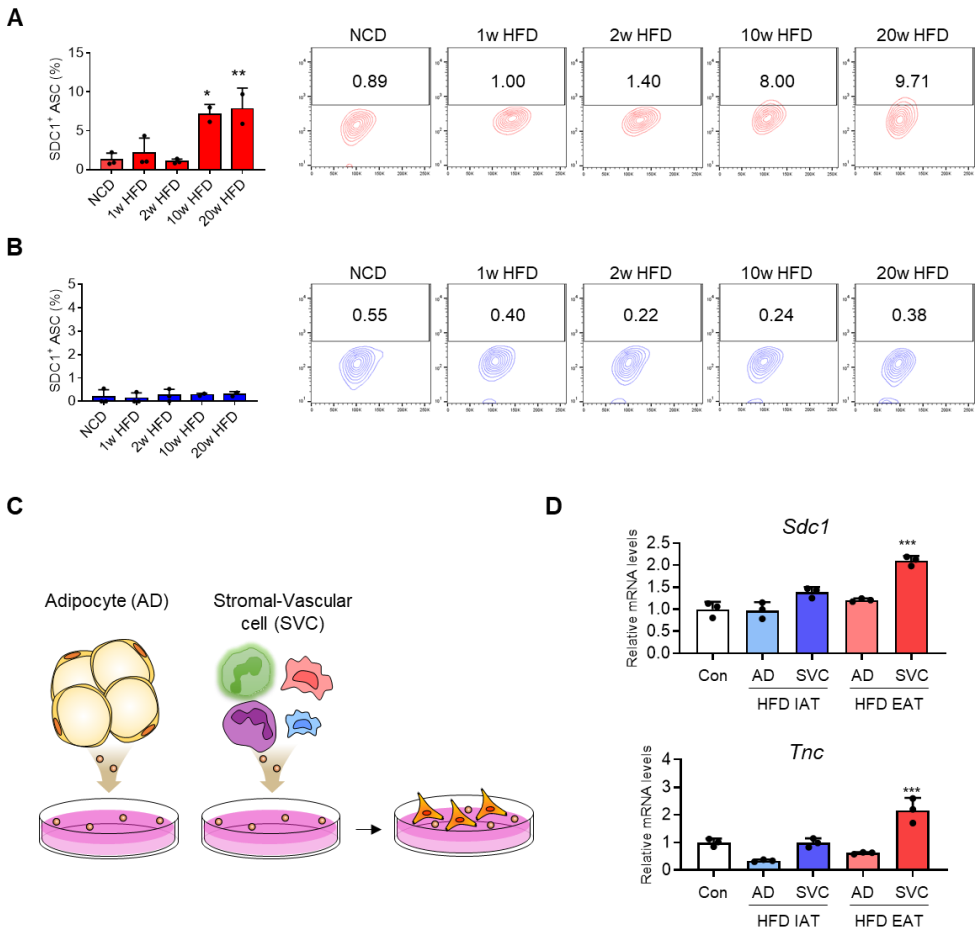


**Figure 26. SDC1$^+$ ASCs are observed in long-term, but not short-term HFD**

(A) Representative FACS plots and proportion of SDC1$^+$ ASCs in EAT upon HFD feeding

(B) Representative FACS plots and proportion of SDC1$^+$ ASCs in IAT upon HFD feeding

(C) Experimental scheme for conditioned media treatment

(D) mRNA levels of Sdc1 and Tnc in plate-attacehd EAT SVFs from NCD-fed mice after conditioned media treatment. Con: control.

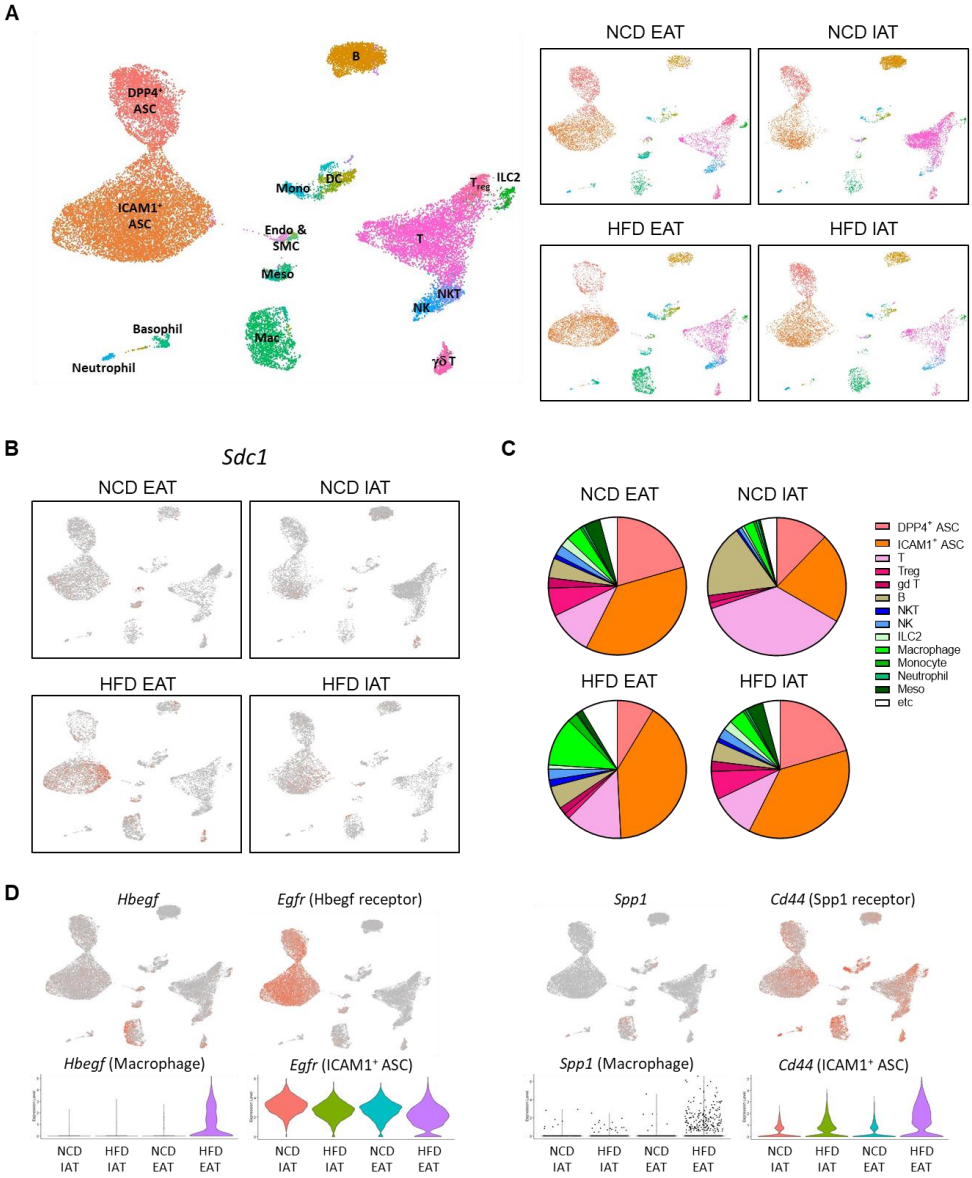


**Figure 27. scRNA-seq reveals potential cell-cell interaction which could mediate the formation of SDC1$^+$ ASCs in obese EAT**

(A) UMAP plot of SVFs in EAT and IAT from NCD- and 16 week HFD-fed mice

(B) Expression of *Sdc1* in each condition

(C) Proportion of cell type in each condition

(D) Candidiate ligand-receptor interaction strengthened in HFD EAT

**IAT-specific CXCL14$^+$ ASCs suppress monocyte infiltration and inflammation**

Unlike EAT, IAT exhibited relatively low levels of inflammatory responses and infiltrated immune cells such as macrophages in obesity (Figures 28A and 28B). It has been recently demonstrated that certain factors secreted from IAT ASCs could suppress monocyte infiltration in obesity [193]. To identify potential anti-inflammatory factor(s), I compared cytokine expression profiles of EAT and IAT ASCs. Compared to EAT ASCs, IAT ASCs selectively expressed CXCL14 (Figures 28C-E), which has been reported to act as an anti-inflammatory factor by inhibiting the CXCL12-CXCR4 pathway during monocyte migration [372, 373]. Consistent with previous reports, CXCL14 inhibited THP-1 monocyte migration mediated by CXCL12-CXCR4 axis (Figures 29A-29C).

In HFD-fed mice, CXCL12 expression was higher in EAT than IAT (Figure 30A). Also, the degree of monocyte infiltration was further elevated in CM from HFD EAT than CM from HFD IAT (Figure 30B). To test the question whether CXCL14 might be indeed involved in monocyte migration, CXCL14 peptides were incubated in CM from EAT and IAT from HFD-fed mice. As indicated in Figures 30B and 30C, CXCL14 peptides actively repressed monocyte migration via, at least partly, suppressing the CXCL12-CXCR4 axis. In addition, experiments with pharmacological inhibitors showed that ERK signaling would be involved in CXCL12-CXCR4-mediated monocyte migration (Figures 30D and 30E). Then, I investigated the effect of CXCL14 secreted from IAT ASC on monocyte infiltration. Knockdown of *Cxcl14* in IAT ASCs increased monocyte migration (Figures 31A and 31B). Further, suppression of *Cxcl14* in IAT, using *in vivo* siRNA injection [374], greatly elevated monocyte infiltration upon HFD (Figures 31C-31E). Together, these

data propose that high expression of CXCL14 in IAT ASCs could contribute to repressed pro-inflammatory responses in obese IAT compared to obese EAT, probably by suppressing CXCL12 activity.

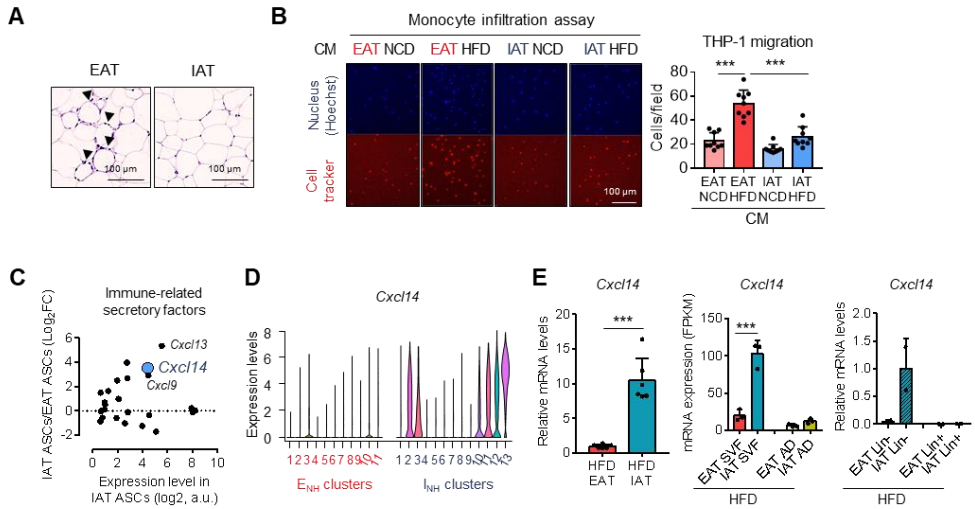


**Figure 28. Specific expression of CXCL14 in IAT ASCs**

(A) Representative histological images of EAT and IAT upon 10 week HFD. Arrows indicate crown-like structure. Scale bar: 100 μm.

(B) (Left) Representative images of monocyte infiltration with EAT or IAT CM from NCD or 10 week HFD-fed mice. (Right) Quantification of monocyte migration. Scale bar: 100 μm.

(C) Differentially expressed genes of immune-related secretory factors (CCLs, CXCLs, and ILs) in EAT and IAT ASC.

(D) A violin plot showing Cxcl14 expression levels in ASC clusters from EAT and IAT of NCD-, 2 week or 10 week HFD-fed mice.

(E) mRNA levels of Cxcl14. (Left) EAT and IAT from 10 week HFD-fed mice. n = 5. (Center) FPKM value in SVFs and adipocyte (AD) fraction from 10 week HFD-fed mice. n = 3. (Right) Sorted Lin$^-$ (CD31$^-$/CD45$^-$) ASCs in EAT and IAT from 10 week HFD-fed mice. 2~3 mice were pooled to each sample.

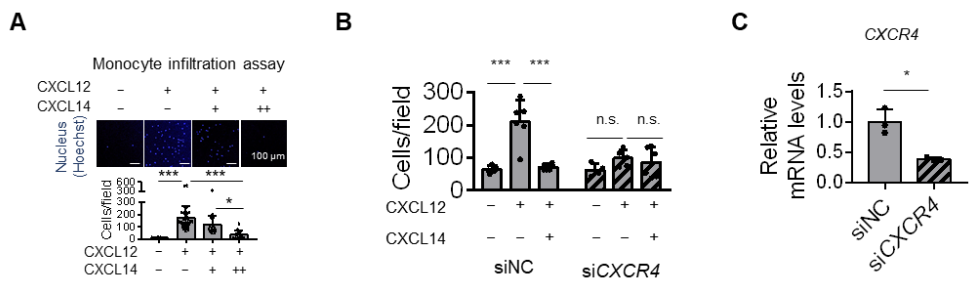


**Figure 29. CXCL14 suppresses CXCL12-CXCR4 mediated monocyte migration**

(A) (Top) Representative images of monocyte infiltration with the absence and presence of CXCL12 and CXCL14 peptides. (Bottom) Quantification of monocyte migration. Scale bar: 100 μm.

(B and C) Monocyte infiltration assay in the absence and presence of CXCL14 and CXCL12 peptides. Negative control siRNA or CXCR4 siRNA was treated to THP-1 monocytes before migration assay. (B) Quantification of monocyte migration. (C) mRNA levels of CXCR4 in THP-1 monocytes. n = 3.

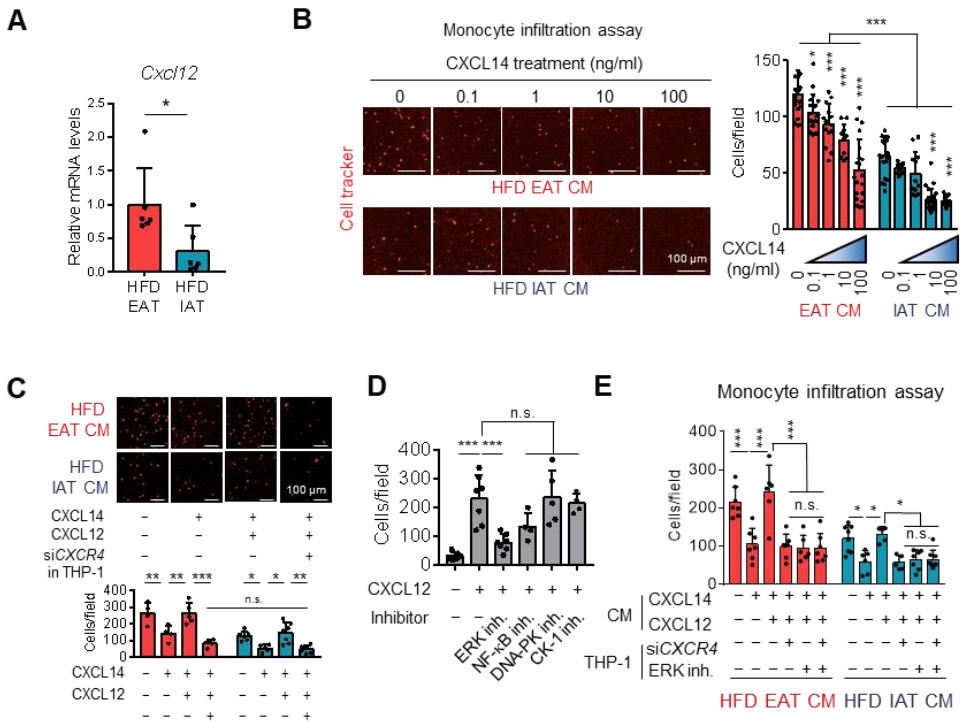


**Figure 30. CXCL14 suppresses monocyte migration into conditioned medium from adipose tissue**

(A) mRNA levels of Cxcl12 in EAT and IAT from 10 week HFD-fed mice. n = 6.

(B) (Left) Representative images of monocyte infiltration in the absence and presence of CXCL14 peptides. (Right) Quantification of monocyte migration. Scale bar: 100 μm.

(C) Monocyte migration in the absence and presence of CXCL14 and CXCL12 peptides. Negative control siRNA or CXCR4 siRNA was treated to THP-1 monocytes before migration assay. (Top) Representative images of monocyte infiltration assay in the absence and presence of CXCL14 and CXCL12 peptides in CM from HFD-fed EAT and IAT. (Bottom) Quantification of monocyte migration. Red: Cell tracker. Scale bar: 100 μm.

(D) Quantification of monocyte infiltration assay with several inhibitors. ERK inhibitor (inh., PD98059, 50 μM), NF-κB inh. (BAY 11-7082, 10 μM), DNA-PK inh. (NU-7441, 1 μM), and CK-1 inh. (IC261, 1 μM) were treated to THP-1 monocytes before migration assay.

(E) Quantification of monocyte migration in the absence and presence of CXCL14 and CXCL12 peptides. ERK inh. (PD98059, 50 μM) and negative control siRNA or CXCR4 siRNA were treated to THP-1 monocytes before migration assay.

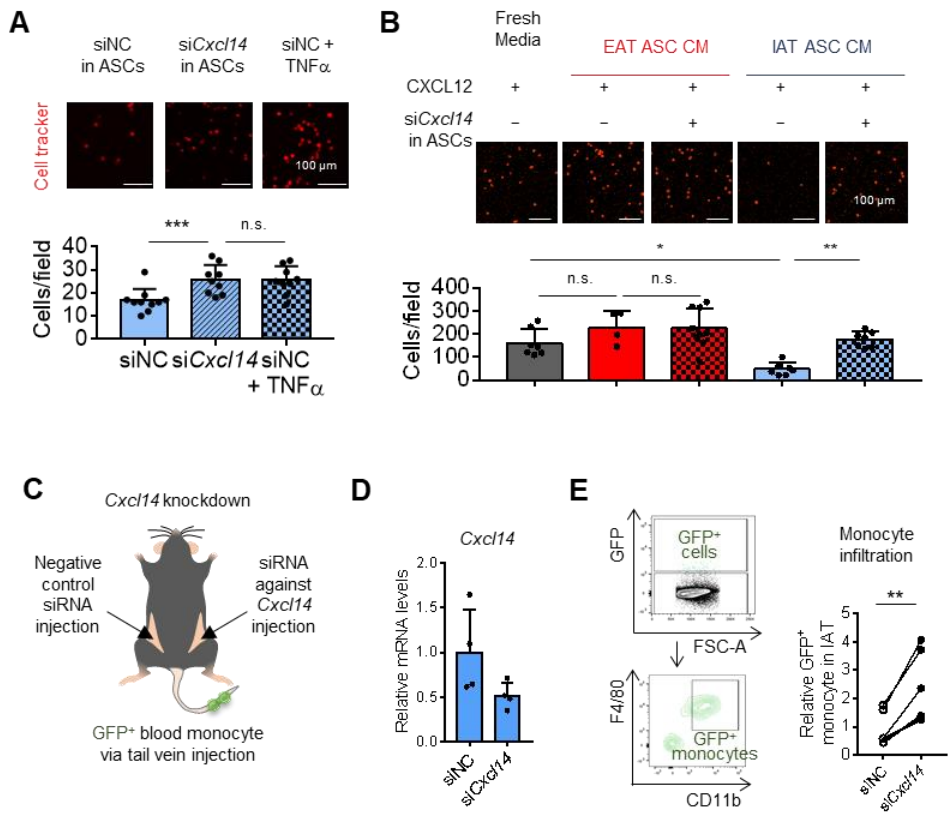


**Figure 31. IAT-specific CXCL14$^{+}$ ASCs suppress monocyte infiltration**

(A) (Top) Representative images of monocyte infiltration by Cxcl14 siRNA in IAT ASCs. (Bottom) Quantification of monocyte migration. Scale bar: 100 μm.

(B) (Top) Representative images of monocyte infiltration assay by Cxcl14 siRNA in EAT and IAT ASCs with CXCL12. (Bottom) Quantification of monocyte migration. Scale bar: 100 μm.

(C) Experimental scheme for *in vivo* monocyte migration assay.

(D) mRNA levels of Cxcl14 in IAT. n = 4.

(E) Representative FACS plots of GFP+ monocytes and quantification of *in vivo* monocyte migration with or without Cxcl14 knockdown in IAT. n = 5. A connected line means data from the same mouse.

# 5. Discussion

In obesity, WAT undergoes numerous remodeling processes, which vary depending on fat depots. Obesity induces inflammatory and fibrotic responses in EAT, while IAT maintains relatively low levels of these features [193]. In this regard, EAT is highly associated with metabolic disease and considered as 'bad fat', while IAT would be a safe storage site. Further, it has been reported that transplantation of IAT, but not EAT, improves metabolic phenotypes, which means IAT has intrinsically beneficial roles and acts as a 'good fat' [195]. However, it is largely unknown how EAT and IAT exhibit different metabolic roles in obesity.

In this study, I found fat-depot specific ASC subpopulations and their potential roles in adipose tissue inflammation and fibrosis. In response to obesogenic stimuli, EAT-specific $SDC1^+$ ASCs were generated. $SDC1^+$ ASCs highly expressed inflammatory and fibrotic genes and localized in CLS, implying their roles in unhealthy adipose tissue remodeling. In contrast, IAT-specific $CXCL14^+$ ASCs would repress monocyte infiltration and excessive immune responses. These data propose that the distinct properties of ASCs from EAT and IAT would mediate the fat depot-specific inflammatory and fibrotic features in obesity.

Accumulation of macrophages in WAT is one of the key events that connect obesity to metabolic complications. Monocyte migration into adipose tissue accounts significant portion of macrophage accumulation in obesity [92, 193]. Although several cytokines and chemokines that could affect monocyte migration have been suggested, fat depot-specific regulatory mechanisms of monocyte migration are incompletely understood [92, 375]. In this study, I showed that specific expression of CXCL14 in IAT ASCs could suppress monocyte migration probably by

suppressing the CXCL12-CXCR4 axis. It has been reported that expression of CXCL12 is increased in obese WAT and promotes macrophage accumulation [376]. Thus, it seems that blocking the action of CXCL12 by CXCL14 would contribute to relatively low inflammatory features of IAT. Notably, metabolically beneficial effects of IAT transplantation are more significant when transplanted into the visceral region compared to the subcutaneous region, which suggests secreted factors from transplanted IAT would modulate neighboring EAT or other organs and mediate the higher metabolic improvement [195]. In this regard, whether CXCL14 could mediate these location-specific effects of IAT transplantation needs further studies.

Close cell-to-cell interactions between mesenchymal stem cells such as ASCs and macrophages have been suggested [301]. Although pro-inflammatory macrophages and fibrogenic ASCs seem to be accumulated in obese EAT, their relationships are not clear [101, 108, 377]. In this study, I found that there were certain ligand-receptor interactions between ASCs and macrophages, whose possible roles appeared to be important in inflammation and fibrosis of WAT. Obese EAT-specific $SDC1^+$ ASCs highly expressed CCL2, a chemokine that mediates macrophage accumulation in obese adipose tissue [92]. Further, certain secreted factors from $SDC1^+$ ASCs such as TGFβ and activin could contribute to the polarization and inflammatory tone of macrophages (Figure 22C) [378, 379]. In addition, macrophages might affect the properties of ASC. scRNA-seq analysis revealed that accumulated macrophages in obesity could mediate the formation of the $SDC1^+$ ASCs by secreting factors such as SPP1. In addition, recent studies have shown that $Trem2^+$ $CD9^+$ lipid-associated or scar-associated macrophages are elevated in obese adipose tissue and various diseases [101, 380-384]. Interestingly,

these macrophages are highly correlated with fibrosis in various tissues and induce fibrosis by secreted factors such as PDGFs, amphiregulin, IL1β, and Spp1 [385]. Together, ASCs and macrophages exhibit dynamic bi-directional interactions with specific ligand-receptor pairs, which would be crucial regulators of inflammation and fibrosis in WAT.

In summary, I dissected heterogeneous ASCs in EAT and IAT and elucidated specific ASC clusters that could contribute to fat depot-selective inflammation and fibrosis in obesity. These data suggest that the unique roles of fat depot-specific ASC subpopulations are important for different pathophysiological features of EAT and IAT in obesity.

**Limitation of study**

The primary goal of this study was to identify and characterize fat depot-specific ASC clusters and their roles in adipose tissue inflammation and fibrosis. Although I explored ASC clusters and identified $SDC1^+$ ASCs and $CXCL14^+$ ASCs, selective removal of $SDC1^+$ and $CXCL14^+$ ASCs and genetic manipulation of key genes in each ASC cluster were not carried out. Using genetically modified models will be beneficial to define the roles of $SDC1^+$ and $CXCL14^+$ ASCs *in vivo*. In addition, experimental validation of ligand-receptor interactions between $SDC1^+$ ASCs and macrophages identified through scRNA-seq was not conducted and needs further investigation.

# CONCLUSION

Adipose tissue is a highly plastic and heterogeneous organ. Understanding the mechanisms by which the different fat depots exhibit their specific functions in response to metabolic stimuli is a fundamental question in adipose tissue biology. It has been suggested that unique features of adipocytes and ASC could mediate fat depot-specific features, including white adipogenesis, beige adipogenesis, inflammation, and fibrosis. However, little is known about the underlying mechanisms and key players in WAT heterogeneity.

In this dissertation, I suggest that fat-depot specific ASC subpopulations determine the unique features of VAT and SAT. The various fat depot-specific clusters identified in this study support this notion. First, $DPP4^{+}$ ES1 and IS1 ASCs have distinct intrinsic features that primarily determine their adipogenic potential. Second, IAT-specific $BST2^{high}$ ASCs appear pivotal in IAT-selective beige adipocyte biogenesis. Third, upon prolonged exposure to obesogenic stimuli, EAT-specific $SDC1^{+}$ ASCs would promote fibro-inflammatory remodeling whereas IAT-specific $CXCL14^{+}$ ASCs suppress monocyte infiltration.

These data suggest that ASCs are key factors in the plasticity and heterogeneity of WAT. Fat depot-specific ASC subpopulations appear to be crucial factors for adipose tissue heterogeneity. In addition, ASC subpopulations and functions could be altered in response to metabolic stimuli, contributing to adipose tissue plasticity. In this thesis, I identified several intrinsic and environmental factors that could influence the formation of fat-depot specific ASC subpopulations. Together, I suggest that the distinct properties of ASC clusters determine the metabolic features of fat depots (Figure 32).

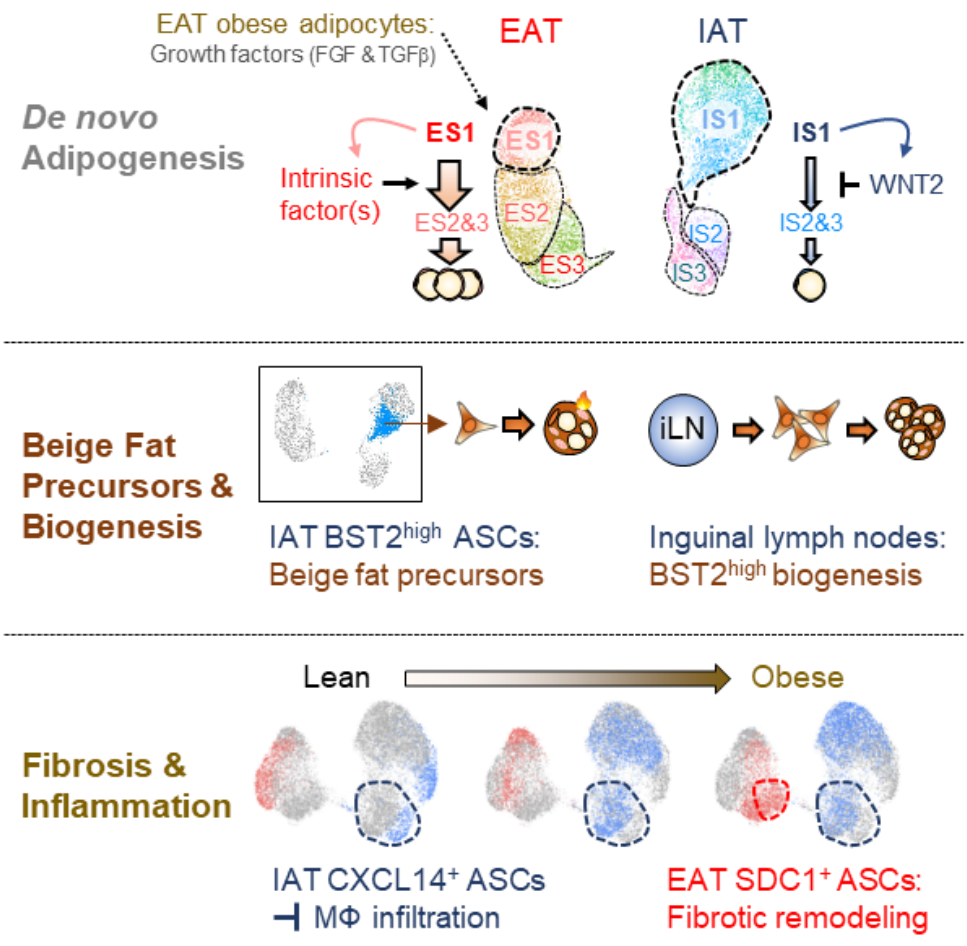


**Figure 32. Graphical abstract of Chapters I and II**

# 1. ASC Subpopulations Determine the Plasticity and Heterogeneity of WAT

For long time, ASCs have been investigated to identify the origin of adipocytes [264, 265]. Numerous investigations have suggested that ASCs perform various functions including white and beige adipogenesis, regulation of immune cells, and production of ECM and growth factors [3, 227]. In addition, several markers of ASC have been reported [231]. However, ASC heterogeneity in EAT and IAT has been poorly explored and its kinetics in response to metabolic stimuli remain elusive. In this study, I identified novel fat depot-specific ASC subpopulations expressing markers such as WNT2, BST2, SDC1, and CXCL14. These ASCs appear to determine the distinct features of EAT and IAT and their responses to metabolic stimuli including adipogenesis, inflammation, and fibrosis.

EAT and IAT have distinct patterns of adipogenesis and metabolic roles. In obesity, white adipogenesis is upregulated in EAT, but not in IAT. Elevated white adipogenesis in EAT could support visceral obesity and contribute to the onset of metabolic disease [185, 386, 387]. In contrast, beige adipogenesis actively occurs in IAT rather than EAT. Beige adipocytes play a metabolically beneficial role by consuming excess energy to generate heat [140]. This study revealed key ASC clusters that could mediate the differences in adipogenesis between EAT and IAT. The intrinsic features and proliferation of ES1 would induce EAT-selective de novo adipogenesis, whereas IAT-specific BST2$^{high}$ ASCs could differentiate into beige adipocytes. Together, this study suggests that ASC subpopulations with different adipogenic capacities would be crucial in the different metabolic features of EAT and IAT.

Adipose tissue inflammation and fibrosis are well-known hallmarks of obesity that contribute to metabolic diseases. EAT exhibits high levels of inflammatory and fibrotic responses in obesity, whereas IAT does not. Although it has been suggested that ASCs could modulate inflammation and fibrosis, ASC subpopulations to fat depot-specificity have been poorly explored. In this study, I examined fat depot-specific ASC clusters and their roles in fibro-inflammatory responses. In obesity, EAT-specific $SDC1^+$ ASCs could facilitate inflammation and fibrosis, whereas IAT-specific $CXCL14^+$ ASCs could suppress monocyte migration, implying that ASCs are essential regulators of adipose tissue remodeling in obesity. In conclusion, ASC subpopulations would be key determinants of WAT heterogeneity and plasticity.

## 2. Identification of Intrinsic and Environmental Factors that Determine the Characteristics of ASC

Various signaling pathways, transcription factors, and epigenetic modulators that control ASC characteristics have been identified [265, 266]. Further, diverse ASC subpopulations, markers, and their functions have been reported [227, 231]. However, the underlying mechanisms that determine the unique features of the different ASC subpopulations remain unclear. Further, the roles of intrinsic factors of ASCs and/or micro-environmental factors of adipose tissue in fat depot-specificity are hardly understood.

In this study, I identified several ASC subpopulations in EAT and IAT and investigated the underlying mechanisms of their formation, dividing them into intrinsic and extrinsic factors. I found that both intrinsic and environmental factors

contribute to the formation of the different ASC subpopulations. The distinct adipogenic potential of DPP4$^{+}$ ES1 and IS1 is likely regulated by intrinsic factors such as WNT2. In contrast, obesity-induced active proliferation of ES1 seems to be regulated by environmental factors such as FGF and TGFβ, secreted by EAT adipocytes. Furthermore, SDC1$^{+}$ ASCs and BST2 $^{high}$ ASCs appear to be modulated by both intrinsic and extrinsic factors. For instance, certain factors secreted by immune cells in obese EAT would mediate the formation of SDC1$^{+}$ ASCs in EAT. Also, lymph nodes could promote the generation of BST2$^{high}$ ASCs in IAT. These findings suggest that immune cells are important regulators of ASC subpopulation formation. However, mechanisms underlying the formation of SDC1$^{+}$ ASCs and BST2$^{high}$ ASCs are not fully investigated and remain to be clarified in future studies.

These intrinsic and environmental factors might be conserved in humans. SNPs related to the waist-to-hip ratio were detected in the promoter/enhancer regions of WNT2 (Figure 10G). Furthermore, human VAT, which has highly developed lymphatic vessels, exhibits higher expression levels of thermogenic genes and markers of BST2$^{high}$ ASCs than SAT (Figure 20) [353]. Therefore, the intrinsic and environmental factors would be potential therapeutic targets for obesity-related metabolic complications.

# ACKNOWLEDGMENTS

Parts of Chapter I and II in this thesis were published in Cell Metabolism (2022) Vol. 34 Issue 3 pp.458-472. In addition, parts of Chapter I and II were presented at the 2020 Korean Society for Molecular and Cellular Biology (KSMCB, online, October 5-7, 2020), 2022 KSMCB (International Conference Center Jeju, Jeju, Korea, September 28-30, 2022), 2023 KSMCB (International Conference Center Jeju, Jeju, Korea, November 6-8, 2023), Experimental Biology 2022 (Pennsylvania Convention Center, Philadelphia, Pennsylvania, USA, April 2-5, 2022), and Keystone Symposia: Adipose Tissue: Energizing Good Fat (Keystone Conference Center, Keystone, Colorado, USA, January 15-19, 2023). This study was supported by the BK21 program and the National Research Foundation, funded by the Korean government (NRF-2018R1A5A1024340 and NRF-2020R1A3B2078617).

# REFERENCES


1. Choe, S.S., et al., *Adipose Tissue Remodeling: Its Role in Energy Metabolism and Metabolic Disorders.* Front Endocrinol (Lausanne), 2016. **7**: p. 30.
2. Luo, L. and M. Liu, *Adipose tissue in control of metabolism.* J Endocrinol, 2016. **231**(3): p. R77-r99.
3. Sakers, A., et al., *Adipose-tissue plasticity in health and disease.* Cell, 2022. **185**(3): p. 419-446.
4. Langin, D., *Adipose tissue lipolysis as a metabolic pathway to define pharmacological strategies against obesity and the metabolic syndrome.* Pharmacol Res, 2006. **53**(6): p. 482-91.
5. Jeon, Y.G., et al., *Physiological and pathological roles of lipogenesis.* Nature Metabolism, 2023. **5**(5): p. 735-759.
6. Zhang, Y., et al., *Positional cloning of the mouse obese gene and its human homologue.* Nature, 1994. **372**(6505): p. 425-32.
7. Maeda, K., et al., *cDNA cloning and expression of a novel adipose specific collagen-like factor, apM1 (AdiPoseMost abundant Gene transcript 1).* Biochemical and biophysical research communications, 1996. **221**(2): p. 286-289.
8. Scherer, P.E., et al., *A novel serum protein similar to C1q, produced exclusively in adipocytes.* Journal of Biological chemistry, 1995. **270**(45): p. 26746-26749.
9. Hu, E., P. Liang, and B.M. Spiegelman, *AdipoQ is a novel adipose-specific gene dysregulated in obesity (*).* Journal of biological chemistry, 1996. **271**(18): p. 10697-10703.
10. Nakano, Y., et al., *Isolation and characterization of GBP28, a novel gelatin-binding protein purified from human plasma.* The Journal of Biochemistry, 1996. **120**(4): p. 803-812.
11. Kershaw, E.E. and J.S. Flier, *Adipose Tissue as an Endocrine Organ.* The Journal of Clinical Endocrinology & Metabolism, 2004. **89**(6): p. 2548-2556.
12. Weisberg, S.P., et al., *Obesity is associated with macrophage accumulation in adipose tissue.* J Clin Invest, 2003. **112**(12): p. 1796-808.
13. Cinti, S., et al., *Adipocyte death defines macrophage localization and function in adipose tissue of obese mice and humans.* J Lipid Res, 2005. **46**(11): p. 2347-55.
14. Grant, R.W. and V.D. Dixit, *Adipose tissue as an immunological organ.* Obesity, 2015. **23**(3): p. 512-518.
15. Man, K., A. Kallies, and A. Vasanthakumar, *Resident and migratory adipose immune cells control systemic metabolism and thermogenesis.* Cellular & Molecular Immunology, 2022. **19**(3): p. 421-431.
16. Lowell, B.B. and B.M. Spiegelman, *Towards a molecular understanding of adaptive thermogenesis.* Nature, 2000. **404**(6778): p. 652-660.
17. Pellegrinelli, V., S. Carobbio, and A. Vidal-Puig, *Adipose tissue plasticity: how fat depots respond differently to pathophysiological cues.* Diabetologia, 2016. **59**(6): p. 1075-88.
18. Lee, M.-J., Y. Wu, and S.K. Fried, *Adipose tissue heterogeneity: Implication of depot differences in adipose tissue for obesity complications.* Molecular Aspects of Medicine, 2013. **34**(1): p. 1-11.
19. Wang, W. and P. Seale, *Control of brown and beige fat development.* Nat Rev Mol Cell Biol, 2016. **17**(11): p. 691-702.
20. Sacks, H. and M.E. Symonds, *Anatomical locations of human brown adipose*

*tissue: functional relevance and implications in obesity and type 2 diabetes.* Diabetes, 2013. **62**(6): p. 1783-90.
21. Zhang, F., et al., *An Adipose Tissue Atlas: An Image-Guided Identification of Human-like BAT and Beige Depots in Rodents.* Cell Metab, 2018. **27**(1): p. 252-262.e3.
22. Harms, M. and P. Seale, *Brown and beige fat: development, function and therapeutic potential.* Nature Medicine, 2013. **19**(10): p. 1252-1263.
23. Nishino, N., et al., *FSP27 contributes to efficient energy storage in murine white adipocytes by promoting the formation of unilocular lipid droplets.* J Clin Invest, 2008. **118**(8): p. 2808-21.
24. Toh, S.Y., et al., *Up-regulation of mitochondrial activity and acquirement of brown adipose tissue-like property in the white adipose tissue of fsp27 deficient mice.* PLoS One, 2008. **3**(8): p. e2890.
25. Nedergaard, J., et al., *UCP1: the only protein able to mediate adaptive non-shivering thermogenesis and metabolic inefficiency.* Biochim Biophys Acta, 2001. **1504**(1): p. 82-106.
26. Feldmann, H.M., et al., *UCP1 ablation induces obesity and abolishes diet-induced thermogenesis in mice exempt from thermal stress by living at thermoneutrality.* Cell Metab, 2009. **9**(2): p. 203-9.
27. Lowell, B.B., et al., *Development of obesity in transgenic mice after genetic ablation of brown adipose tissue.* Nature, 1993. **366**(6457): p. 740-2.
28. Tseng, Y.H., et al., *New role of bone morphogenetic protein 7 in brown adipogenesis and energy expenditure.* Nature, 2008. **454**(7207): p. 1000-4.
29. Nedergaard, J., T. Bengtsson, and B. Cannon, *Unexpected evidence for active brown adipose tissue in adult humans.* American Journal of Physiology-Endocrinology and Metabolism, 2007. **293**(2): p. E444-E452.
30. Cypess, A.M., et al., *Identification and importance of brown adipose tissue in adult humans.* N Engl J Med, 2009. **360**(15): p. 1509-17.
31. Inagaki, T., J. Sakai, and S. Kajimura, *Transcriptional and epigenetic control of brown and beige adipose cell fate and function.* Nat Rev Mol Cell Biol, 2016. **17**(8): p. 480-95.
32. Cohen, P. and S. Kajimura, *The cellular and functional complexity of thermogenic fat.* Nat Rev Mol Cell Biol, 2021. **22**(6): p. 393-409.
33. Shamsi, F., C.-H. Wang, and Y.-H. Tseng, *The evolving view of thermogenic adipocytes — ontogeny, niche and function.* Nature Reviews Endocrinology, 2021. **17**(12): p. 726-744.
34. Sun, W., et al., *Plasticity and heterogeneity of thermogenic adipose tissue.* Nat Metab, 2021. **3**(6): p. 751-761.
35. Frühbeck, G., et al., *Regulation of adipocyte lipolysis.* Nutr Res Rev, 2014. **27**(1): p. 63-93.
36. Shimano, H. and R. Sato, *SREBP-regulated lipid metabolism: convergent physiology - divergent pathophysiology.* Nat Rev Endocrinol, 2017. **13**(12): p. 710-730.
37. Duerre, D.J. and A. Galmozzi, *Deconstructing Adipose Tissue Heterogeneity One Cell at a Time.* Front Endocrinol (Lausanne), 2022. **13**: p. 847291.
38. Maniyadath, B., et al., *Adipose tissue at single-cell resolution.* Cell Metabolism, 2023. **35**(3): p. 386-413.
39. Czech, M.P., et al., *Insulin signalling mechanisms for triacylglycerol storage.* Diabetologia, 2013. **56**(5): p. 949-964.
40. Taniguchi, C.M., B. Emanuelli, and C.R. Kahn, *Critical nodes in signalling pathways: insights into insulin action.* Nat Rev Mol Cell Biol, 2006. **7**(2): p. 85-96.

41. Suzuki, K. and T. Kono, *Evidence that insulin causes translocation of glucose transport activity to the plasma membrane from an intracellular storage site.* Proc Natl Acad Sci U S A, 1980. **77**(5): p. 2542-5.
42. Cheatham, B., et al., *Phosphatidylinositol 3-kinase activation is required for insulin stimulation of pp70 S6 kinase, DNA synthesis, and glucose transporter translocation.* Mol Cell Biol, 1994. **14**(7): p. 4902-11.
43. Wu, Q., et al., *FATP1 is an insulin-sensitive fatty acid transporter involved in diet-induced obesity.* Mol Cell Biol, 2006. **26**(9): p. 3455-67.
44. Sadur, C.N. and R.H. Eckel, *Insulin stimulation of adipose tissue lipoprotein lipase. Use of the euglycemic clamp technique.* J Clin Invest, 1982. **69**(5): p. 1119-25.
45. Semenkovich, C.F., et al., *Insulin regulation of lipoprotein lipase activity in 3T3-L1 adipocytes is mediated at posttranscriptional and posttranslational levels.* J Biol Chem, 1989. **264**(15): p. 9030-8.
46. Kim, J.B., et al., *Nutritional and insulin regulation of fatty acid synthetase and leptin gene expression through ADD1/SREBP1.* J Clin Invest, 1998. **101**(1): p. 1-9.
47. Herman, M.A., et al., *A novel ChREBP isoform in adipose tissue regulates systemic glucose metabolism.* Nature, 2012. **484**(7394): p. 333-8.
48. Nielsen, T.S., et al., *Dissecting adipose tissue lipolysis: molecular regulation and implications for metabolic disease.* J Mol Endocrinol, 2014. **52**(3): p. R199-222.
49. Greenberg, A.S., et al., *Perilipin, a major hormonally regulated adipocyte-specific phosphoprotein associated with the periphery of lipid storage droplets.* J Biol Chem, 1991. **266**(17): p. 11341-6.
50. Subramanian, V., et al., *Perilipin A Mediates the Reversible Binding of CGI-58 to Lipid Droplets in 3T3-L1 Adipocytes *.* Journal of Biological Chemistry, 2004. **279**(40): p. 42062-42071.
51. Cerk, I.K., L. Wechselberger, and M. Oberer, *Adipose Triglyceride Lipase Regulation: An Overview.* Curr Protein Pept Sci, 2018. **19**(2): p. 221-233.
52. Kraemer, F.B. and W.-J. Shen, *Hormone-sensitive lipase.* Journal of Lipid Research, 2002. **43**(10): p. 1585-1594.
53. Schreiber, R., H. Xie, and M. Schweiger, *Of mice and men: The physiological role of adipose triglyceride lipase (ATGL).* Biochimica et Biophysica Acta (BBA) - Molecular and Cell Biology of Lipids, 2019. **1864**(6): p. 880-899.
54. Schoiswohl, G., et al., *Impact of Reduced ATGL-Mediated Adipocyte Lipolysis on Obesity-Associated Insulin Resistance and Inflammation in Male Mice.* Endocrinology, 2015. **156**(10): p. 3610-24.
55. Schoiswohl, G., et al., *Adipose triglyceride lipase plays a key role in the supply of the working muscle with fatty acids.* J Lipid Res, 2010. **51**(3): p. 490-9.
56. Blüher, M., et al., *Adipose tissue selective insulin receptor knockout protects against obesity and obesity-related glucose intolerance.* Dev Cell, 2002. **3**(1): p. 25-38.
57. Friesen, M., et al., *Adipocyte insulin receptor activity maintains adipose tissue mass and lifespan.* Biochem Biophys Res Commun, 2016. **476**(4): p. 487-492.
58. Kusminski, C.M., P.E. Bickel, and P.E. Scherer, *Targeting adipose tissue in the treatment of obesity-associated diabetes.* Nat Rev Drug Discov, 2016. **15**(9): p. 639-660.
59. González-Muniesa, P., et al., *Obesity.* Nature Reviews Disease Primers, 2017. **3**(1): p. 17034.
60. Klein, S., et al., *Why does obesity cause diabetes?* Cell Metab, 2022. **34**(1): p.

11-20.
61. Ghaben, A.L. and P.E. Scherer, *Adipogenesis and metabolic health.* Nat Rev Mol Cell Biol, 2019. **20**(4): p. 242-258.
62. Vishvanath, L. and R.K. Gupta, *Contribution of adipogenesis to healthy adipose tissue expansion in obesity.* J Clin Invest, 2019. **129**(10): p. 4022-4031.
63. Arner, E., et al., *Adipocyte turnover: relevance to human adipose tissue morphology.* Diabetes, 2010. **59**(1): p. 105-9.
64. Acosta, J.R., et al., *Increased fat cell size: a major phenotype of subcutaneous white adipose tissue in non-obese individuals with type 2 diabetes.* Diabetologia, 2016. **59**(3): p. 560-70.
65. Senol-Cosar, O., et al., *Tenomodulin promotes human adipocyte differentiation and beneficial visceral adipose tissue expansion.* Nat Commun, 2016. **7**: p. 10686.
66. Kusminski, C.M., et al., *MitoNEET-driven alterations in adipocyte mitochondrial activity reveal a crucial adaptive process that preserves insulin sensitivity in obesity.* Nat Med, 2012. **18**(10): p. 1539-49.
67. Shepherd, P.R., et al., *Adipose cell hyperplasia and enhanced glucose disposal in transgenic mice overexpressing GLUT4 selectively in adipose tissue.* J Biol Chem, 1993. **268**(30): p. 22243-6.
68. Kim, J.Y., et al., *Obesity-associated improvements in metabolic profile through expansion of adipose tissue.* J Clin Invest, 2007. **117**(9): p. 2621-37.
69. Fujiwara, T., et al., *Characterization of new oral antidiabetic agent CS-045. Studies in KK and ob/ob mice and Zucker fatty rats.* Diabetes, 1988. **37**(11): p. 1549-58.
70. McLaughlin, T.M., et al., *Pioglitazone increases the proportion of small cells in human abdominal subcutaneous adipose tissue.* Obesity (Silver Spring), 2010. **18**(5): p. 926-31.
71. Shao, M., et al., *De novo adipocyte differentiation from Pdgfrbeta(+) preadipocytes protects against pathologic visceral adipose expansion in obesity.* Nat Commun, 2018. **9**(1): p. 890.
72. Jernås, M., et al., *Separation of human adipocytes by size: hypertrophic fat cells display distinct gene expression.* Faseb j, 2006. **20**(9): p. 1540-2.
73. Berger, J.J. and R.J. Barnard, *Effect of diet on fat cell size and hormone-sensitive lipase activity.* J Appl Physiol (1985), 1999. **87**(1): p. 227-32.
74. Kim, J.I., et al., *Lipid-overloaded enlarged adipocytes provoke insulin resistance independent of inflammation.* Mol Cell Biol, 2015. **35**(10): p. 1686-99.
75. Sarvari, A.K., et al., *Plasticity of Epididymal Adipose Tissue in Response to Diet-Induced Obesity at Single-Nucleus Resolution.* Cell Metab, 2021. **33**(2): p. 437-453 e5.
76. Rohm, T.V., et al., *Inflammation in obesity, diabetes, and related disorders.* Immunity, 2022. **55**(1): p. 31-55.
77. Zatterale, F., et al., *Chronic adipose tissue inflammation linking obesity to insulin resistance and type 2 diabetes.* Frontiers in physiology, 2020. **10**: p. 1607.
78. Gregor, M.F. and G.S. Hotamisligil, *Inflammatory mechanisms in obesity.* Annual review of immunology, 2011. **29**: p. 415-445.
79. Reilly, S.M. and A.R. Saltiel, *Adapting to obesity with adipose tissue inflammation.* Nat Rev Endocrinol, 2017. **13**(11): p. 633-643.
80. Hotamisligil, G.S., N.S. Shargill, and B.M. Spiegelman, *Adipose expression of tumor necrosis factor-alpha: direct role in obesity-linked insulin resistance.* Science, 1993. **259**(5091): p. 87-91.

81. Cheung, A.T., et al., *An in vivo model for elucidation of the mechanism of tumor necrosis factor-alpha (TNF-alpha)-induced insulin resistance: evidence for differential regulation of insulin signaling by TNF-alpha.* Endocrinology, 1998. **139**(12): p. 4928-35.
82. Hotamisligil, G., *Mechanisms of TNF-a-induced insulin resistance.* Experimental and clinical endocrinology & diabetes, 1999. **107**(02): p. 119-125.
83. Peraldi, P. and B. Spiegelman, *TNF-a and insulin resistance: summary and future prospects.* Molecular and cellular biochemistry, 1998. **182**: p. 169-175.
84. Yuan, M., et al., *Reversal of obesity- and diet-induced insulin resistance with salicylates or targeted disruption of Ikkbeta.* Science, 2001. **293**(5535): p. 1673-7.
85. Lumeng, C.N., J.L. Bodzin, and A.R. Saltiel, *Obesity induces a phenotypic switch in adipose tissue macrophage polarization.* J Clin Invest, 2007. **117**(1): p. 175-84.
86. Lumeng, C.N., et al., *Phenotypic Switching of Adipose Tissue Macrophages With Obesity Is Generated by Spatiotemporal Differences in Macrophage Subtypes.* Diabetes, 2008. **57**(12): p. 3239-3246.
87. de Luca, C. and J.M. Olefsky, *Inflammation and insulin resistance.* FEBS Lett, 2008. **582**(1): p. 97-105.
88. Hotamisligil, G.S., et al., *IRS-1-mediated inhibition of insulin receptor tyrosine kinase activity in TNF-alpha- and obesity-induced insulin resistance.* Science, 1996. **271**(5249): p. 665-8.
89. Shi, H., et al., *TLR4 links innate immunity and fatty acid-induced insulin resistance.* J Clin Invest, 2006. **116**(11): p. 3015-25.
90. Könner, A.C. and J.C. Brüning, *Toll-like receptors: linking inflammation to metabolism.* Trends in Endocrinology & Metabolism, 2011. **22**(1): p. 16-23.
91. Lancaster, G.I., et al., *Evidence that TLR4 Is Not a Receptor for Saturated Fatty Acids but Mediates Lipid-Induced Inflammation by Reprogramming Macrophage Metabolism.* Cell Metab, 2018. **27**(5): p. 1096-1110.e5.
92. Kanda, H., et al., *MCP-1 contributes to macrophage infiltration into adipose tissue, insulin resistance, and hepatic steatosis in obesity.* J Clin Invest, 2006. **116**(6): p. 1494-505.
93. Halberg, N., et al., *Hypoxia-inducible factor 1alpha induces fibrosis and insulin resistance in white adipose tissue.* Mol Cell Biol, 2009. **29**(16): p. 4467-83.
94. Feuerer, M., et al., *Lean, but not obese, fat is enriched for a unique population of regulatory T cells that affect metabolic parameters.* Nat Med, 2009. **15**(8): p. 930-9.
95. Nishimura, S., et al., *CD8+ effector T cells contribute to macrophage recruitment and adipose tissue inflammation in obesity.* Nat Med, 2009. **15**(8): p. 914-20.
96. Winer, D.A., et al., *B cells promote insulin resistance through modulation of T cells and production of pathogenic IgG antibodies.* Nat Med, 2011. **17**(5): p. 610-7.
97. Wensveen, F.M., et al., *NK cells link obesity-induced adipose stress to inflammation and insulin resistance.* Nat Immunol, 2015. **16**(4): p. 376-85.
98. Huh, J.Y., et al., *A novel function of adipocytes in lipid antigen presentation to iNKT cells.* Mol Cell Biol, 2013. **33**(2): p. 328-39.
99. Wernstedt Asterholm, I., et al., *Adipocyte inflammation is essential for healthy adipose tissue expansion and remodeling.* Cell Metab, 2014. **20**(1): p. 103-18.
100. Park, J., et al., *Activation of invariant natural killer T cells stimulates adipose*

*tissue remodeling via adipocyte death and birth in obesity.* Genes Dev, 2019. **33**(23-24): p. 1657-1672.
101. Jaitin, D.A., et al., *Lipid-Associated Macrophages Control Metabolic Homeostasis in a Trem2-Dependent Manner.* Cell, 2019. **178**(3): p. 686-698 e14.
102. Sun, K., et al., *Fibrosis and adipose tissue dysfunction.* Cell Metab, 2013. **18**(4): p. 470-7.
103. Sun, K., X. Li, and P.E. Scherer, *Extracellular Matrix (ECM) and Fibrosis in Adipose Tissue: Overview and Perspectives.* Compr Physiol, 2023. **13**(1): p. 4387-4407.
104. Marcelin, G., E.L. Gautier, and K. Clement, *Adipose Tissue Fibrosis in Obesity: Etiology and Challenges.* Annu Rev Physiol, 2022. **84**: p. 135-155.
105. Tanaka, M., et al., *Macrophage-inducible C-type lectin underlies obesity-induced adipose tissue fibrosis.* Nat Commun, 2014. **5**: p. 4982.
106. Vila, I.K., et al., *Immune cell Toll-like receptor 4 mediates the development of obesity- and endotoxemia-associated adipose tissue fibrosis.* Cell Rep, 2014. **7**(4): p. 1116-29.
107. Jang, J.E., et al., *Nitric Oxide Produced by Macrophages Inhibits Adipocyte Differentiation and Promotes Profibrogenic Responses in Preadipocytes to Induce Adipose Tissue Fibrosis.* Diabetes, 2016. **65**(9): p. 2516-28.
108. Marcelin, G., et al., *A PDGFRalpha-Mediated Switch toward CD9(high) Adipocyte Progenitors Controls Obesity-Induced Adipose Tissue Fibrosis.* Cell Metab, 2017. **25**(3): p. 673-685.
109. Hasegawa, Y., et al., *Repression of Adipose Tissue Fibrosis through a PRDM16-GTF2IRD1 Complex Improves Systemic Glucose Homeostasis.* Cell Metab, 2018. **27**(1): p. 180-194 e6.
110. Pellegrinelli, V., et al., *Human adipocyte function is impacted by mechanical cues.* J Pathol, 2014. **233**(2): p. 183-95.
111. Massagué, J. and D. Sheppard, *TGFb signaling in health and disease.* Cell, 2023. **186**(19): p. 4007-4037.
112. Khan, T., et al., *Metabolic dysregulation and adipose tissue fibrosis: role of collagen VI.* Mol Cell Biol, 2009. **29**(6): p. 1575-91.
113. Sun, K., et al., *Endotrophin triggers adipose tissue fibrosis and metabolic dysfunction.* Nat Commun, 2014. **5**: p. 3485.
114. Kim, M., C. Lee, and J. Park, *Extracellular matrix remodeling facilitates obesity-associated cancer progression.* Trends in Cell Biology, 2022.
115. Hepler, C., et al., *Identification of functionally distinct fibro-inflammatory and adipogenic stromal subpopulations in visceral adipose tissue of adult mice.* Elife, 2018. **7**.
116. Park, J.S., et al., *The effect of matrix stiffness on the differentiation of mesenchymal stem cells in response to TGF-β.* Biomaterials, 2011. **32**(16): p. 3921-3930.
117. Iwayama, T., et al., *PDGFRα signaling drives adipose tissue fibrosis by targeting progenitor cell plasticity.* Genes Dev, 2015. **29**(11): p. 1106-19.
118. Lafontan, M. and D. Langin, *Lipolysis and lipid mobilization in human adipose tissue.* Progress in lipid research, 2009. **48**(5): p. 275-297.
119. Reynisdottir, S., et al., *Effects of weight reduction on the regulation of lipolysis in adipocytes of women with upper-body obesity.* Clinical science, 1995. **89**(4): p. 421-429.
120. Kim, A.Y., et al., *Obesity-induced DNA hypermethylation of the adiponectin gene mediates insulin resistance.* Nat Commun, 2015. **6**: p. 7585.
121. Ouchi, N., et al., *Adipokines in inflammation and metabolic disease.* Nat Rev

Immunol, 2011. **11**(2): p. 85-97.
122. Crewe, C., et al., *Extracellular vesicle-based interorgan transport of mitochondria from energetically stressed adipocytes.* Cell Metab, 2021. **33**(9): p. 1853-1868 e11.
123. Flaherty, S.E., et al., *A lipase-independent pathway of lipid release and immune modulation by adipocytes.* Science, 2019. **363**(6430): p. 989-993.
124. Borcherding, N., et al., *Dietary lipids inhibit mitochondria transfer to macrophages to divert adipocyte-derived mitochondria into the blood.* Cell Metab, 2022. **34**(10): p. 1499-1513.e8.
125. Mei, R., et al., *Role of Adipose Tissue Derived Exosomes in Metabolic Disease.* Front Endocrinol (Lausanne), 2022. **13**: p. 873865.
126. Sun, K., C.M. Kusminski, and P.E. Scherer, *Adipose tissue remodeling and obesity.* J Clin Invest, 2011. **121**(6): p. 2094-101.
127. Blondin, D.P., et al., *Contributions of white and brown adipose tissues and skeletal muscles to acute cold-induced metabolic responses in healthy men.* J Physiol, 2015. **593**(3): p. 701-14.
128. Schreiber, R., et al., *Cold-Induced Thermogenesis Depends on ATGL-Mediated Lipolysis in Cardiac Muscle, but Not Brown Adipose Tissue.* Cell Metab, 2017. **26**(5): p. 753-763.e7.
129. Shin, H., et al., *Lipolysis in Brown Adipocytes Is Not Essential for Cold-Induced Thermogenesis in Mice.* Cell Metab, 2017. **26**(5): p. 764-777.e5.
130. Shamsi, F., C.H. Wang, and Y.H. Tseng, *The evolving view of thermogenic adipocytes - ontogeny, niche and function.* Nat Rev Endocrinol, 2021. **17**(12): p. 726-744.
131. Shao, M., et al., *Cellular Origins of Beige Fat Cells Revisited.* Diabetes, 2019. **68**(10): p. 1874-1885.
132. Wu, J., et al., *Beige adipocytes are a distinct type of thermogenic fat cell in mouse and human.* Cell, 2012. **150**(2): p. 366-76.
133. Long, J.Z., et al., *A smooth muscle-like origin for beige adipocytes.* Cell Metab, 2014. **19**(5): p. 810-20.
134. Wang, Q.A., et al., *Tracking adipogenesis during white adipose tissue development, expansion and regeneration.* Nat Med, 2013. **19**(10): p. 1338-44.
135. Jiang, H., et al., *Dense Intra-adipose Sympathetic Arborizations Are Essential for Cold-Induced Beiging of Mouse White Adipose Tissue.* Cell Metab, 2017. **26**(4): p. 686-692 e3.
136. Chi, J., et al., *Three-Dimensional Adipose Tissue Imaging Reveals Regional Variation in Beige Fat Biogenesis and PRDM16-Dependent Sympathetic Neurite Density.* Cell Metab, 2018. **27**(1): p. 226-236 e3.
137. Cao, W., et al., *p38 mitogen-activated protein kinase is the central regulator of cyclic AMP-dependent transcription of the brown fat uncoupling protein 1 gene.* Mol Cell Biol, 2004. **24**(7): p. 3057-67.
138. Seale, P., et al., *PRDM16 controls a brown fat/skeletal muscle switch.* Nature, 2008. **454**(7207): p. 961-7.
139. Seale, P., et al., *Transcriptional control of brown fat determination by PRDM16.* Cell Metab, 2007. **6**(1): p. 38-54.
140. Cohen, P., et al., *Ablation of PRDM16 and beige adipose causes metabolic dysfunction and a subcutaneous to visceral fat switch.* Cell, 2014. **156**(1-2): p. 304-16.
141. Lee, M.W., et al., *Activated type 2 innate lymphoid cells regulate beige fat biogenesis.* Cell, 2015. **160**(1-2): p. 74-87.
142. Brestoff, J.R., et al., *Group 2 innate lymphoid cells promote beiging of white*

*adipose tissue and limit obesity.* Nature, 2015. **519**(7542): p. 242-6.
143. Huang, Z., et al., *The FGF21-CCL11 Axis Mediates Beiging of White Adipose Tissues by Coupling Sympathetic Nervous System to Type 2 Immunity.* Cell Metab, 2017. **26**(3): p. 493-508 e4.
144. Cheong, L.Y., et al., *Fibroblastic reticular cells in lymph node potentiate white adipose tissue beiging through neuro-immune crosstalk in male mice.* Nat Commun, 2023. **14**(1): p. 1213.
145. Oguri, Y., et al., *CD81 Controls Beige Fat Progenitor Cell Growth and Energy Balance via FAK Signaling.* Cell, 2020. **182**(3): p. 563-577 e20.
146. Lynch, L., et al., *iNKT Cells Induce FGF21 for Thermogenesis and Are Required for Maximal Weight Loss in GLP1 Therapy.* Cell Metab, 2016. **24**(3): p. 510-519.
147. Agueda-Oyarzabal, M. and B. Emanuelli, *Immune Cells in Thermogenic Adipose Depots: The Essential but Complex Relationship.* Front Endocrinol (Lausanne), 2022. **13**: p. 839360.
148. Shabalina, I.G., et al., *UCP1 in brite/beige adipose tissue mitochondria is functionally thermogenic.* Cell Rep, 2013. **5**(5): p. 1196-203.
149. Ikeda, K., et al., *UCP1-independent signaling involving SERCA2b-mediated calcium cycling regulates beige fat thermogenesis and systemic glucose homeostasis.* Nat Med, 2017. **23**(12): p. 1454-1465.
150. Kazak, L., et al., *A creatine-driven substrate cycle enhances energy expenditure and thermogenesis in beige fat.* Cell, 2015. **163**(3): p. 643-55.
151. Rahbani, J.F., et al., *Creatine kinase B controls futile creatine cycling in thermogenic fat.* Nature, 2021. **590**(7846): p. 480-485.
152. Oeckl, J., et al., *Loss of UCP1 function augments recruitment of futile lipid cycling for thermogenesis in murine brown fat.* Mol Metab, 2022. **61**: p. 101499.
153. Flachs, P., et al., *Induction of lipogenesis in white fat during cold exposure in mice: link to lean phenotype.* Int J Obes (Lond), 2017. **41**(3): p. 372-380.
154. Altshuler-Keylin, S., et al., *Beige Adipocyte Maintenance Is Regulated by Autophagy-Induced Mitochondrial Clearance.* Cell Metabolism, 2016. **24**(3): p. 402-419.
155. Roh, H.C., et al., *Warming Induces Significant Reprogramming of Beige, but Not Brown, Adipocyte Cellular Identity.* Cell Metab, 2018. **27**(5): p. 1121-1137.e5.
156. Wang, Y., et al., *Adipocyte Liver Kinase b1 Suppresses Beige Adipocyte Renaissance Through Class IIa Histone Deacetylase 4.* Diabetes, 2017. **66**(12): p. 2952-2963.
157. Tchkonia, T., et al., *Mechanisms and metabolic implications of regional differences among fat depots.* Cell Metab, 2013. **17**(5): p. 644-656.
158. Gesta, S., Y.H. Tseng, and C.R. Kahn, *Developmental origin of fat: tracking obesity to its source.* Cell, 2007. **131**(2): p. 242-56.
159. Vague, J., *The degree of masculine differentiation of obesities: a factor determining predisposition to diabetes, atherosclerosis, gout, and uric calculous disease.* The American journal of clinical nutrition, 1956. **4**(1): p. 20-34.
160. Jensen, M.D., et al., *Influence of body fat distribution on free fatty acid metabolism in obesity.* J Clin Invest, 1989. **83**(4): p. 1168-73.
161. Miyazaki, Y., et al., *Abdominal fat distribution and peripheral and hepatic insulin resistance in type 2 diabetes mellitus.* Am J Physiol Endocrinol Metab, 2002. **283**(6): p. E1135-43.
162. Amato, M.C., et al., *Visceral Adiposity Index: A reliable indicator of visceral*

*fat function associated with cardiometabolic risk.* Diabetes Care, 2010. **33**(4): p. 920-922.
163. Ibrahim, M.M., *Subcutaneous and visceral adipose tissue: structural and functional differences.* Obesity Reviews, 2010. **11**(1): p. 11-18.
164. Chait, A. and L.J. den Hartigh, *Adipose Tissue Distribution, Inflammation and Its Metabolic Consequences, Including Diabetes and Cardiovascular Disease.* Front Cardiovasc Med, 2020. **7**: p. 22.
165. Fonseca, V., *Effect of thiazolidinediones on body weight in patients with diabetes mellitus.* Am J Med, 2003. **115 Suppl 8A**: p. 42s-48s.
166. Laplante, M., et al., *PPAR-gamma activation mediates adipose depot-specific effects on gene expression and lipoprotein lipase activity: mechanisms for modulation of postprandial lipemia and differential adipose accretion.* Diabetes, 2003. **52**(2): p. 291-9.
167. Li, H., et al., *Fibroblast growth factor 21 increases insulin sensitivity through specific expansion of subcutaneous fat.* Nature Communications, 2018. **9**(1): p. 272.
168. Lu, Q., et al., *Induction of adipocyte hyperplasia in subcutaneous fat depot alleviated type 2 diabetes symptoms in obese mice.* Obesity, 2014. **22**(7): p. 1623-1631.
169. Kabir, M., et al., *Molecular evidence supporting the portal theory: a causative link between visceral adiposity and hepatic insulin resistance.* American journal of physiology-endocrinology and metabolism, 2005. **288**(2): p. E454-E461.
170. Rytka, J.M., et al., *The Portal Theory Supported by Venous Drainage-Selective Fat Transplantation.* Diabetes, 2010. **60**(1): p. 56-63.
171. Item, F. and D. Konrad, *Visceral fat and metabolic inflammation: the portal theory revisited.* Obes Rev, 2012. **13 Suppl 2**: p. 30-9.
172. Yan, H., et al., *Gut Microbiome Alterations in Patients With Visceral Obesity Based on Quantitative Computed Tomography.* Front Cell Infect Microbiol, 2021. **11**: p. 823262.
173. Le Roy, C.I., et al., *Dissecting the role of the gut microbiota and diet on visceral fat mass accumulation.* Sci Rep, 2019. **9**(1): p. 9758.
174. Nie, X., et al., *A metagenome-wide association study of gut microbiome and visceral fat accumulation.* Comput Struct Biotechnol J, 2020. **18**: p. 2596-2609.
175. Hayward, M.G. and W.R. Keatinge, *Roles of subcutaneous fat and thermoregulatory reflexes in determining ability to stabilize body temperature in water.* J Physiol, 1981. **320**: p. 229-51.
176. Hwang, I. and J.B. Kim, *Two Faces of White Adipose Tissue with Heterogeneous Adipogenic Progenitors.* Diabetes Metab J, 2019. **43**(6): p. 752-762.
177. Petrus, P., et al., *Depot-specific differences in fatty acid composition and distinct associations with lipogenic gene expression in abdominal adipose tissue of obese women.* Int J Obes (Lond), 2017. **41**(8): p. 1295-1298.
178. Yang, R.Z., et al., *Identification of omentin as a novel depot-specific adipokine in human adipose tissue: possible role in modulating insulin action.* Am J Physiol Endocrinol Metab, 2006. **290**(6): p. E1253-61.
179. Fain, J.N., et al., *Comparison of the Release of Adipokines by Adipose Tissue, Adipose Tissue Matrix, and Adipocytes from Visceral and Subcutaneous Abdominal Adipose Tissues of Obese Humans.* Endocrinology, 2004. **145**(5): p. 2273-2282.
180. Arner, P., *Differences in lipolysis between human subcutaneous and omental adipose tissues.* Ann Med, 1995. **27**(4): p. 435-8.

181. Tchkonia, T., et al., *Fat depot origin affects adipogenesis in primary cultured and cloned human preadipocytes.* Am J Physiol Regul Integr Comp Physiol, 2002. **282**(5): p. R1286-96.
182. Tchkonia, T., et al., *Abundance of two human preadipocyte subtypes with distinct capacities for replication, adipogenesis, and apoptosis varies among fat depots.* Am J Physiol Endocrinol Metab, 2005. **288**(1): p. E267-77.
183. Tchkonia, T., et al., *Fat depot-specific characteristics are retained in strains derived from single human preadipocytes.* Diabetes, 2006. **55**(9): p. 2571-8.
184. Macotela, Y., et al., *Intrinsic differences in adipocyte precursor cells from different white fat depots.* Diabetes, 2012. **61**(7): p. 1691-9.
185. Jeffery, E., et al., *Rapid depot-specific activation of adipocyte precursor cells at the onset of obesity.* Nat Cell Biol, 2015. **17**(4): p. 376-85.
186. Jeffery, E., et al., *The Adipose Tissue Microenvironment Regulates Depot-Specific Adipogenesis in Obesity.* Cell Metab, 2016. **24**(1): p. 142-50.
187. Park, J., et al., *Targeted erasure of DNA methylation by TET3 drives adipogenic reprogramming and differentiation.* Nat Metab, 2022. **4**(7): p. 918-931.
188. Gustafson, B., A. Nerstedt, and U. Smith, *Reduced subcutaneous adipogenesis in human hypertrophic obesity is linked to senescent precursor cells.* Nat Commun, 2019. **10**(1): p. 2757.
189. Rask-Andersen, M., et al., *Genome-wide association study of body fat distribution identifies adiposity loci and sex-specific genetic effects.* Nature Communications, 2019. **10**(1): p. 339.
190. Shungin, D., et al., *New genetic loci link adipose and insulin biology to body fat distribution.* Nature, 2015. **518**(7538): p. 187-196.
191. Strissel, K.J., et al., *Adipocyte death, adipose tissue remodeling, and obesity complications.* Diabetes, 2007. **56**(12): p. 2910-8.
192. Harman-Boehm, I., et al., *Macrophage infiltration into omental versus subcutaneous fat across different populations: effect of regional adiposity and the comorbidities of obesity.* J Clin Endocrinol Metab, 2007. **92**(6): p. 2240-7.
193. Hwang, I., et al., *GABA-stimulated adipose-derived stem cells suppress subcutaneous adipose inflammation in obesity.* Proc Natl Acad Sci U S A, 2019. **116**(24): p. 11936-11945.
194. Zuriaga, M.A., et al., *Humans and Mice Display Opposing Patterns of "Browning" Gene Expression in Visceral and Subcutaneous White Adipose Tissue Depots.* Front Cardiovasc Med, 2017. **4**: p. 27.
195. Tran, T.T., et al., *Beneficial effects of subcutaneous fat transplantation on metabolism.* Cell Metab, 2008. **7**(5): p. 410-20.
196. Hocking, S.L., D.J. Chisholm, and D.E. James, *Studies of regional adipose transplantation reveal a unique and beneficial interaction between subcutaneous adipose tissue and the intra-abdominal compartment.* Diabetologia, 2008. **51**(5): p. 900-2.
197. Foster, M.T., et al., *Transplantation of non-visceral fat to the visceral cavity improves glucose tolerance in mice: investigation of hepatic lipids and insulin sensitivity.* Diabetologia, 2011. **54**(11): p. 2890-2899.
198. Tran, T.T. and C.R. Kahn, *Transplantation of adipose tissue and stem cells: role in metabolism and disease.* Nature Reviews Endocrinology, 2010. **6**(4): p. 195-213.
199. Hocking, S.L., et al., *Subcutaneous fat transplantation alleviates diet-induced glucose intolerance and inflammation in mice.* Diabetologia, 2015. **58**(7): p. 1587-600.

200. Kwok, K.H., K.S. Lam, and A. Xu, *Heterogeneity of white adipose tissue: molecular basis and clinical implications.* Exp Mol Med, 2016. **48**: p. e215.
201. Gesta, S., et al., *Evidence for a role of developmental genes in the origin of obesity and body fat distribution.* Proc Natl Acad Sci U S A, 2006. **103**(17): p. 6676-81.
202. Tchkonia, T., et al., *Identification of depot-specific human fat cell progenitors through distinct expression profiles and developmental gene patterns.* Am J Physiol Endocrinol Metab, 2007. **292**(1): p. E298-307.
203. Yamamoto, Y., et al., *Adipose depots possess unique developmental gene signatures.* Obesity (Silver Spring), 2010. **18**(5): p. 872-878.
204. Gehrke, S., et al., *Epigenetic Regulation of Depot-Specific Gene Expression in Adipose Tissue.* PLOS ONE, 2013. **8**(12): p. e82516.
205. Chau, Y.Y., et al., *Visceral and subcutaneous fat have different origins and evidence supports a mesothelial source.* Nat Cell Biol, 2014. **16**(4): p. 367-75.
206. Sanchez-Gurmaches, J., W.Y. Hsiao, and D.A. Guertin, *Highly selective in vivo labeling of subcutaneous white adipocyte precursors with Prx1-Cre.* Stem Cell Reports, 2015. **4**(4): p. 541-50.
207. Han, J., et al., *The spatiotemporal development of adipose tissue.* Development, 2011. **138**(22): p. 5027-37.
208. Baglioni, S., et al., *Functional differences in visceral and subcutaneous fat pads originate from differences in the adipose stem cell.* PLoS One, 2012. **7**(5): p. e36569.
209. Hocking, S.L., et al., *Intrinsic Depot-Specific Differences in the Secretome of Adipose Tissue, Preadipocytes, and Adipose Tissue-Derived Microvascular Endothelial Cells.* Diabetes, 2010. **59**(12): p. 3008-3016.
210. Grandl, G., et al., *Depot specific differences in the adipogenic potential of precursors are mediated by collagenous extracellular matrix and Flotillin 2 dependent signaling.* Mol Metab, 2016. **5**(10): p. 937-947.
211. Gesta, S., et al., *Mesodermal developmental gene Tbx15 impairs adipocyte differentiation and mitochondrial respiration.* Proceedings of the National Academy of Sciences, 2011. **108**(7): p. 2771-2776.
212. Lee, K.Y., et al., *Shox2 is a molecular determinant of depot-specific adipocyte function.* Proc Natl Acad Sci U S A, 2013. **110**(28): p. 11409-14.
213. Loh, N.Y., et al., *LRP5 regulates human body fat distribution by modulating adipose progenitor biology in a dose- and depot-specific fashion.* Cell Metab, 2015. **21**(2): p. 262-273.
214. Ding, H., et al., *Fasting induces a subcutaneous-to-visceral fat switch mediated by microRNA-149-3p and suppression of PRDM16.* Nat Commun, 2016. **7**: p. 11533.
215. Lee, K.Y., et al., *Tbx15 Defines a Glycolytic Subpopulation and White Adipocyte Heterogeneity.* Diabetes, 2017. **66**(11): p. 2822-2829.
216. Ng, Y., et al., *HOXC10 suppresses browning of white adipose tissues.* Exp Mol Med, 2017. **49**(2): p. e292.
217. Akama, T. and T.H. Chun, *Transcription factor 21 (TCF21) promotes proinflammatory interleukin 6 expression and extracellular matrix remodeling in visceral adipose stem cells.* J Biol Chem, 2018. **293**(17): p. 6603-6610.
218. Sun, W., et al., *Tbx15 is required for adipocyte browning induced by adrenergic signaling pathway.* Mol Metab, 2019. **28**: p. 48-57.
219. Zhang, X., et al., *A Novel Regulator of Preadipocyte Differentiation, Transcription Factor TCF21, Functions Partially Through Promoting LPL Expression.* Front Physiol, 2019. **10**: p. 458.

220. Ma, M., et al., *HOXC10 promotes proliferation and attenuates lipid accumulation of sheep bone marrow mesenchymal stem cells.* Molecular and Cellular Probes, 2020. **49**: p. 101491.
221. Markan, K.R., et al., *Adipose TBX1 regulates β-adrenergic sensitivity in subcutaneous adipose tissue and thermogenic capacity in vivo.* Molecular Metabolism, 2020. **36**: p. 100965.
222. Kumar, V., et al., *Dynamics of HOX gene expression and regulation in adipocyte development.* Gene, 2021. **768**: p. 145308.
223. Tan, H.Y.A., et al., *HOXC10 Suppresses Browning to Maintain White Adipocyte Identity.* Diabetes, 2021. **70**(8): p. 1654-1663.
224. Erdos, E., et al., *Unique role for lncRNA HOTAIR in defining depot-specific gene expression patterns in human adipose-derived stem cells.* Genes Dev, 2022.
225. Kuo, F.C., et al., *HOTAIR interacts with PRC2 complex regulating the regional preadipocyte transcriptome and human fat distribution.* Cell Rep, 2022. **40**(4): p. 111136.
226. Liu, Q., et al., *Tcf21 marks visceral adipose mesenchymal progenitors and functions as a rate-limiting factor during visceral adipose tissue development.* Cell Rep, 2023. **42**(3): p. 112166.
227. Cannavino, J. and R.K. Gupta, *Mesenchymal stromal cells as conductors of adipose tissue remodeling.* Genes Dev, 2023.
228. Plikus, M.V., et al., *Fibroblasts: Origins, definitions, and functions in health and disease.* Cell, 2021. **184**(15): p. 3852-3872.
229. Soliman, H., et al., *Multipotent stromal cells: One name, multiple identities.* Cell Stem Cell, 2021. **28**(10): p. 1690-1707.
230. Cawthorn, W.P., E.L. Scheller, and O.A. MacDougald, *Adipose tissue stem cells meet preadipocyte commitment: going back to the future.* J Lipid Res, 2012. **53**(2): p. 227-46.
231. Ferrero, R., P. Rainer, and B. Deplancke, *Toward a Consensus View of Mammalian Adipocyte Stem and Progenitor Cell Heterogeneity.* Trends Cell Biol, 2020. **30**(12): p. 937-950.
232. Hepler, C., L. Vishvanath, and R.K. Gupta, *Sorting out adipocyte precursors and their role in physiology and disease.* Genes Dev, 2017. **31**(2): p. 127-140.
233. Berry, R., E. Jeffery, and M.S. Rodeheffer, *Weighing in on adipocyte precursors.* Cell Metab, 2014. **19**(1): p. 8-20.
234. Sebo, Z.L. and M.S. Rodeheffer, *Assembling the adipose organ: adipocyte lineage segregation and adipogenesis in vivo.* Development, 2019. **146**(7).
235. Berry, D.C., et al., *The developmental origins of adipose tissue.* Development, 2013. **140**(19): p. 3939-49.
236. Hausman, G.J., D.R. Campion, and R.J. Martin, *Search for the adipocyte precursor cell and factors that promote its differentiation.* J Lipid Res, 1980. **21**(6): p. 657-70.
237. Green, H. and O. Kehinde, *Sublines of mouse 3T3 cells that accumulate lipid.* Cell, 1974. **1**(3): p. 113-116.
238. Green, H. and M. Meuth, *An established pre-adipose cell line and its differentiation in culture.* Cell, 1974. **3**(2): p. 127-33.
239. Tran, K.V., et al., *The vascular endothelium of the adipose tissue gives rise to both white and brown fat cells.* Cell Metab, 2012. **15**(2): p. 222-9.
240. Zuk, P.A., et al., *Multilineage cells from human adipose tissue: implications for cell-based therapies.* Tissue Eng, 2001. **7**(2): p. 211-28.
241. Rodeheffer, M.S., K. Birsoy, and J.M. Friedman, *Identification of white adipocyte progenitor cells in vivo.* Cell, 2008. **135**(2): p. 240-9.

242. Tang, W., et al., *White fat progenitor cells reside in the adipose vasculature.* Science, 2008. **322**(5901): p. 583-6.
243. Lee, Y.H., et al., *In vivo identification of bipotential adipocyte progenitors recruited by beta3-adrenoceptor activation and high-fat feeding.* Cell Metab, 2012. **15**(4): p. 480-91.
244. Berry, R. and M.S. Rodeheffer, *Characterization of the adipocyte cellular lineage in vivo.* Nat Cell Biol, 2013. **15**(3): p. 302-8.
245. Gupta, R.K., et al., *Zfp423 expression identifies committed preadipocytes and localizes to adipose endothelial and perivascular cells.* Cell Metab, 2012. **15**(2): p. 230-9.
246. Wang, Y. and H.S. Sul, *Pref-1 regulates mesenchymal cell commitment and differentiation through Sox9.* Cell Metab, 2009. **9**(3): p. 287-302.
247. Hudak, C.S., et al., *Pref-1 marks very early mesenchymal precursors required for adipose tissue development and expansion.* Cell Rep, 2014. **8**(3): p. 678-87.
248. Moitra, J., et al., *Life without white fat: a transgenic mouse.* Genes Dev, 1998. **12**(20): p. 3168-81.
249. Merrick, D., et al., *Identification of a mesenchymal progenitor cell hierarchy in adipose tissue.* Science, 2019. **364**(6438).
250. Emont, M.P., et al., *A single-cell atlas of human and mouse white adipose tissue.* Nature, 2022.
251. Jiang, Z., et al., *PDGFRb(+) mesenchymal cells, but not NG2(+) mural cells, contribute to cardiac fat.* Cell Rep, 2021. **34**(5): p. 108697.
252. Cattaneo, P., et al., *Parallel Lineage-Tracing Studies Establish Fibroblasts as the Prevailing In Vivo Adipocyte Progenitor.* Cell Rep, 2020. **30**(2): p. 571-582 e2.
253. Westcott, G.P., et al., *Mesothelial cells are not a source of adipocytes in mice.* Cell Rep, 2021. **36**(2): p. 109388.
254. Angueira, A.R., et al., *Defining the lineage of thermogenic perivascular adipose tissue.* Nat Metab, 2021. **3**(4): p. 469-484.
255. Shamsi, F., et al., *Vascular smooth muscle-derived Trpv1(+) progenitors are a source of cold-induced thermogenic adipocytes.* Nat Metab, 2021. **3**(4): p. 485-495.
256. Tajbakhsh, S., *Stem cell: what's in a name?* Nature Reports Stem Cells, 2009.
257. Buechler, M.B., et al., *Cross-tissue organization of the fibroblast lineage.* Nature, 2021. **593**(7860): p. 575-579.
258. Lendahl, U., L. Muhl, and C. Betsholtz, *Identification, discrimination and heterogeneity of fibroblasts.* Nature Communications, 2022. **13**(1): p. 3409.
259. Jun, S., et al., *Control of murine brown adipocyte development by GATA6.* Dev Cell, 2023.
260. Rao, J., et al., *Reconstructing human brown fat developmental trajectory in vitro.* Dev Cell, 2023.
261. Sebo, Z.L., et al., *A mesodermal fate map for adipose tissue.* Development, 2018. **145**(17).
262. Dominguez, M.H., et al., *Graded mesoderm assembly governs cell fate and morphogenesis of the early mammalian heart.* Cell, 2023. **186**(3): p. 479-496.e23.
263. Chen, A., et al., *Spatiotemporal transcriptomic atlas of mouse organogenesis using DNA nanoball-patterned arrays.* Cell, 2022. **185**(10): p. 1777-1792.e21.
264. Rosen, E.D. and O.A. MacDougald, *Adipocyte differentiation from the inside out.* Nature Reviews Molecular Cell Biology, 2006. **7**(12): p. 885-896.
265. Cristancho, A.G. and M.A. Lazar, *Forming functional fat: a growing*

*understanding of adipocyte differentiation.* Nat Rev Mol Cell Biol, 2011. **12**(11): p. 722-34.
266. Lefterova, M.I., et al., *PPARgamma and the global map of adipogenesis and beyond.* Trends Endocrinol Metab, 2014. **25**(6): p. 293-302.
267. Hong, K.Y., et al., *Perilipin+ embryonic preadipocytes actively proliferate along growing vasculatures for adipose expansion.* Development, 2015. **142**(15): p. 2623-2632.
268. Zhang, Q., et al., *Distinct functional properties of murine perinatal and adult adipose progenitor subpopulations.* Nature Metabolism, 2022. **4**(8): p. 1055-1070.
269. Spalding, K.L., et al., *Dynamics of fat cell turnover in humans.* Nature, 2008. **453**(7196): p. 783-7.
270. Kim, S.M., et al., *Loss of white adipose hyperplastic potential is associated with enhanced susceptibility to insulin resistance.* Cell Metab, 2014. **20**(6): p. 1049-58.
271. Vishvanath, L., et al., *Pdgfrbeta+ Mural Preadipocytes Contribute to Adipocyte Hyperplasia Induced by High-Fat-Diet Feeding and Prolonged Cold Exposure in Adult Mice.* Cell Metab, 2016. **23**(2): p. 350-9.
272. Lee, Y.H., A.P. Petkova, and J.G. Granneman, *Identification of an adipogenic niche for adipose tissue remodeling and restoration.* Cell Metab, 2013. **18**(3): p. 355-67.
273. Burl, R.B., et al., *Deconstructing Adipogenesis Induced by beta3-Adrenergic Receptor Activation with Single-Cell Expression Profiling.* Cell Metab, 2018. **28**(2): p. 300-309 e4.
274. Ross, S.E., et al., *Inhibition of adipogenesis by Wnt signaling.* Science, 2000. **289**(5481): p. 950-3.
275. Christodoulides, C., et al., *Adipogenesis and WNT signalling.* Trends Endocrinol Metab, 2009. **20**(1): p. 16-24.
276. Takada, I., A.P. Kouzmenko, and S. Kato, *Wnt and PPARgamma signaling in osteoblastogenesis and adipogenesis.* Nat Rev Rheumatol, 2009. **5**(8): p. 442-7.
277. Hammarstedt, A., et al., *WISP2 regulates preadipocyte commitment and PPARγ activation by BMP4.* Proc Natl Acad Sci U S A, 2013. **110**(7): p. 2563-8.
278. Blázquez-Medela, A.M., M. Jumabay, and K.I. Boström, *Beyond the bone: Bone morphogenetic protein signaling in adipose tissue.* Obes Rev, 2019. **20**(5): p. 648-658.
279. Petrus, P., et al., *Transforming Growth Factor-beta3 Regulates Adipocyte Number in Subcutaneous White Adipose Tissue.* Cell Rep, 2018. **25**(3): p. 551-560 e5.
280. Choy, L. and R. Derynck, *Transforming growth factor-β inhibits adipocyte differentiation by Smad3 interacting with CCAAT/enhancer-binding protein (C/EBP) and repressing C/EBP transactivation function.* Journal of Biological Chemistry, 2003. **278**(11): p. 9609-9619.
281. Lacasa, D., et al., *Macrophage-secreted factors impair human adipogenesis: involvement of proinflammatory state in preadipocytes.* Endocrinology, 2007. **148**(2): p. 868-77.
282. Keophiphath, M., et al., *Macrophage-secreted factors promote a profibrotic phenotype in human preadipocytes.* Mol Endocrinol, 2009. **23**(1): p. 11-24.
283. Haylett, W.L. and W.F. Ferris, *Adipocyte-progenitor cell communication that influences adipogenesis.* Cell Mol Life Sci, 2020. **77**(1): p. 115-128.
284. Meissburger, B., et al., *Regulation of adipogenesis by paracrine factors from*

*adipose stromal-vascular fraction - a link to fat depot-specific differences.* Biochimica et Biophysica Acta (BBA) - Molecular and Cell Biology of Lipids, 2016. **1861**(9, Part A): p. 1121-1131.
285. Wang, S., et al., *Adipocyte Piezo1 mediates obesogenic adipogenesis through the FGF1/FGFR1 signaling pathway in mice.* Nat Commun, 2020. **11**(1): p. 2303.
286. Hu, L., et al., *IGF1 Promotes Adipogenesis by a Lineage Bias of Endogenous Adipose Stem/Progenitor Cells.* STEM CELLS, 2015. **33**(8): p. 2483-2495.
287. Chang, H.R., et al., *Macrophage and adipocyte IGF1 maintain adipose tissue homeostasis during metabolic stresses.* Obesity (Silver Spring), 2016. **24**(1): p. 172-83.
288. Cao, Z., R.M. Umek, and S.L. McKnight, *Regulated expression of three C/EBP isoforms during adipose conversion of 3T3-L1 cells.* Genes & development, 1991. **5**(9): p. 1538-1552.
289. Wu, Z., et al., *Conditional ectopic expression of C/EBP beta in NIH-3T3 cells induces PPAR gamma and stimulates adipogenesis.* Genes & development, 1995. **9**(19): p. 2350-2363.
290. Tang, Q.-Q., T.C. Otto, and M.D. Lane, *CCAAT/enhancer-binding protein β is required for mitotic clonal expansion during adipogenesis.* Proceedings of the National Academy of Sciences, 2003. **100**(3): p. 850-855.
291. Siersbæk, R., et al., *Extensive chromatin remodelling and establishment of transcription factor 'hotspots' during early adipogenesis.* Embo j, 2011. **30**(8): p. 1459-72.
292. Siersbæk, R., et al., *Dynamic Rewiring of Promoter-Anchored Chromatin Loops during Adipocyte Differentiation.* Mol Cell, 2017. **66**(3): p. 420-435.e5.
293. Kim, J.B., et al., *ADD1/SREBP1 activates PPARγ through the production of endogenous ligand.* Proceedings of the national academy of sciences, 1998. **95**(8): p. 4333-4337.
294. Kim, J.B. and B.M. Spiegelman, *ADD1/SREBP1 promotes adipocyte differentiation and gene expression linked to fatty acid metabolism.* Genes and Development, 1996. **10**(9): p. 1096-1107.
295. Tontonoz, P., et al., *ADD1: a novel helix-loop-helix transcription factor associated with adipocyte determination and differentiation.* Molecular and cellular biology, 1993. **13**(8): p. 4753-4759.
296. Chawla, A., et al., *Peroxisome proliferator-activated receptor (PPAR) gamma: adipose-predominant expression and induction early in adipocyte differentiation.* Endocrinology, 1994. **135**(2): p. 798-800.
297. Tontonoz, P., et al., *PPAR gamma 2 regulates adipose expression of the phosphoenolpyruvate carboxykinase gene.* Molecular and cellular biology, 1995.
298. Spiegelman, B.M., *PPAR-gamma: adipogenic regulator and thiazolidinedione receptor.* Diabetes, 1998. **47**(4): p. 507-514.
299. Lin, F.-T. and M.D. Lane, *CCAAT/enhancer binding protein alpha is sufficient to initiate the 3T3-L1 adipocyte differentiation program.* Proceedings of the National Academy of Sciences, 1994. **91**(19): p. 8757-8761.
300. Naik, S., et al., *Two to Tango: Dialog between Immunity and Stem Cells in Health and Disease.* Cell, 2018. **175**(4): p. 908-920.
301. Buechler, M.B., W. Fu, and S.J. Turley, *Fibroblast-macrophage reciprocal interactions in health, fibrosis, and cancer.* Immunity, 2021. **54**(5): p. 903-915.
302. Koliaraki, V., et al., *The mesenchymal context in inflammation, immunity and cancer.* Nat Immunol, 2020. **21**(9): p. 974-982.
303. Mahlakõiv, T., et al., *Stromal cells maintain immune cell homeostasis in*

*adipose tissue via production of interleukin-33.* Science Immunology, 2019. **4**(35): p. eaax0416.
304. Goldberg, E.L., et al., *IL-33 causes thermogenic failure in aging by expanding dysfunctional adipose ILC2.* Cell Metab, 2021. **33**(11): p. 2277-2287 e5.
305. Shan, B., et al., *Cold-responsive adipocyte progenitors couple adrenergic signaling to immune cell activation to promote beige adipocyte accrual.* Genes Dev, 2021. **35**(19-20): p. 1333-1338.
306. Poulain-Godefroy, O. and P. Froguel, *Preadipocyte response and impairment of differentiation in an inflammatory environment.* Biochemical and Biophysical Research Communications, 2007. **356**(3): p. 662-667.
307. Kaplan, J.L., et al., *Adipocyte progenitor cells initiate monocyte chemoattractant protein-1-mediated macrophage accumulation in visceral adipose tissue.* Molecular Metabolism, 2015. **4**(11): p. 779-794.
308. Bruun, J.M., et al., *Monocyte chemoattractant protein-1 release is higher in visceral than subcutaneous human adipose tissue (AT): implication of macrophages resident in the AT.* J Clin Endocrinol Metab, 2005. **90**(4): p. 2282-9.
309. Kaplan, J.L., et al., *Adipocyte progenitor cells initiate monocyte chemoattractant protein-1-mediated macrophage accumulation in visceral adipose tissue.* Mol Metab, 2015. **4**(11): p. 779-94.
310. Dahlgren, M.W., et al., *Adventitial Stromal Cells Define Group 2 Innate Lymphoid Cell Tissue Niches.* Immunity, 2019. **50**(3): p. 707-722 e6.
311. Rana, B.M.J., et al., *A stromal cell niche sustains ILC2-mediated type-2 conditioning in adipose tissue.* J Exp Med, 2019. **216**(9): p. 1999-2009.
312. Liew, F.Y., J.P. Girard, and H.R. Turnquist, *Interleukin-33 in health and disease.* Nat Rev Immunol, 2016. **16**(11): p. 676-689.
313. Spallanzani, R.G., et al., *Distinct immunocyte-promoting and adipocyte-generating stromal components coordinate adipose tissue immune and metabolic tenors.* Sci Immunol, 2019. **4**(35).
314. Cautivo, K.M. and A.B. Molofsky, *Regulation of metabolic health and adipose tissue function by group 2 innate lymphoid cells.* Eur J Immunol, 2016. **46**(6): p. 1315-25.
315. Han, J.M., et al., *IL-33 Reverses an Obesity-Induced Deficit in Visceral Adipose Tissue ST2+ T Regulatory Cells and Ameliorates Adipose Tissue Inflammation and Insulin Resistance.* J Immunol, 2015. **194**(10): p. 4777-83.
316. Pakshir, P., et al., *The myofibroblast at a glance.* J Cell Sci, 2020. **133**(13).
317. Iwayama, T., et al., *PDGFRalpha signaling drives adipose tissue fibrosis by targeting progenitor cell plasticity.* Genes Dev, 2015. **29**(11): p. 1106-19.
318. Distler, J.H.W., et al., *Shared and distinct mechanisms of fibrosis.* Nat Rev Rheumatol, 2019. **15**(12): p. 705-730.
319. Rabhi, N., et al., *Obesity-induced senescent macrophages activate a fibrotic transcriptional program in adipocyte progenitors.* Life Sci Alliance, 2022. **5**(5).
320. Min, S.Y., et al., *Diverse repertoire of human adipocyte subtypes develops from transcriptionally distinct mesenchymal progenitor cells.* Proc Natl Acad Sci U S A, 2019. **116**(36): p. 17970-17979.
321. Schwalie, P.C., et al., *A stromal cell population that inhibits adipogenesis in mammalian fat depots.* Nature, 2018. **559**(7712): p. 103-108.
322. Nguyen, H.P., et al., *Aging-dependent regulatory cells emerge in subcutaneous fat to inhibit adipogenesis.* Dev Cell, 2021. **56**(10): p. 1437-1451 e3.
323. Spallanzani, R.G., et al., *Distinct immunocyte-promoting and adipocyte-generating stromal components coordinate adipose tissue immune and*

*metabolic tenors.* Science Immunology, 2019. **4**(35): p. eaaw3658.
324. Esteve, D., et al., *Lobular architecture of human adipose tissue defines the niche and fate of progenitor cells.* Nat Commun, 2019. **10**(1): p. 2549.
325. Gu, W., et al., *Single-Cell RNA-Sequencing and Metabolomics Analyses Reveal the Contribution of Perivascular Adipose Tissue Stem Cells to Vascular Remodeling.* Arterioscler Thromb Vasc Biol, 2019. **39**(10): p. 2049-2066.
326. Lee, K.Y., et al., *Developmental and functional heterogeneity of white adipocytes within a single fat depot.* Embo j, 2019. **38**(3).
327. Rajbhandari, P., et al., *Single cell analysis reveals immune cell-adipocyte crosstalk regulating the transcription of thermogenic adipocytes.* Elife, 2019. **8**.
328. Vijay, J., et al., *Single-cell analysis of human adipose tissue identifies depot- and disease-specific cell types.* Nature Metabolism, 2020. **2**(1): p. 97-109.
329. Zhong, L., et al., *Single cell transcriptomics identifies a unique adipose lineage cell population that regulates bone marrow environment.* Elife, 2020. **9**.
330. Farup, J., et al., *Human skeletal muscle CD90(+) fibro-adipogenic progenitors are associated with muscle degeneration in type 2 diabetic patients.* Cell Metab, 2021. **33**(11): p. 2201-2214 e11.
331. Hildreth, A.D., et al., *Single-cell sequencing of human white adipose tissue identifies new cell states in health and obesity.* Nature Immunology, 2021. **22**(5): p. 639-653.
332. Burl, R.B., et al., *Deconstructing cold-induced brown adipocyte neogenesis in mice.* Elife, 2022. **11**.
333. Massier, L., et al., *An integrated single cell and spatial transcriptomic map of human white adipose tissue.* Nature Communications, 2023. **14**(1): p. 1438.
334. Yang Loureiro, Z., et al., *Wnt signaling preserves progenitor cell multipotency during adipose tissue development.* Nature Metabolism, 2023.
335. Palani, N.P., et al., *Adipogenic and SWAT cells separate from a common progenitor in human brown and white adipose depots.* Nature Metabolism, 2023.
336. Chouchani, E.T. and S. Kajimura, *Metabolic adaptation and maladaptation in adipose tissue.* Nat Metab, 2019. **1**(2): p. 189-200.
337. Rosen, E.D. and B.M. Spiegelman, *What we talk about when we talk about fat.* Cell, 2014. **156**(1-2): p. 20-44.
338. Choi, Y.H. and J.K. Kim, *Dissecting Cellular Heterogeneity Using Single-Cell RNA Sequencing.* Mol Cells, 2019. **42**(3): p. 189-199.
339. Stuart, T., et al., *Comprehensive Integration of Single-Cell Data.* Cell, 2019. **177**(7): p. 1888-1902.e21.
340. Kolodziejczyk, A.A., et al., *Single Cell RNA-Sequencing of Pluripotent States Unlocks Modular Transcriptional Variation.* Cell Stem Cell, 2015. **17**(4): p. 471-85.
341. Han, J.S., et al., *Hypoxia Restrains Lipid Utilization via Protein Kinase A and ATGL Downregulation through Hypoxia Inducible Factor.* Molecular and Cellular Biology, 2019. **39**(2): p. e00390-18.
342. Kong, J., et al., *Spatiotemporal contact between peroxisomes and lipid droplets regulates fasting-induced lipolysis via PEX5.* Nature communications, 2020. **11**(1): p. 578-578.
343. Lee, J.H., et al., *RNF20 suppresses tumorigenesis by inhibiting SREBP1c-PTTG1 axis in kidney cancer.* Mol Cell Biol, 2017. **37**(22): p. e00265-17.
344. Hu, W., et al., *Patient Adipose Stem Cell-Derived Adipocytes Reveal Genetic Variation that Predicts Antidiabetic Drug Response.* Cell Stem Cell, 2019.

**24**(2): p. 299-308 e6.
345. Setty, M., et al., *Characterization of cell fate probabilities in single-cell data with Palantir.* Nature Biotechnology, 2019. **37**(4): p. 451-460.
346. Boyle, K.B., et al., *The transcription factors Egr1 and Egr2 have opposing influences on adipocyte differentiation.* Cell Death Differ, 2009. **16**(5): p. 782-9.
347. Villanueva, C.J., et al., *TLE3 is a dual-function transcriptional coregulator of adipogenesis.* Cell Metab, 2011. **13**(4): p. 413-427.
348. Chen, Y., et al., *Thermal stress induces glycolytic beige fat formation via a myogenic state.* Nature, 2019. **565**(7738): p. 180-185.
349. Yoneshiro, T., et al., *BCAA catabolism in brown fat controls energy homeostasis through SLC25A44.* Nature, 2019. **572**(7771): p. 614-619.
350. Shapira, S.N. and P. Seale, *Transcriptional Control of Brown and Beige Fat Development and Function.* Obesity (Silver Spring), 2019. **27**(1): p. 13-21.
351. Bénézech, C., et al., *Lymphotoxin-β Receptor Signaling through NF-κB2-RelB Pathway Reprograms Adipocyte Precursors as Lymph Node Stromal Cells.* Immunity, 2012. **37**(4): p. 721-734.
352. van de Pavert, S.A., et al., *Chemokine CXCL13 is essential for lymph node initiation and is induced by retinoic acid and neuronal stimulation.* Nat Immunol, 2009. **10**(11): p. 1193-9.
353. Redondo, P.A.G., et al., *Lymphatic vessels in human adipose tissue.* Cell Tissue Res, 2020. **379**(3): p. 511-520.
354. Shungin, D., et al., *New genetic loci link adipose and insulin biology to body fat distribution.* Nature, 2015. **518**(7538): p. 187-196.
355. Pischon, T., et al., *General and abdominal adiposity and risk of death in Europe.* N Engl J Med, 2008. **359**(20): p. 2105-20.
356. Jonker, J.W., et al., *A PPARgamma-FGF1 axis is required for adaptive adipose remodelling and metabolic homeostasis.* Nature, 2012. **485**(7398): p. 391-4.
357. Hepler, C., et al., *Identification of functionally distinct fibro-inflammatory and adipogenic stromal subpopulations in visceral adipose tissue of adult mice.* Elife, 2018. **7**: p. e39636.
358. Merrick, D., et al., *Identification of a mesenchymal progenitor cell hierarchy in adipose tissue.* Science, 2019. **364**(6438): p. eaav2501.
359. Sohn, J.H., et al., *Effects of Three Thiazolidinediones on Metabolic Regulation and Cold-Induced Thermogenesis.* Mol Cells, 2018. **41**(10): p. 900-908.
360. Villarroya, F., et al., *Toward an Understanding of How Immune Cells Control Brown and Beige Adipobiology.* Cell Metab, 2018. **27**(5): p. 954-961.
361. Rajbhandari, P., et al., *IL-10 Signaling Remodels Adipose Chromatin Architecture to Limit Thermogenesis and Energy Expenditure.* Cell, 2018. **172**(1-2): p. 218-233 e17.
362. Rajbhandari, P., et al., *Single cell analysis reveals immune cell-adipocyte crosstalk regulating the transcription of thermogenic adipocytes.* Elife, 2019. **8**: p. e49501.
363. Saltiel, A.R. and J.M. Olefsky, *Inflammatory mechanisms linking obesity and metabolic disease.* J Clin Invest, 2017. **127**(1): p. 1-4.
364. Ham, M., et al., *Glucose-6-phosphate dehydrogenase deficiency improves insulin resistance with reduced adipose tissue inflammation in obesity.* Diabetes, 2016.
365. Sillat, T., et al., *Basement membrane collagen type IV expression by human mesenchymal stem cells during adipogenic differentiation.* Journal of Cellular and Molecular Medicine, 2012. **16**(7): p. 1485-1495.
366. Neal, J.W. and N.A. Clipstone, *A constitutively active NFATc1 mutant induces*

*a transformed phenotype in 3T3-L1 fibroblasts.* J Biol Chem, 2003. **278**(19): p. 17246-54.
367. Pham, T.X., et al., *Transcriptional analysis of lung fibroblasts identifies PIM1 signaling as a driver of aging-associated persistent fibrosis.* JCI Insight, 2022. **7**(6).
368. Dubey, S., et al., *Inhibition of RUNX1 blocks the differentiation of lung fibroblasts to myofibroblasts.* J Cell Physiol, 2022. **237**(4): p. 2169-2182.
369. Lee, Y.S., et al., *Inflammation is necessary for long-term but not short-term high-fat diet-induced insulin resistance.* Diabetes, 2011. **60**(10): p. 2474-83.
370. Hoeft, K., et al., *Platelet-instructed SPP1(+) macrophages drive myofibroblast activation in fibrosis in a CXCL4-dependent manner.* Cell Rep, 2023. **42**(2): p. 112131.
371. Coulis, G., et al., *Single-cell and spatial transcriptomics identify a macrophage population associated with skeletal muscle fibrosis.* Science Advances, 2023. **9**(27): p. eadd9984.
372. Hara, T. and K. Tanegashima, *CXCL14 antagonizes the CXCL12-CXCR4 signaling axis.* Biomol Concepts, 2014. **5**(2): p. 167-73.
373. Tanegashima, K., et al., *Dimeric peptides of the C-terminal region of CXCL14 function as CXCL12 inhibitors.* FEBS Lett, 2013. **587**(23): p. 3770-5.
374. Nguyen, T.T.P., et al., *SREBP-1c impairs ULK1 sulfhydration-mediated autophagic flux to promote hepatic steatosis in high-fat-diet-fed mice.* Mol Cell, 2021.
375. Ramkhelawon, B., et al., *Netrin-1 promotes adipose tissue macrophage retention and insulin resistance in obesity.* Nat Med, 2014. **20**(4): p. 377-84.
376. Kim, D., et al., *CXCL12 secreted from adipose tissue recruits macrophages and induces insulin resistance in mice.* Diabetologia, 2014. **57**(7): p. 1456-65.
377. Fujisaka, S., et al., *Regulatory Mechanisms for Adipose Tissue M1 and M2 Macrophages in Diet-Induced Obese Mice.* Diabetes, 2009. **58**(11): p. 2574-2582.
378. Sierra-Filardi, E., et al., *Activin A skews macrophage polarization by promoting a proinflammatory phenotype and inhibiting the acquisition of anti-inflammatory macrophage markers.* Blood, 2011. **117**(19): p. 5092-101.
379. Gong, D., et al., *TGFβ signaling plays a critical role in promoting alternative macrophage activation.* BMC Immunology, 2012. **13**(1): p. 31.
380. Hill, D.A., et al., *Distinct macrophage populations direct inflammatory versus physiological changes in adipose tissue.* Proceedings of the National Academy of Sciences, 2018. **115**(22): p. E5096-E5105.
381. Ramachandran, P., et al., *Resolving the fibrotic niche of human liver cirrhosis at single-cell level.* Nature, 2019. **575**(7783): p. 512-518.
382. Mulder, K., et al., *Cross-tissue single-cell landscape of human monocytes and macrophages in health and disease.* Immunity, 2021. **54**(8): p. 1883-1900.e5.
383. Fabre, T., et al., *Identification of a broadly fibrogenic macrophage subset induced by type 3 inflammation.* Sci Immunol, 2023. **8**(82): p. eadd8945.
384. Zhang, K., et al., *TREM2(hi) resident macrophages protect the septic heart by maintaining cardiomyocyte homeostasis.* Nat Metab, 2023. **5**(1): p. 129-146.
385. Bhattacharya, M. and P. Ramachandran, *Immunology of human fibrosis.* Nature Immunology, 2023. **24**(9): p. 1423-1433.
386. Jeon, Y.G., et al., *RNF20 Functions as a Transcriptional Coactivator for PPARgamma by Promoting NCoR1 Degradation in Adipocytes.* Diabetes, 2020. **69**(1): p. 20-34.
387. Jung, B.C., et al., *TET3 plays a critical role in white adipose development and diet-induced remodeling.* Cell Rep, 2023. **42**(10): p. 113196.

# 국문 초록

지방조직은 핵심 대사기관으로 에너지의 저장과 방출, 호르몬 및 대사물질 분비를 통해 전신적 에너지대사를 조절한다. 포유류의 지방조직은 크게 에너지 저장에 특화된 백색지방조직과 열을 소모하여 에너지를 생성하는 갈색지방조직으로 구분된다. 백색지방조직은 해부학적으로 다시 내장지방조직과 피하지방조직으로 나눌 수 있다. 마우스에서는 생식소 주변 epididymal adipose tissue (EAT) 가 내장지방 연구의 주요 모델로서, 사타구니 주변 inguinal adipose tissue (IAT) 는 피하지방 연구의 주요 모델로서 사용되고 있다.

EAT 와 IAT 는 해부학적 위치 뿐 아니라 발생학적 기원과 대사자극 등에 대한 반응에서도 차이를 보인다. 발생학적 측면에서 EAT 는 Wt1 및 Pax3 를 발현하는 세포계통에서 형성되는 반면, IAT 는 EAT 와는 다른 Prrx1 을 발현하는 세포계통에서 형성된다. EAT 는 복강에 존재하는 장과 같은 기관들과 긴밀하게 상호작용을 할 수 있는 반면 IAT 는 상대적으로 신체의 바깥쪽에 위치하여 물리적 충격에 대한 보호 및 단열기능 등을 수행한다. 또한 EAT 와 IAT 는 대사자극에 대하여 다른 반응도를 나타낸다. 비만 시 EAT 에는 만성 염증반응과 섬유화반응이 항진되나 이러한 현상은 IAT 에서는 크게 나타나지 않는다. 반면 추위자극 시에 열 생성에 기여하는 베이지 지방세포 형성은 IAT 에서 높게 나타나지만 EAT 에서는 거의 관찰되지 않는다.

최근 일련의 연구결과들은 지방조직 줄기세포 (adipose stem cells, ASCs) 고유의 특성이 EAT 와 IAT 사이의 차이점을 매개한다고 제시하였다. 예를 들어, EAT 와 IAT ASC 에서 분화된 지방세포는 기능적으로 상이한 측면이 있다. 비만 시 EAT 내 ASC 는 항진된 지방세포분화에 기여하지만 IAT 에서는

상대적으로 지방세포분화가 낮게 유지된다. 추위노출 시 IAT 에서는 일부 ASC 가 베이지 지방세포로 분화한다. 또한 IAT ASC 는 지방조직의 염증반응을 억제할 수 있음이 제안되었다. 나아가 최근 단일세포 전사체분석기법 (single-cell RNA sequencing, scRNA-seq) 을 활용한 연구결과들은 ASC 가 기능적으로 상이한 아집단으로 구성되어 있는 이질적인 세포군임을 제안하였다. 그럼에도 불구하고 EAT 와 IAT 특이적인 ASC 아집단에 대한 비교연구는 시도된 바가 없다.

1 장에서 EAT 와 IAT 를 대상으로 ASC 의 지방세포분화 (adipogenesis) 정도와 기전을 비교분석하였다. 그 결과 ASC 의 백색지방세포분화가 EAT 에서 IAT 보다 활발히 일어나는 기전을 규명하였고 IAT 특이적인 베이지 지방세포의 전구세포군을 동정하였다. 단일세포 전사체분석을 통해 EAT 와 IAT ASC 가 상이한 세포군으로 구성되며, 이들을 임의적으로 3 개의 지방세포 분화단계로 구분하고 분석하였다. 상대적으로 지방세포 분화능이 높은 2,3 단계의 세포군들이 IAT 보다 EAT 에 다량으로 존재함을 관찰하였고 ASC 의 내재적 인자가 이를 제어함을 규명하였다. 또한 비만 시 EAT ASC 들이 특이적으로 분열능이 증가하여 지방세포분화 증가에 기여함을 관찰하였다. 또한 IAT 특이적으로 BST2 를 높게 발현하고 증가된 베이지 지방세포 분화능을 가진 ASC 아집단을 동정하였으며, 해당 아집단의 형성이 림프절에 의해 조절됨을 규명하였다.

2 장에서 비만 시 EAT 특이적으로 염증반응과 섬유화반응을 촉진하는 $SDC1^+$ ASC 와 IAT 특이적으로 염증반응을 억제하는 $CXCL14^+$ ASC 를 동정하고 그 특성을 규명하였다. 비만 시 EAT 에서는 IAT 에 비해 항진된 염증반응 및 섬유화반응이 타나난다. 이를 관장하는 ASC 아집단을 동정하기 위해 정상 및 비만 마우스의 EAT 와 IAT ASC 를 대상으로 단일세포 전사체분석 결과를

심층분석하였다. 분화경로분석기법을 통해 EAT 와 IAT 의 ASC 들을 비교한 결과 비만 시 EAT 에서만 나타나는 ASC 아집단을 발견하고 SDC1 을 그 표지마커로 동정하였다. $SDC1^{+}$ ASC 는 염증반응 및 섬유화반응 관련 유전자를 높게 발현하였다. 반면 특정 IAT ASC 아집단은 CXCL14 유전자를 높게 발현하였으며, CXCL14 는 CXCL12 의 작용을 억제하여 대식세포의 침윤과 염증반응을 억제하였다. 이러한 결과는 EAT 및 IAT 특이적인 $SDC1^{+}$ ASC 및 $CXCL14^{+}$ ASC 가 비만에 의한 EAT 및 IAT 특이적 염증반응과 섬유화반응을 매개함을 암시한다.

종합적으로, 본 학위논문은 ASC 가 내장지방과 피하지방이 가진 고유한 대사기능의 수행에 있어 핵심적인 세포군임을 시사한다. EAT ASC 는 내재적 특성으로 인하여 높은 백색지방세포 분화능을 나타내는 반면 IAT 특이적인 $BST2^{high}$ ASC 는 상대적으로 높은 베이지 지방세포 분화능을 보유하고 있다. 나아가 EAT 특이적인 $SDC1^{+}$ ASC 와 IAT 특이적인 $CXCL14^{+}$ ASC 는 염증반응과 섬유화반응을 각각 다른방향으로 제어하였다. 본 학위논문의 연구결과를 통하여 지방조직 내 ASC 이질성에 대한 이해를 넓히고 새로운 시각을 제공할 수 있으리라 기대하며, 이를 통해 내장지방과 피하지방간의 차이점 이해를 통한 새로운 통찰을 제공하기를 희망한다.

주요어: 지방조직, 백색지방조직, 내장지방, 피하지방, 지방조직 줄기세포, 지방세포분화, 염증반응, 섬유화반응

학번: 2018-23827